Universidad de Huelva

Departamento de Química "Profesor José Carlos Vílchez Martín"

Supramolecular cucurbituril complexes for applications in bio-relevant contexts

Memoria para optar al grado de doctora
presentada por:

Cátia Diana Parente Caldeira Carvahlo

Fecha de lectura: 21 de diciembre de 2015

Bajo la dirección del doctor:

Uwe Pischel

Huelva, 2015

Facultad de Ciencias Experimentales
Dpto. de Química
"Prof. José Carlos Vílchez Martín"

Supramolecular Cucurbituril Complexes for Applications in Bio-relevant Contexts

by

Cátia Diana Parente Caldeira Carvalho

Oriented by Dr. Uwe Pischel

PROGRAMA OFICIAL DE DOCTORADO EN CIENCIA Y TECNOLOGÍA QUÍMICA

Huelva, 2015

Authorship Verification

I declare to be the author of this thesis, which derives entirely from the work developed under the supervision of Prof. Dr. Uwe Pischel. I confirm that where the thesis is based on consulted/quoted published papers, or where jointly work was performed, I have made clear what the contributions of others were.

(Cátia Diana Parente Caldeira Carvalho)

Acknowledgements

First, I would like to express my gratitude to my supervisor Prof. Dr. Uwe Pischel for the constant help, guidance, motivation, and the countless hours of attention devoted throughout the course of my PhD work.

I also would like to thank the professors Prof. Dr. José Paulo da Silva, Prof. Dr. Werner M. Nau, Prof. Dr. Joakim Andréasson, Prof. Dr. Vera Ribeiro, and their group members for the continuous collaboration, help, contributions, and specially for receiving me in their laboratories and for letting me use their facilities.

The Spanish Ministry of Economy and Competitiveness, Madrid (grant CTQ2011-28390), the Portuguese Foundation for Science and Technology, Lisbon (doctoral fellowship SFRH/BD/81628/2011), and the POCTEP program (RISE and I2TEP projects) are gratefully acknowledged for the provided financial support. The University of Huelva, especially the Center for Research in Sustainable Chemistry (CIQSO), I thank for providing all professional and administrative means to develop this thesis work.

I wish to acknowledge all former and present group members for the friendly atmosphere, help, and support. I am particularly thankful to my friends Dr. Vânia Pais and Dr. Patricia Remón for many fruitful discussions and advices. My colleagues, Julián Vázquez, Antonio Alfaro, and Miguel Romero I thank for their brilliant humor and friendship. My special gratitude goes to Julián y Antonio for their help with some of the figures of this thesis. To Zoe Dominguez I am indebted for the synthetic work required for Chapter 5.

Last but not least, I would like to express my heartfelt gratitude to all the people who always encouraged me. To my friends and family, that always motivated and continuously supported me throughout my career, particularly my mother that always helped me to fulfill my dreams. My dear husband I thank from the deepest of my heart for all his help and sacrifice. Jorge, this thesis is dedicated to you.

Abstract

In the last decade, macrocyclic hosts have been used as an exciting new tool in functional supramolecular chemistry applications ranging from sensing, via drug delivery to catalysis and materials chemistry. This doctoral thesis describes the development of new supramolecular systems based on cucurbiturils for biologically related applications. Adequate water solubility, low toxicity, and capacity to form strong host-guest complexes, establish cucurbituril chemistry as a powerful tool to investigate and possibly modulate biological systems and functions. Likewise, their ability to tune photophysical and chemical properties of encapsulated guests were exploited by the use of UV/vis, mass spectrometry, liquid chromatography, NMR, and fluorescence-based techniques. Moreover, taking advantage of molecular biology procedures the effects of cucurbiturils on enzymatic activity were investigated.

In this work, for the first time a proof-of-principle for the photo-triggered delivery of a drug by disassembly of its host-guest complex with CB7, taking advantage of a pH jump, is described. Additionally, an anchor approach was developed, which enabled the improvement of the hydrolytic stability of spiropyrans in aqueous solution without compromising their switching performance. Furthermore, it is described for the first time that CB6 and CB7 can influence directly enzymatic activity of endonucleases, which can be reversibly controlled by the use of strong competitors for the macrocyclic host cavity. This consolidates the possibility of supramolecular control of biocatalytic processes. Finally, the chemically and photonically driven operation of a supramolecular keypad lock device with a ternary anthracene-guest/CB8 host complex is described. The reversible and robust photoinduced cycloaddition reaction in the cavity of the host is remarkable.

In general terms, this work broadens further the use of cucurbituril macrocyclic hosts in the context of functional chemistry and biological applications.

Resumen

En la última década, los anfitriones macrocíclicos se han utilizado como una nueva herramienta excitante para aplicaciones de la química supramolecular funcional, que van desde la detección de analitos, la administración y el transporte de fármacos, a la catálisis y la química de materiales. Esta tesis doctoral describe el desarrollo de nuevos sistemas supramoleculares basados en cucurbiturilos para aplicaciones biológicas. Una solubilidad en agua adecuada, una baja toxicidad, y la capacidad para formar complejos fuertes anfitrión-huésped, dan lugar a que la química de los cucurbiturilos sea una herramienta poderosa para investigar y posiblemente controlar sistemas biológicos y sus funciones. Del mismo modo, su capacidad para modular propiedades fotofísicas y químicas de los huéspedes encapsulados se han explotado por medio del uso de técnicas basadas en absorción UV/vis, espectrometría de masas, cromatografía líquida, RMN y técnicas basadas en fluorescencia. Por otra parte, tomando ventaja de procedimientos de biología molecular, se investigaron también los efectos de los cucurbiturilos sobre la actividad enzimática.

En este trabajo, por primera vez, se describe una prueba de concepto para la liberación foto-inducida de un fármaco modelo por la disociación de un complejo anfitrión-huésped con CB7, aprovechando un salto en el pH. Igualmente, se desarrolló un sistema basado en un anclaje, que permitió mejorar la estabilidad hidrolítica de los espiropiranos en solución acuosa sin comprometer su rendimiento como interruptores. Además, se desvela, por primera vez, que el CB6 y CB7 pueden influir directamente en la actividad enzimática de las endonucleasas, las cuales pueden ser controladas de forma reversible mediante el uso de competidores fuertes por del macrociclo. Con esto se consolida la posibilidad de tener un control supramolecular de los procesos biocatalíticos. Por último, se describe una operación lógica impulsada químicamente y mediante irradiación con luz resultando en un dispositivo *keypad lock* supramolecular. Ésta operación se ha llevado a cabo por un complejo ternario antraceno-huésped/CB8-anfitrión. Es de remarcar la reacción de cicloadición fotoinducida reversible y robusta dentro de la cavidad del huésped.

En términos generales, este trabajo amplía aún más el uso de los anfitriones macrocíclicos cucurbiturilos en el contexto de la química funcional y para aplicaciones biológicas.

Table of Contents

Chapter 1

Introduction

The main focus of this thesis is to demonstrate the applicability of cucurbituril macrocycles in topics that are relevant to biological contexts. In this chapter, briefly some principles of supramolecular chemistry, with particular emphasis on the cucurbituril family, their distinct complexation properties and applications will be introduced.

1.1 Supramolecular Chemistry

Supramolecular chemistry is commonly defined as the "chemistry beyond the molecule", implying any organized system in which two or more molecular entities are held together by non-covalent interactions.[1] Despite the lack of a more precise definition, but may be also because of this broad description, supramolecular chemistry evolved as a major field of science. It is situated at a multidisciplinary intersection between chemistry, physics, biology, and nanotechnology, providing exciting applications,[2] ranging from prime examples of academic ingenuity to day-by-day applications.

The foundation of the supramolecular chemistry began with insights into the chemistry of the living systems and remotes back to the late 19th century. Among the pioneering ideas we can find the concept of coordination chemistry (Alfred Werner, 1893),[3] the lock-and-key principle jointly with the notion of selective binding (Emil Fischer, 1894),[4] and the perception of what is a receptor (Paul Ehrlich, 1906).[5] The term "supermolecules" was coined by Wolf and coworkers in 1937 to describe entities of higher organization resulting from the association of coordinately saturated species.[6] The first artificial molecular receptor (crown

ethers)[7] was reported by Pederson in 1967, followed by Cram's contributions (carcerands) and the establishment of host-guest chemistry.[8,9] Finally, in 1978 Lehn (cryptands) was the first to propose the term "supramolecular chemistry" in order to contextualize this type of chemistry as "chemistry beyond the molecule". Together, Pedersen, Cram, and Lehn, received the Nobel Prize in Chemistry (1987) for their crucial contributions to the foundations of this field.[10-12]

According to Lehn, a supramolecular complex is characterized by its structural conformation, thermodynamics (enthalpy and entropy of formation), and dynamics (kinetics of formation and dissociation). Supramolecular structures are the result of additive and often cooperative interactions. The most common types of supramolecular interactions are electrostatic, cation-π, π-π stacking, hydrophobic, hydrogen bonding, and van-der-Waals forces. These interactions are reversible and weaker compared with the covalent bond, and their dynamic nature determines their predominant role in many biological processes. It is therefore not surprising that supramolecular chemistry takes its inspiration from the chemistry of living systems and the development of a simple host-guest system provides the opportunity to unveil several natural processes.

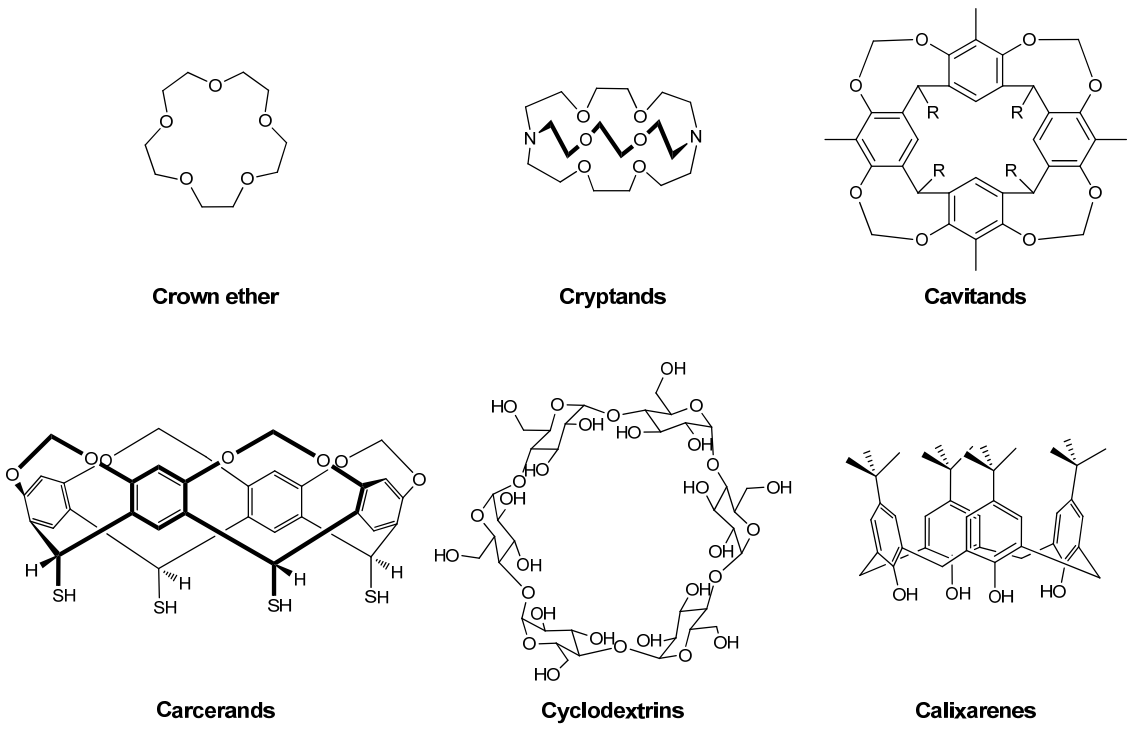

Scheme 1.1 – General representation of crown ethers, cryptands, cavitands, carcerands, cyclodextrins and calixarenes macrocyclic host molecules.

Following the discovery of crown ethers by Pederson,[7] cryptands by Lehn,[13] and cavitands and carcerands by Cram,[14] many research groups understood the potential implications of developing and studying macrocyclic host molecules (differing in size and shape, see Scheme 1.1). Since then, many other macrocyclic families emerged, like cyclodextrins,[15] calixarenes,[16] and cucurbiturils[17]. As a result, supramolecular chemistry has become an attractive approach to address biological problems,[18] and among the existing hosts, the cucurbituril family is nowadays one of the most promising.

1.2 The Cucurbituril Family

Cucurbiturils (CB*n*) are a re-discovered family of macrocyclic host compounds readily assembled by an acid-catalyzed condensation reaction of glycoril and formaldehyde, forming cyclic oligomers of *n* glycoluril units bridged by 2*n* methylene groups (Scheme 1.2). Their synthesis was first reported by Behrend and coworkers in 1905 (named as Behrend's polymer).[19] However, their nature remained elusive until 1981, when Mock *et al.*[17] described the chemical and structural properties of cucurbit[6]uril (CB6). The particular name emerges from the structural resemblance to the pumpkin family (lat.: *cucurbitacea*). In the following years, other members of the CB*n* family (*n* = 5, 7, 8, and 10) were disclosed and successfully isolated by Kim,[20] Day,[21] and Nau,[22] which broadened the scope of CB*n* chemistry enormously.

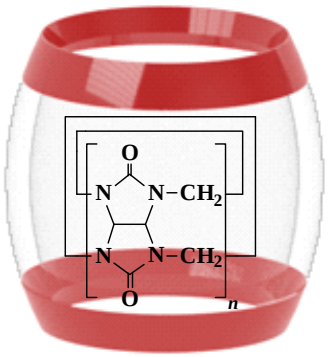

Scheme 1.2 – Representation of the CB*n* structure.

CB*n* are highly symmetrical, with a central hydrophobic cavity accessible by two aligned carbonyl-rimmed portals, see Scheme 1.2. CB*n* are also weak bases, which become only protonated in strongly acidic media (acidity dissociation constant, pK_a ≤ 3.0), in which H^+ may diminish the affinity for the encapsulation of molecules.[23,24] With respect to their size, CB*n* are 9.1 Å deep and the portals guarding the entries are approximately 2 Å narrower than the cavity itself. This results in constrictive binding that may produce significant steric barriers for guest association and dissociation.[25] Depending on the number of glycoluril units of the CB*n* homologues, ranging from CB5 to CB10, the outer diameter, internal cavity, volume, and molecular weight increase progressively (Table 1.1). One of the outstanding features of CB*n* is their high thermal stability, without any signs of decomposition observed up to 573 K.[26,27] On the other hand, the solubility in aqueous solvents is a potential limitation for the use of these macrocycles in biological applications. Nonetheless, CB5 and CB7 homologues stand by an appreciable solubility (Table 1.1). In any case, the only moderate solubility in water is compensated by the extraordinarily high guest binding constants (see below). The solubility of the macrocycles increases by the addition of salts or by providing strongly acidic conditions.[26,27]

Table 1.1 – Dimensions and physical properties of CB*n*.

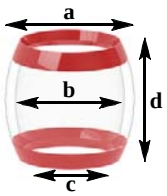

Properties[a]		**CB5**	**CB6**	**CB7**	**CB8**	**CB10**[b]
MW		830	996	1163	1329	1661
Outer diameter (Å)	**a**	13.1	14.4	16.0	17.5	-
Cavity (Å)	**b**	4.4	5.8	7.3	8.8	~11.7
	c	2.4	3.9	5.4	6.9	~10.0
Height (Å)	**d**	9.1	9.1	9.1	9.1	9.1
Cavity volume (Å^3)		82	164	279	479	870
Solubility in water (mM)		~3 - 4	0.05	5	<0.1	<0.05
Stability (K)		>693	698	643	>693	>573
pK_a		-	3.02	2.20	-	-

[a] Values according with [22-31]; [b] Determined for the CB[5]@CB[10] complex.

In 2013, Tao discovered a twisted CB14 homologue which does not have a normal cavity like most CB*n*, but rather the appearance of a folded, figure-of-eight conformation.[32] Functionalized, inverted, nor-sec, and various CB*n* congeners have also been discovered,[33] comprising distinct properties in the complexation of guests.

1.2.1 Host-Guest Complexation

The hydrophobic interior of CB*n* macrocycles is a potential inclusion site for several nonpolar molecules (guest), allowing an assembly of host-guest complexes. The CB*n* cavity features a low polarizability and a polarity that is lower than water but higher than ethanol.[34-36] As a result, the environment that a guest experiences is quite similar to that of alcohols or alcohol-water mixtures. In contrast, the carbonyl-rimmed portals are hydrophilic and have a high hydrogen-bonding and ion-dipole interaction ability (Scheme 1.3).[25,37,38] The hydrophilic nature of the two portals and the non-polarizable hydrophobic interior make neutral and positively charged molecules preferable guests for CB*n*. Interestingly, CB5 can also accommodate anionic guests, such as Cl^- and NO_3^- ions.[30,39] Note that the relative importance of the electrostatic interactions and the hydrophobic effect may change as the cavity size increases.

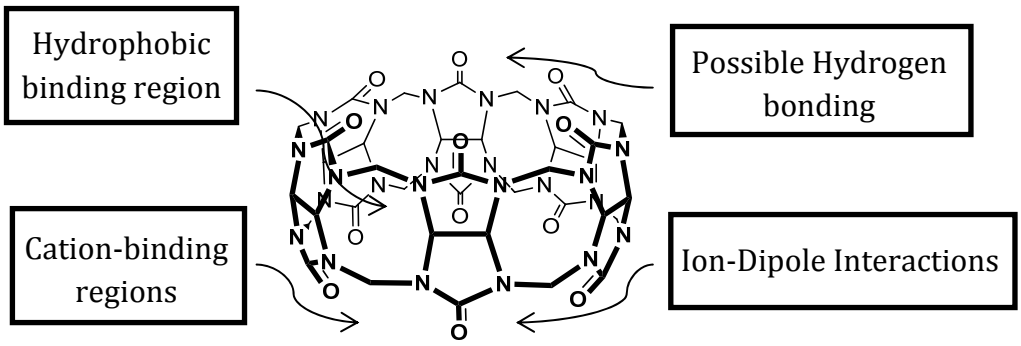

Scheme 1.3 – Representation of the different binding regions of CB6.

The CB*n* portals are important steric barriers to the association and dissociation of guests, where the distinct binding possibilities and restriction environment have profound implications in the formation of stable host-guest complexes.[17,26,27] The binding capacity of these macrocycles equals and most often largely exceeds that of other host molecules (10^6 to 10^{17} M^{-1}), such as cyclodextrins and crown ethers.[27,40] In this regard the role of released high-energy water was emphasized as a crucial factor for the observed high binding constants.[41]

The binding constant (or affinity constant, K_b) between a host and the guest determines the viability of the host-guest pair in many applications. This value is usually determined by titration experiments, for example by following a spectroscopic property of the guest in dependence on the concentration of macrocycle.[42] The host-guest spectroscopic properties can also be recorded in dependence on the concentration of an competitive guest (competitive displacement titration),[43] and then plotted and fitted with an appropriate binding model. This is possible due to the transparency CB*n* in a large optical window (>300 nm), making them optimal hosts for optical applications.

A simple prediction about the formation of a particular host-guest complex obeys the "packing coefficient" rule (ratio of volumes between the guest and the host cavity), which should be around 0.55 ± 0.09 for optimal binding efficiency.[44,45] However, the formation of stable inclusion complexes is a delicate equilibrium between hydrophobicity, charge, shape, and size of the guest and the host. Taking these principles into account, Blatov and coworkers developed a computational technique that identifies suitable guests for each member of the CB*n* family.[46] Notably, another type of complexation can occur between the guest and host, not by total or partial immersion in the host cavity, but by association with the host portals alone. This type of association is termed exclusion complex.[47]

Changes of enthalpy and entropy are the commonly investigated thermodynamic parameters for host-guest complexations, accessible by isothermal titration calorimetry. The complexation with CB*n* is often enthalpically driven.[48-54] Enthalpy changes account mainly for the stabilization of the guest by the host, through hydrophobicity and dipole interactions. Entropy mainly contributes to the release

of solvent molecules from the interior host cavity or the desolvation of highly polar or charged guest molecules.

From the viewpoint of kinetics, it seems that the encapsulated guests determine the velocity of the exchange (ingression and egression rates) on the NMR time scale. Smaller guests tend to display fast exchange kinetics (middled NMR signals are detected), whereas larger guests favor slow exchange (separate signals are observed for the free and bound guests). A significant number of guests adopt intermediate exchange rates, leading often to the observation of NMR signal broadening.[55]

1.2.2 Biocompatibility

In order to use CB*n* in biological applications, they should not only be water-soluble (see above for detailed solubility), but also biocompatible. The biocompatibility is related with the overall low toxicity of many host macrocycles in biological systems.[56] Furthermore, the CB*n* host should also beneficially influence the encapsulated guest by improving its solubility and its chemical and physical stability (see next section, and Scheme 1.4).[29] Comprehensive toxicity, phamacokinetic and pharmacodynamic profiles for CB*n* have yet to be determined, but several studies point out positive predictions for the bio-safety of these macrocycles.[29,57,58]

*In vitro a*nd *in vivo* studies revealed that CB*n* (*n* = 5, 7, and 8) and its complexes are remarkably inert and can effectively cross cell membranes. Likewise, up to millimolar concentrations of free macrocycle have shown practically no cytotoxicity in animal and human cell lines.[57-63] In mice both CB7 and CB7/CB8 1:1 mixture are non-toxic at concentrations well above those necessary for drug delivery applications.[57] Furthermore, it was demonstrated that CB7 does not cross the blood-brain barrier, and accumulation in the liver and spleen was very low with respect to that in the kidneys.[64] This suggests that the macrocycle is quickly excreted by the urine without chemical modifications.

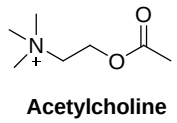

Acetylcholine

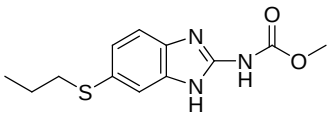

Albendazole

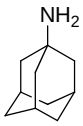

Amantadine

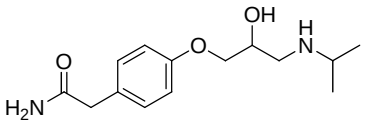

Atenolol

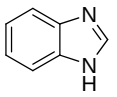

Benzimidazole

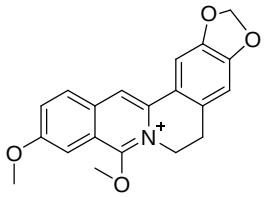

Berberine

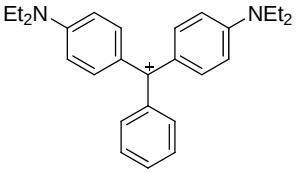

Brilliant Green

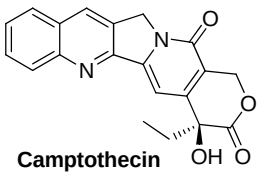

Camptothecin

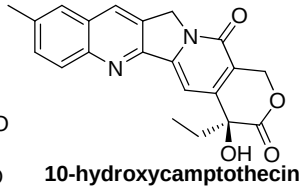

10-hydroxycamptothecin

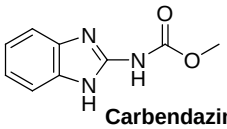

Carbendazim

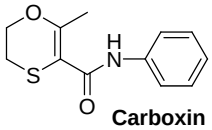

Carboxin

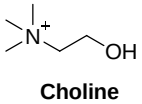

Choline

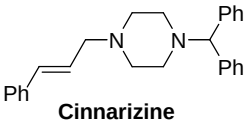

Cinnarizine

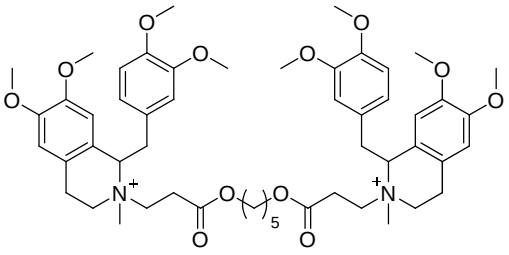

Cisatracurium

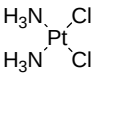

Cisplatin

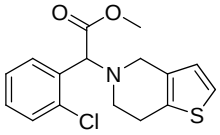

Clopidogrel

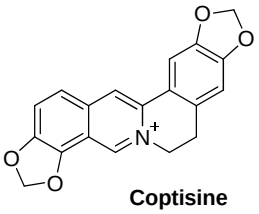

Coptisine

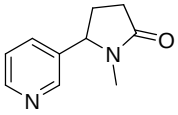

Cotinine

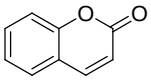

Coumarin

Cp_2MoCl_2

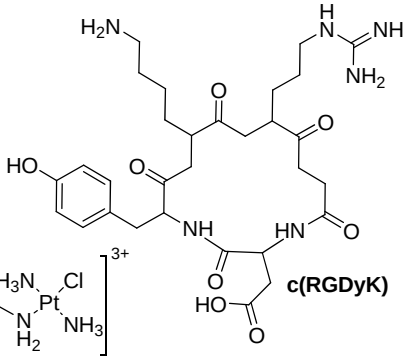

c(RGDyK)

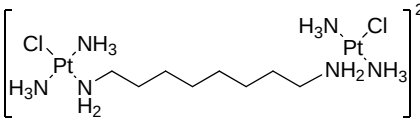

CT008

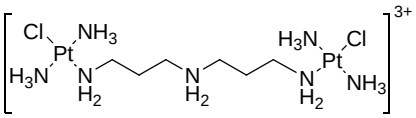

CT033

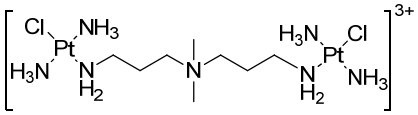

CT233

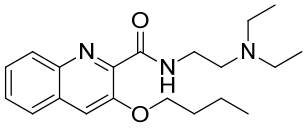

Dibucaine

Diiodine

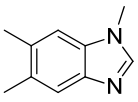

α-DMB

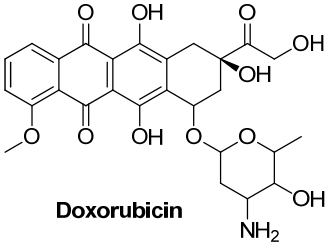

Doxorubicin

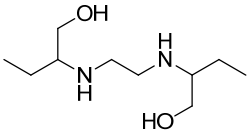

Ethambutol

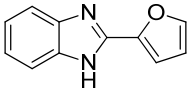

Fuberidazole

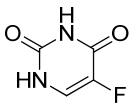

5-Fluorocuracil

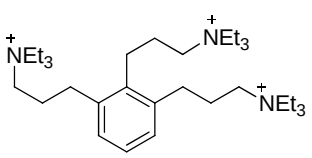

Gallamine

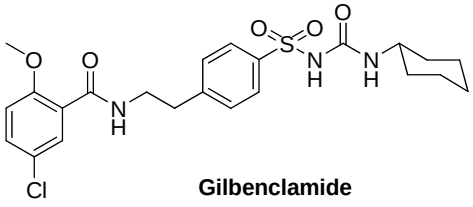

Gilbenclamide

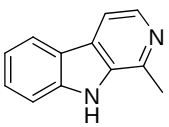

Harmane

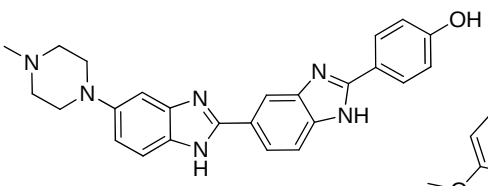

Hoechst 33258

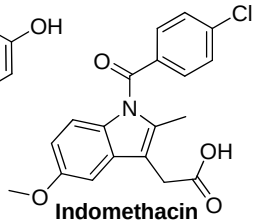

Indomethacin

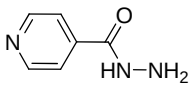

Isoniazid

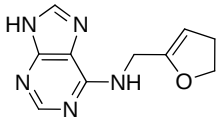

Kinetin

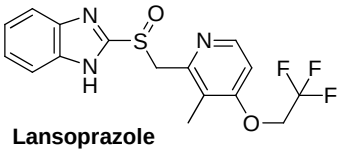

Lansoprazole

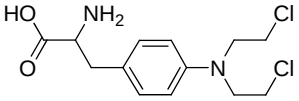

Melphalan

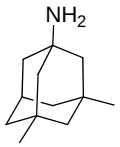

Memantine

1-Methylcyclopropene

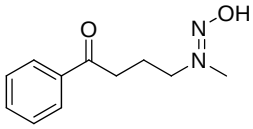

(4-methylnitrosamino)-1-(3-pyridyl)-1-butanone

N-nitrosodimethylamine

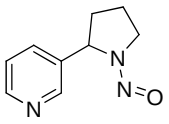

N-nitrosonomicatin

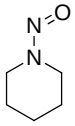

N-nitrosopiperidine

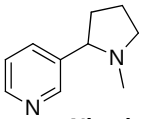

Nicotine

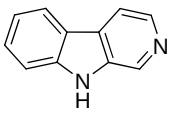

Norharmane

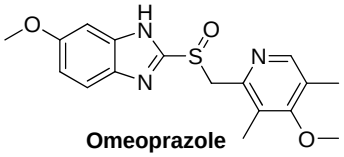

Omeoprazole

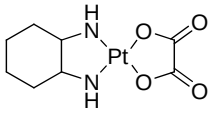

Oxaliplatin

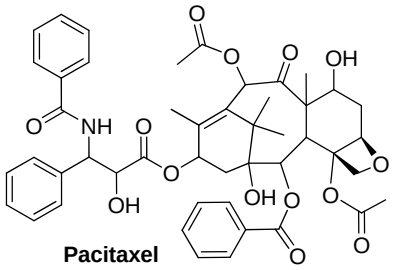

Pacitaxel

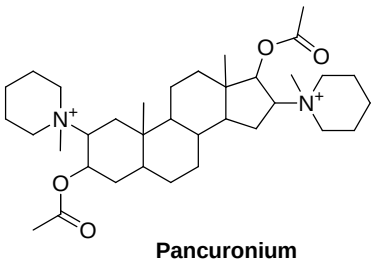

Pancuronium

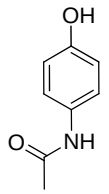

Paracetamol

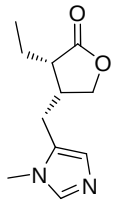

Pilocarpine

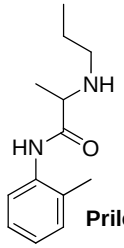

Prilocaine

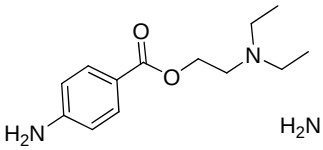

Procaine

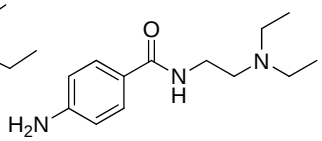

Procainamide

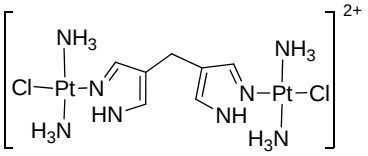

[trans-[{Pt(NH$_3$)$_2$Cl}]$_2$ μ-dpzm]$^{2+}$

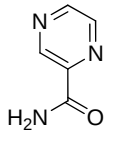

Pyrazinarride

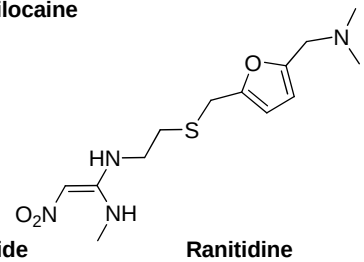

Ranitidine

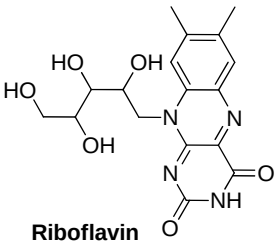

Riboflavin

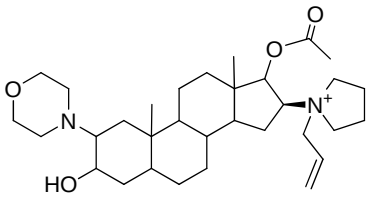

Rocuronium

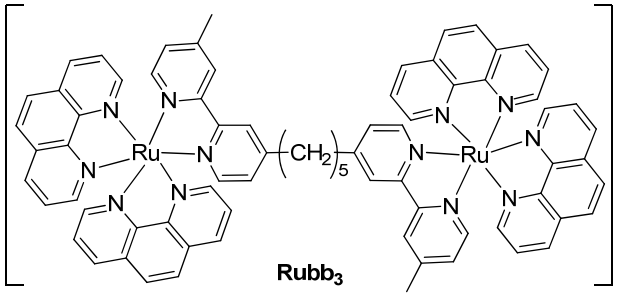

Rubb$_3$

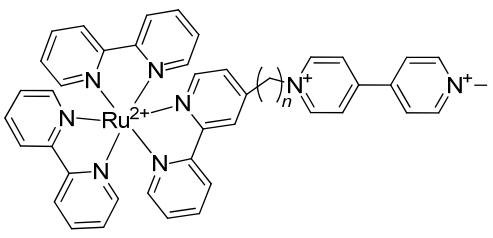

Ruthenium(II)tris-bipyridyl-(CH$_2$)$_n$-MV^{2+}

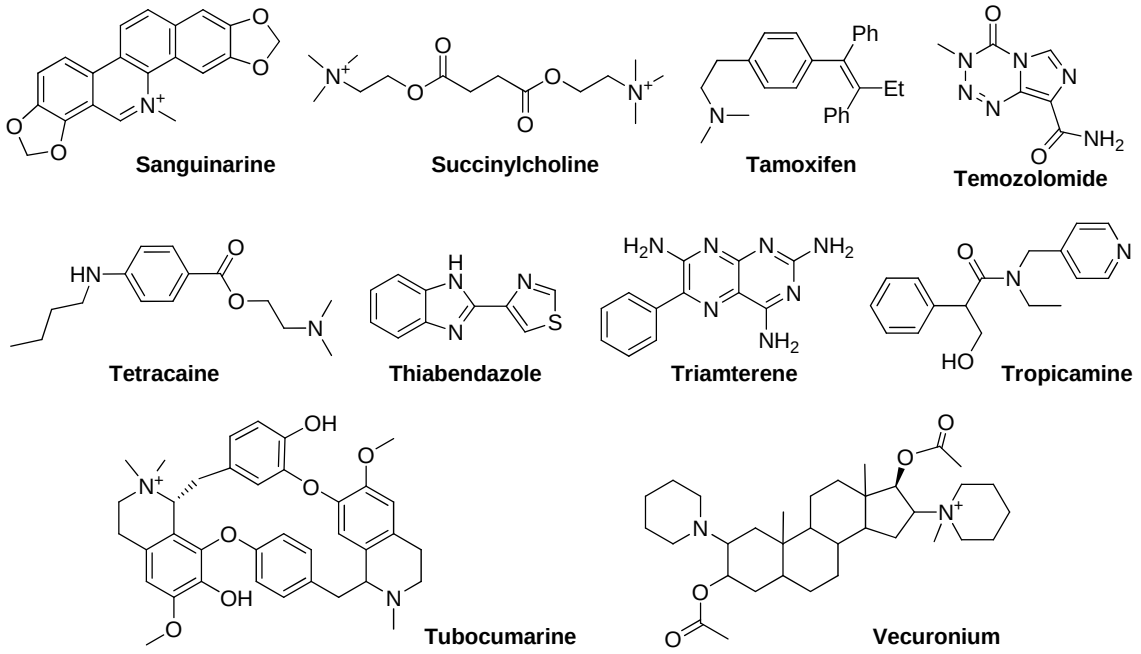

Scheme 1.4 – Structural composition of drugs and biologically active molecules that benefit from CB*n*-guest assemblies.

Recently, it was revealed that the solubility of CB*n* in biologically relevant media could actually be much higher than previously considered. It was shown that in simulated gastric fluid CB6 is soluble at concentrations of up to 4 mM, and in other fluids, it can go as high as 45 mM.[29,65] Such promotion effects in solubility are probably related to the high salt content and acid concentrations in these media.

All these recent discovered features increased the interest in CB*n* macrocycles and in their use in biological applications. Recent studies unveiled that CB6 can be easily applied in drug formulations for oral administration,[65] and that when used as an ingredient of a topical cream, it does not permeate easily through skin and therefore may have more likely application in localized skin treatments than it does for transdermal drug delivery.[66]

Unfortunately, there is no toxicological information related to CB6 and CB10. Moreover, CB5 and CB10 cannot be considered for biological applications due to their cavity size. While CB5 is too small to incorporate drugs, CB10 is usually too large to strongly bind a guest molecule.[27,29]

1.2.3 Applications Based on CB*n* Encapsulation

Over the past few years, several studies highlighted the potential of CB*n* chemistry in a broad range of biological applications, including catalysis,[33,67] polymers and nanostructures,[68-74] molecular tools,[75-79] drug delivery,[29,80-85] supramolecular tandem enzyme assays,[86-88] chromatography,[89,90] chiral recognition,[91-94] waste treatment,[49,95-99] sensors and switches,[100-105] ion channels,[106] biotechnology,[107-110] and supramolecular logic,[111,112] just to cite a few examples. This variety is only possible due to the extraordinary effects upon guest encapsulation, allowing a tuning of the guest properties.

When guest molecules are encapsulated in the CB*n* cavity, their physical and chemical properties are modified due to an altered microenvironment, as well as confinement and isolation from the surrounding medium.[113] Since the present work is projected for bio-relevant contexts, the next sections demonstrate host-induced guest alterations, highlighting assemblies with potential use in biological applications.

1.2.3.1 Solubilization and Deaggregation

CB*n* macrocycles are able to improve the solubility of poorly water-soluble or insoluble guest molecules, including metal complexes, drugs or fluorescent dyes.[42,114-118] For example, CB7 encapsulation improves the water solubility of a vast array of benzimidazole drugs, including lansoprazole, omeoprazole, albendazole, carbendazim, thiabendazole, and fuberidazole (structures presented in Scheme 1.4).[113,116,117] This phenomenon is often termed host-induced guest solubilization, also known for cyclodextrin macrocycles,[119] and opens a window to study poorly soluble or insoluble molecules in water. In some cases, such as for cationic guests, CB*n* complexes become more soluble than the uncomplexed CB*n* hosts due to higher guest solubility.[29,113,117,120] For example, the CB8 solubility increases to the millimolar range when complexed with some cationic anticancer drugs, whereas the intrinsic CB8 solubility is set at the micromolar scale.[120]

Enhanced solubility upon CB*n* encapsulation benefits guest molecule desorption from material surfaces. Indeed, CB7 and its complexes have low propensity to adsorb to glass and polymer materials.[114] For instance, CB7 suppresses adsorption of the commonly used dye rhodamine 6G on glass, plastic, and quartz surfaces, improving its use in a variety of biotechnological applications.[37] CB7 can also prevent aggregation of guests, often improving their photophysical properties in biological applications.[37,117,121-123]

Note that, in some cases, CB*n* host are able to assist and even promote dimer formation of guests inside their cavity,[124,125] causing an undesirable fluorescence quenching, but sometimes leading to other interesting properties like photocycloadditions.[33,83,126-130]

1.2.3.2 Stabilization

Upon encapsulation inside the CB*n* cavity, guest molecules can also take advantage of isolation or protection from the bulk solvent. For example, the complexation with CB*n* may improve the chemical stability of guests susceptible to oxidation or hydrolysis.[84,114] In this context the impressive stabilization of the active form of a benzimidazole class of proton pump inhibitors, which decompose 500 times slower when encapsulated in CB7 is cited here.[116] Furthermore, the physical barrier imposed by CB*n* macrocycles has been proven to be an enormous advantage against the reactivity of several guests with molecules in the medium. The best examples are reflected in the protection of drugs towards reactions with nucleophiles and electrophiles,[116,131-133] but also in the reduction or complete suppression of fluorescence quenching of dyes by external additives.[22,114]

Owing to the chemical inertness of their cavities, CB*n* efficiently suppress unimolecular guest photochemical reactivity and photodecomposition, thereby improving their photostability. CB*n* are excellent stabilizing additives because they do not act as quenchers themselves, unlike other macrocyclic hosts.[114] For instance, CB7 encapsulation improves the photostability of Hoechst 34580, a common nuclear stain.[134] The photostabilization was enhanced by a factor of *ca.* 6,

where after irradiation 40% of the dye molecules underwent photobleaching, in contrast with 7% in presence of CB7. Simultaneously, the encapsulation reduced binding of the dye toward DNA, demonstrating the potential of CB*n* in microscopy imaging, particularly in time-lapse microscopy. Although it has been mostly explored in the context of fluorescent dyes,[37,114,135-138] this supramolecular approach has been successfully used to photostabilize drugs,[113] often with more promising performances than cyclodextrins.

Another interesting feature of CB*n* is their ability to occasionally stabilize a specific isomer relative to another.[139-143] For example, *cis*-diaminostilbene dihydrochloride encapsulated in CB7 does not spontaneously isomerize to the *trans* isomer at room temperature, as a result of the strong host–guest interactions, including strong hydrogen bonds between the two protonated amino groups of the guest and the portal oxygen atoms of the host.[142] This modulation of the properties of isomerizable guest molecules can be very advantageous and allows exerting control of the equilibrium between isomers.

The stabilization provided by CB*n* combined with the favorable solubilization and deaggregation effects, is a valuable tool for improving storage capacity and working stability of guest, particularly dyes. Notably, stabilization of drug complexes has also been reported in the solid state. For instance, in its solid CB7 complex oxaliplatin was stable for more than one year, while the free drug already decomposed in much shorter period.[133] Additionally, CB7 may confer thermal stability to the guests in the solid state.[144,145]

1.2.3.3 Fluorescence Enhancement (Brightness, Quantum Yield, and Lifetime)

It is well known that the inclusion of a guest in microheterogeneous media, such as the CB*n* cavity, may cause significant changes in the photophysical properties.[102] As mentioned above, these changes occur because of the relocation of the guest molecule into a more hydrophobic environment with reduced polarizability and geometrical confinement (restriction of the rotational and vibration freedom). In consequence, for a wide variety of fluorescent dyes a suppression of nonradiative decay pathways and increase of fluorescence is observed.[114] It is possible to study

supramolecular complexes with a large bandwidth of spectroscopic techniques, such as nuclear magnetic resonance (NMR) spectroscopy, circular dichroism (CD), spectrophotometry, and spectrofluorometry.[146] Having in mind the pronounced changes upon encapsulation of fluorescent guests, fluorescence-based techniques are preferred because of their high sensitivity and specificity. Wagner and coworkers were the first to reported fluorescence enhancement phenomena upon complexation with CB*n*.[34,147,148] The authors observed 5 and 25 times enhanced quantum yield for 2-anilinonaphthalene-6-sulfonate with CB6 and CB7, respectively. Since then, many reports pursued these phenomena,[102,114] and verified that the positive effects are most commonly observed for cationic guests (Scheme 1.5), enabling a direct determination of the binding constants.[149,150] This broadened the applicability of chromophore/CB*n* in a variety of domains, such as biosensors, where the fluorescent dye may serve as probe to signal the binding of an analyte by an indicator displacement strategy (next section). [43,151]

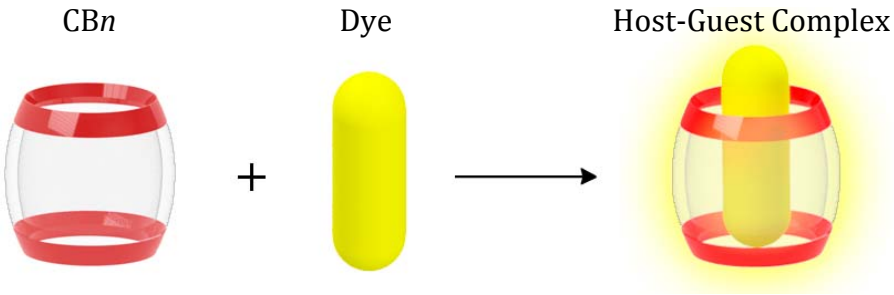

Scheme 1.5 – Fluorescence enhancement of dyes upon total or partial encapsulation in CB*n*.

The product of the molar absorption coefficient (ε) and fluorescence quantum yield (Φ_f) defines the brightness, and it is used to characterize the usefulness of a dye in fluorescence-based applications (sensing, bioimaging, luminescent materials, *etc.*). Generally, complexation with CB*n* increases brightness of fluorescent dyes, particularly for chromophores with very low fluorescence quantum yields in water and high quantum yields in nonpolar solvents. Complexation with CB*n* increases the brightness of several classes of dyes with

different chemical properties, including several acridines, xanthenes, quinine-imines, arylmethanes, coumarines, alkaloids, and many (hetero)aromatic molecules.[102,114] The formation of inclusion complexes with this type of dyes causes a remarkable fluorescence enhancement that can be very advantageous for fluorescence-based imaging.[152]

Longer fluorescence lifetimes of dyes upon supramolecular encapsulation are also a common characteristic, being a direct consequence of the low polarizability experienced by the dye upon assembly with a CB*n*. According to the Strickler-Berg equation,[153] there is a decrease of the radiative decay rate (the quotient of fluorescence quantum yield and fluorescence lifetime), leading to a "slower" emission of the complex fluorescence, resulting in an increased fluorescence lifetime (τ).[114] Such property could be a valuable asset in fluorescence lifetime imaging microscopy, where CB7 could serve as a useful additive and contrast agent, or even in time-resolved fluorescence assays to monitor, for example, enzymatic transformations.[22,154]

1.2.3.4 CB*n*-Assisted Guest Protonation

The complexation with macrocyclic hosts affects the protonation equilibria of guest molecules. Encapsulation in CB*n* is no exception and is being extensively used as a tool to alter the chemical reactivity of guests, for example with the objective to improve drug delivery systems,[113,131] prodrug activation strategies,[116] and biosensor technologies.[114,155]

Host-assisted guest protonation is accomplished by unspecific hydrophobic interactions of the organic water-soluble molecule encapsulated in the nonpolar cavity, resulting in distinct pK_a values. Moreover, specific electrostatic interactions between protonated groups or negatively charged moieties of the guest and the negative charge density of the host lead to pK_a shifts. With CB*n*, positive and negative pK_a shifts were already observed for a variety of encapsulated guest molecules.[114,145,156-158] Commonly, guests have a high propensity to become protonated upon complexation, which increases their pK_a values due to stabilization of the positive charge by the macrocycle. This protonation can usually

be spectroscopically followed by pH-dependent changes of the UV/vis absorption spectra or the fluorescence spectral fingerprints.

Commonly the guest pK_a shifts caused by most host systems are found to be between 2 and 3 units.[42,114,159,160] However, CB*n* are known to cause even larger shifts in the ground and excited states of guests.[81,113,116,159,161,162] For example, a pK_a shift of 4.5 units of a diamine-anchored carbazole-based dye has been reported upon complexation with CB6.[161] This shift value is close to what is observed for enzymes in their biological environment.[163] As expected, the host-induced pK_a shift upon guest encapsulation is directly reflected in the magnitude of the host-guest binding constant, due to the different protonation states of the guest. Accordingly, a four-state thermodynamic cycle can be projected to assign the relationship between the binding strength and the acidity constants of the guest in the free and complexed state (Scheme 1.6). Based on this model, the pK_a' value of the complexed guest can be easily calculated through the pK_a value of the free guest and the CB*n* binding constants of the unprotonated and protonated guest forms.

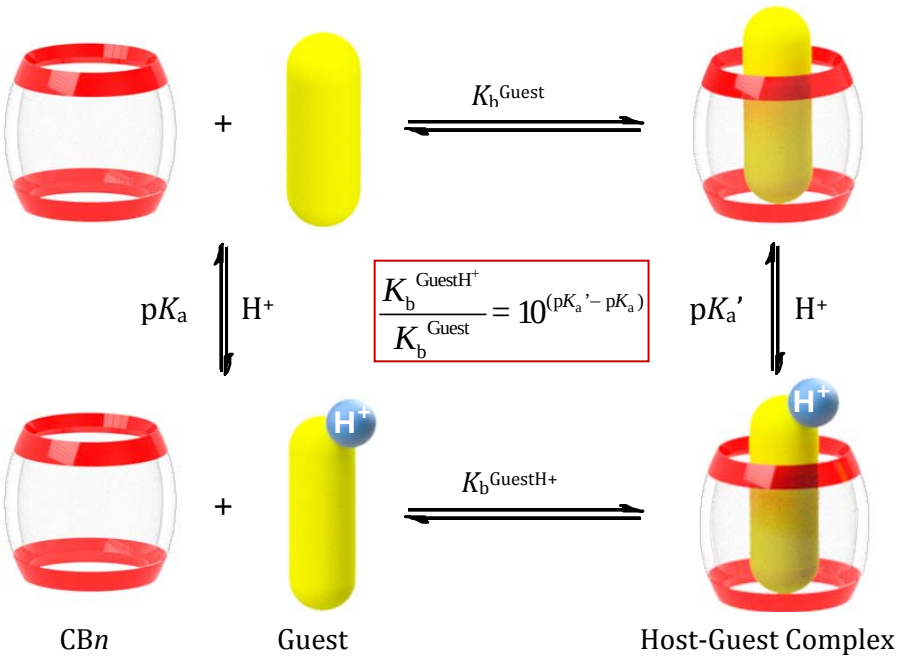

Scheme 1.6 – Thermodynamic cycle which determines supramolecular pK_a shifts through protonated and unprotonated guest binding affinity with CB*n*.

In the case of chromophoric guests, their host-assisted protonation can cause a remarkable change in their electronic properties and consequently their photophysical properties. This is being explored for many applications, such as indicator displacement assays and tandem assays (see next section), allowing the determination of enzyme activity and enantiomeric excess.[88,164,165] Furthermore, the protonation of fluorescent guests can considerably influence their photoinduced electron transfer pathways, excited state properties, and intermolecular charge transfer states. A nice example was reported for the Dapoxyl dye,[114] whose locally excited state emission band can only be seen below pH 4.2, but upon encapsulation in CB7 its visible until pH 6.0.

1.2.3.5 Modulation of Guest Recognition

The ability of CB*n* macrocycles to bind reversibly to molecules allows a controlled modulation of host-guest complexes. Guest uptake or release can be achieved by single or combined pH changes, CB*n* binding competitors, and/or irradiation as an external *stimuli* (Scheme 1.7). Indeed, many biological applications of CB*n* were developed around this approach and a few selected ones are highlighted below.

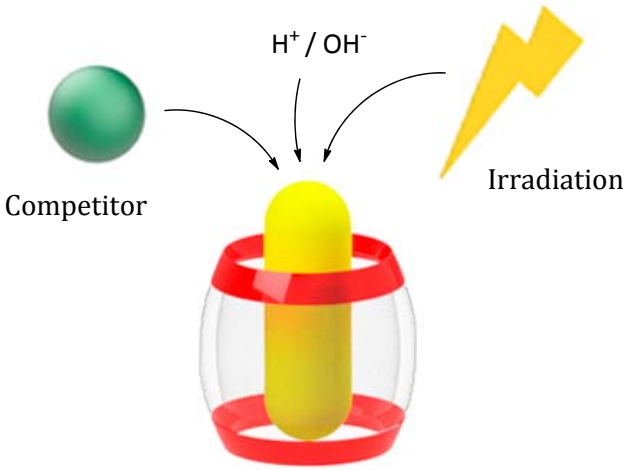

Scheme 1.7 – Representation of the *stimuli* that can modulate CB*n*-guest complexation, including pH changes, competitors, and irradiation.

Nowadays, CB*n* are being survey as drug delivery systems. To date, two different strategies have been explored to stimulate the release of a variety of drugs from the CB*n* cavity. Primarily, cations are known to bind to the carbonyl rims of the macrocycles.[27,55] Being so, they can act as competitors and consequently displace the encapsulated drug. The degree of the displacement depends on the concentration of the cation. This concept was used to release the Neutral Red dye (used as a drug model) from the CB7 cavity and relocate it into the hydrophobic cavity of BSA protein, solely by the presence of salts.[166] The second mechanism relies on the fact that unprotonated drugs have lower binding affinities to CB*n* than their protonated forms. If the pH value is such that it causes a diminished binding affinity between the macrocycle and the drug, an effective drug release can be achieved, triggered by a pH change or gradient attainable in the human body. One example of this approach was obtained by a photo-controlled drug release of the Hoechst 33258 drug from CB7,[167] achievable by a phototriggered pH jump. This will be discussed in detail in Chapter 2.

An important application of CB*n* is their use in conjugation with sensors and molecular switches (see Chapter 3). Several examples of fluorescence-based systems have already been described, where changing the pK_a values by adding CB*n* host to the guest, modulates the dye's fluorescence intensity, which is reversed upon decomplexation. Again, the simplest way to achieve such result is by adding a competitor, which can be indirectly detected by the fluorescence of the dye.[168] Various host-dye systems ("reporter pairs") for analyte sensing have been reported,[102] with two possible responses, fluorescence decrease (switch-OFF) or increase (switch-ON) upon analyte binding. One example is a switch-OFF detection of insulin by the CB7-acridine orange reporter pair.[169] Another case study was developed around the CB7-Dapoxyl pair, enabling the construction of a multiparameter sensing array for different amino acids.[52] This type of sensor arrays has been used to detect not only amino acids, but also structurally similar amines, biological metabolites, as well as quaternary ammonium salts, and even to discriminate between them.[104,170-172]

The Nau group developed a different approach for the measurement of enzymatic activity: supramolecular tandem enzyme assays.[164] The assay's principle relies on

the self-assembly of a CB*n*-dye reporter pair and the differential binding of substrates and products to the macrocycle. With such assays, the enzymatic activity can be followed label-free and in real time by observing the corresponding fluorescence modulation of the dye.[88,173]

Chemical transformations inside the CB*n* macrocycle, often in form of photoreactions, are very interesting examples of supramolecular catalysis and the use of templating effects.[33] Several examples of photodimerizations, photofragmentation, and photolysis reactions catalyzed or template by CB*n* have been reported.[127,174-180] Photocycloadditions are often promoted inside CB*n* cavities and in Chapter 5 this phenomenon is demonstrated for harnessing molecular information processing.

In conclusion, CB*n* chemistry is proven to be a highly useful tool to study and control biological processes, with extraordinary effects upon guest encapsulation. In the following chapters, I will demonstrate a series of bio-inspired applications by taking advantage of CB*n*-guest complexes, where each topic is introduced with additional specific bibliographic information.

References

(1) Menger, F. M. *Proc. Natl. Acad. Sci.* **2002**, *99*, 4818.

(2) Dodziuk, H. *Introduction to Supramolecular Chemistry*; Kluwer Academic Publishers, 2002.

(3) Werner, A. *Z. Anorg. Chem.* **1893**, *3*, 267.

(4) Fischer, E. *Ber. Dtsch. Chem. Ges.* **1894**, *27*, 2985.

(5) Ehrlich, P. *Studies on Immunity*; Wiley: New York, 1906.

(6) Wolf, K. L.; Frahm, H.; Harms, H. Z. *Phys. Chem. (B)* **1937**, *36*, 237.

(7) Pedersen, C. J. *J. Am. Chem. Soc.* **1967**, *89*, 7017.

(8) Cram, D. J.; Cram, J. M. *Science* **1974**, *183*, 803.

(9) Kyba, E. P.; Helgeson, R. C.; Madan, K.; Gokel, G. W.; Tarnowski, T. L.; Moore, S. S.; Cram, D. J. *J. Am. Chem. Soc.* **1977**, *99*, 2564.

(10) Cram, D. J. *Angew. Chem. Int. Ed.* **1988**, *27*, 1009.

(11) Lehn, J.-M. *Angew. Chem. Int. Ed.* **1988**, *27*, 89.

(12) Pedersen, C. J. *Angew. Chem. Int. Ed.* **1988**, *27*, 1021.

(13) Lehn, J. M.; Sauvage, J. P. *J. Am. Chem. Soc.* **1975**, *97*, 6700.

(14) Moran, J. R.; Karbach, S.; Cram, D. J. *J. Am. Chem. Soc.* **1982**, *104*, 5826.

(15) Szejtli, J. *Cyclodextrin Technology*; Springer: New York, 1988; Vol. 1.

(16) Gutsche, C. D. *Calixarenes*; Royal Society of Chemistry: Cambridge, 1989.

(17) Freeman, W. A.; Mock, W. L.; Shih, N. Y. *J. Am. Chem. Soc.* **1981**, *103*, 7367.

(18) Uhlenheuer, D. A.; Petkau, K.; Brunsveld, L. *Chem. Soc. Rev.* **2010**, *39*, 2817.

(19) Behrend, R.; Meyer, E.; Rusche, F. *Justus Liebigs Ann. Chem.* **1905**, *339*, 1.

(20) Kim, J.; Jung, I.-S.; Kim, S.-Y.; Lee, E.; Kang, J.-K.; Sakamoto, S.; Yamaguchi, K.; Kim, K. *J. Am. Chem. Soc.* **2000**, *122*, 540.

(21) Day, A.; Arnold, A. P.; Blanch, R. J.; Snushall, B. *J. Org. Chem.* **2001**, *66*, 8094.

(22) Marquez, C.; Fang, H.; Nau, W. M. *IEEE Trans. NanoBiosci.* **2004**, *3*, 39.

(23) Hwang, I.; Jeon, W. S.; Kim, H.-J.; Kim, D.; Kim, H.; Selvapalam, N.; Fujita, N.; Shinkai, S.; Kim, K. *Angew. Chem. Int. Ed.* **2007**, *46*, 210.

(24) Buschmann, H. J.; Cleve, E.; Schollmeyer, E. *Inorg. Chim. Acta* **1992**, *193*, 93.

(25) Márquez, C.; Hudgins, R. R.; Nau, W. M. *J. Am. Chem. Soc.* **2004**, *126*, 5806.

(26) Lee, J. W.; Samal, S.; Selvapalam, N.; Kim, H.-J.; Kim, K. *Acc. Chem. Res.* **2003**, *36*, 621.

(27) Lagona, J.; Mukhopadhyay, P.; Chakrabarti, S.; Isaacs, L. *Angew. Chem. Int. Ed.* **2005**, *44*, 4844.

(28) Liu, S.; Zavalij, P. Y.; Isaacs, L. *J. Am. Chem. Soc.* **2005**, *127*, 16798.

(29) Walker, S.; Oun, R.; McInnes, F. J.; Wheate, N. J. *Isr. J. Chem.* **2011**, *51*, 616.

(30) Day, A. I.; Blanch, R. J.; Arnold, A. P.; Lorenzo, S.; Lewis, G. R.; Dance, I. *Angew. Chem. Int. Ed.* **2002**, *41*, 275.

(31) Marquez, C.; Nau, W. M. *Angew. Chem. Int. Ed.* **2001**, *40*, 4387.

(32) Cheng, X.-J.; Liang, L.-L.; Chen, K.; Ji, N.-N.; Xiao, X.; Zhang, J.-X.; Zhang, Y.-Q.; Xue, S.-F.; Zhu, Q.-J.; Ni, X.-L.; Tao, Z. *Angew. Chem. Int. Ed.* **2013**, *52*, 7252.

(33) Assaf, K. I.; Nau, W. M. *Chem. Soc. Rev.* **2015**, *44*, 394.

(34) Rankin, M. A.; Wagner, B. D. *Supramol. Chem.* **2004**, *16*, 513.

(35) Megyesi, M.; Biczók, L.; Jablonkai, I. *J. Phys. Chem. C* **2008**, *112*, 3410.

(36) Assaf, K. I.; Nau, W. M. *Supramol. Chem.* **2014**, *26*, 657.

(37) Mohanty, J.; Nau, W. M. *Angew. Chem. Int. Ed.* **2005**, *44*, 3750.

(38) Marquez, C.; Nau, W. M. *Angew. Chem. Int. Ed.* **2001**, *40*, 3155.

(39) Liu, J.-X.; Long, L.-S.; Huang, R.-B.; Zheng, L.-S. *Inorg. Chem.* **2007**, *46*, 10168.

(40) Cao, L.; Šekutor, M.; Zavalij, P. Y.; Mlinarić-Majerski, K.; Glaser, R.; Isaacs, L. *Angew. Chem. Int. Ed.* **2014**, *53*, 988.

(41) Biedermann, F.; Uzunova, V. D.; Scherman, O. A.; Nau, W. M.; De Simone, A. *J. Am. Chem. Soc.* **2012**, *134*, 15318.

(42) Ghosh, I.; Nau, W. M. *Adv. Drug Del. Rev.* **2012**, *64*, 764.

(43) Bakirci, H.; Nau, W. M. *Adv. Funct. Mater.* **2006**, *16*, 237.

(44) Nau, W. M.; Florea, M.; Assaf, K. I. *Isr. J. Chem.* **2011**, *51*, 559.

(45) Mecozzi, S.; Rebek, J. J. *Chem. Eur. J.* **1998**, *4*, 1016.

(46) Szejtli, J. *Chem. Rev.* **1998**, *98*, 1743.

(47) Choudhury, S. D.; Mohanty, J.; Upadhyaya, H. P.; Bhasikuttan, A. C.; Pal, H. *J. Phys. Chem. B* **2009**, *113*, 1891.

(48) Rekharsky, M. V.; Mori, T.; Yang, C.; Ko, Y. H.; Selvapalam, N.; Kim, H.; Sobransingh, D.; Kaifer, A. E.; Liu, S.; Isaacs, L.; Chen, W.; Moghaddam, S.; Gilson, M. K.; Kim, K.; Inoue, Y. *Proc. Natl. Acad. Sci.* **2007**, *104*, 20737.

(49) Rekharsky, M. V.; Ko, Y. H.; Selvapalam, N.; Kim, K.; Inoue, Y. *Supramol. Chem.* **2007**, *19*, 39.

(50) Kim, H.-J.; Jeon, W. S.; Ko, Y. H.; Kim, K. *Proc. Natl. Acad. Sci.* **2002**, *99*, 5007.

(51) Buschmann, H. J.; Jansen, K.; Meschke, C.; Schollmeyer, E. *J. Solution Chem.* **1998**, *27*, 135.

(52) Bailey, D. M.; Hennig, A.; Uzunova, V. D.; Nau, W. M. *Chem. Eur. J.* **2008**, *14*, 6069.

(53) Biedermann, F.; Vendruscolo, M.; Scherman, O. A.; De Simone, A.; Nau, W. M. *J. Am. Chem. Soc.* **2013**, *135*, 14879.

(54) Biedermann, F.; Nau, W. M.; Schneider, H.-J. *Angew. Chem. Int. Ed.* **2014**, *53*, 11158.

(55) Masson, E.; Ling, X.; Joseph, R.; Kyeremeh-Mensah, L.; Lu, X. *RSC Adv.* **2012**, *2*, 1213.

(56) Davis, M. E.; Brewster, M. E. *Nat. Rev. Drug Discov.* **2004**, *3*, 1023.

(57) Uzunova, V. D.; Cullinane, C.; Brix, K.; Nau, W. M.; Day, A. I. *Org. Biomol. Chem.* **2010**, *8*, 2037.

(58) Hettiarachchi, G.; Nguyen, D.; Wu, J.; Lucas, D.; Ma, D.; Isaacs, L.; Briken, V. *PLoS One* **2010**, *5*, e10514.

(59) Montes-Navajas, P.; Gonzalez-Bejar, M.; Scaiano, J. C.; Garcia, H. *Photochem. Photobiol. Sci.* **2009**, *8*, 1743.

(60) McNoleg, O. *Comput Geosci* **1996**, *22*, 585.

(61) Oun, R.; Floriano, R. S.; Isaacs, L.; Rowan, E. G.; Wheate, N. J. *Toxicol. Res.* **2014**, *3*, 447.

(62) Ma, W.-J.; Chen, J.-M.; Jiang, L.; Yao, J.; Lu, T.-B. *Mol. Pharm.* **2013**, *10*, 4698.

(63) Cao, L.; Hettiarachchi, G.; Briken, V.; Isaacs, L. *Angew. Chem. Int. Ed.* **2013**, *52*, 12033.

(64) Day, A. I.; G., C. J. In *Supramolecular Chemistry: From Molecules to Nanomaterials*; Gale, P. A., Steed, J. W., Eds.; Wiley: 2012; Vol. 3, p 983.

(65) Walker, S.; Kaur, R.; McInnes, F. J.; Wheate, N. J. *Mol. Pharm.* **2010**, *7*, 2166.

(66) Seif, M.; Impelido, M. L.; Apps, M. G.; Wheate, N. J. *PLoS One* **2014**, *9*, e85361.

(67) Vallavoju, N.; Sivaguru, J. *Chem. Soc. Rev.* **2014**, *43*, 4084.

(68) del Barrio, J.; Horton, P. N.; Lairez, D.; Lloyd, G. O.; Toprakcioglu, C.; Scherman, O. A. *J. Am. Chem. Soc.* **2013**, *135*, 11760.

(69) Liu, Y.; Huang, Z.; Tan, X.; Wang, Z.; Zhang, X. *Chem. Commun.* **2013**, *49*, 5766.

(70) Ma, X.; Tian, H. *Acc. Chem. Res.* **2014**, *47*, 1971.

(71) Ling, Y.; Kaifer, A. E. *Chem. Mater.* **2006**, *18*, 5944.

(72) Eelkema, R.; Maeda, K.; Odell, B.; Anderson, H. L. *J. Am. Chem. Soc.* **2007**, *129*, 12384.

(73) Gurbuz, S.; Idris, M.; Tuncel, D. *Org. Biomol. Chem.* **2015**, *13*, 330.

(74) Lan, Y.; Wu, Y.; Karas, A.; Scherman, O. A. *Angew. Chem. Int. Ed.* **2014**, *53*, 2166.

(75) Smith, L. C.; Leach, D. G.; Blaylock, B. E.; Ali, O. A.; Urbach, A. R. *J. Am. Chem. Soc.* **2015**, *137*, 3663.

(76) Ramaekers, M.; Wijnands, S. P. W.; van Dongen, J. L. J.; Brunsveld, L.; Dankers, P. Y. W. *Chem. Commun.* **2015**, *51*, 3147.

(77) Lee, D.-W.; Park, K. M.; Gong, B.; Shetty, D.; Khedkar, J. K.; Baek, K.; Kim, J.; Ryu, S. H.; Kim, K. *Chem. Commun.* **2015**, *51*, 3098.

(78) Ko, Y. H.; Hwang, I.; Lee, D.-W.; Kim, K. *Isr. J. Chem.* **2011**, *51*, 506.

(79) Urbach, A. R.; Ramalingam, V. *Isr. J. Chem.* **2011**, *51*, 664.

(80) Berdnikova, D. V.; Aliyeu, T. M.; Paululat, T.; Fedorov, Y. V.; Fedorova, O. A.; Ihmels, H. *Chem. Commun.* **2015**, *51*, 4906.

(81) Macartney, D. H. *Isr. J. Chem.* **2011**, *51*, 600.

(82) Wang, L.; Li, L.-l.; Fan, Y.-s.; Wang, H. *Adv. Mater.* **2013**, *25*, 3888.

(83) Bush, M. E.; Bouley, N. D.; Urbach, A. R. *J. Am. Chem. Soc.* **2005**, *127*, 14511.

(84) Wang, R.; Macartney, D. H. *Org. Biomol. Chem.* **2008**, *6*, 1955.

(85) Kemp, S.; Wheate, N.; Wang, S.; Collins, J. G.; Ralph, S.; Day, A.; Higgins, V.; Aldrich-Wright, J. *J Biol Inorg Chem* **2007**, *12*, 969.

(86) Ghale, G.; Nau, W. M. *Acc. Chem. Res.* **2014**, *47*, 2150.

(87) Florea, M.; Nau, W. M. *Org. Biomol. Chem.* **2010**, *8*, 1033.

(88) Hennig, A.; Bakirci, H.; Nau, W. M. *Nat Meth* **2007**, *4*, 629.

(89) Ma, L.; Liu, S.-M.; Yao, L.; Xu, L. *J. Chromatogr. A* **2015**, *1376*, 64.

(90) Li, L.-S.; Wang, S.-W.; Chen, X.-Q.; Liu, C.; Xu, L.-L. *Chin. J. Chem .* **2008**, *26*, 307.

(91) Huang, W.-H.; Zavalij, P. Y.; Isaacs, L. *Angew. Chem.* **2007**, *119*, 7569.

(92) Biedermann, F.; Nau, W. M. *Angew. Chem. Int. Ed.* **2014**, *53*, 5694.

(93) Mandadapu, V.; Day, A. I.; Ghanem, A. *Chirality* **2014**, *26*, 712.

(94) Rekharsky, M. V.; Yamamura, H.; Inoue, C.; Kawai, M.; Osaka, I.; Arakawa, R.; Shiba, K.; Sato, A.; Ko, Y. H.; Selvapalam, N.; Kim, K.; Inoue, Y. *J. Am. Chem. Soc.* **2006**, *128*, 14871.

(95) Nagy, H. J.; Sallay, P.; Varga, M. L.; Rusznák, I.; Bakó, P.; Víg, A. *Text Res J* **2009**, *79*, 1312.

(96) Karcher, S.; Kornmüller, A.; Jekel, M. *Water Res.* **2001**, *35*, 3309.

(97) Kornmüller, A.; Karcher, S.; Jekel, M. *Water Res.* **2001**, *35*, 3317.

(98) Dantz, D. A.; Meschke, C.; Buschmann, H.-J.; Schollmeyer, E. *Supramol. Chem.* **1998**, *9*, 79.

(99) Karcher, S.; Kornmüller, A.; Jekel, M. *Water Sci. Technol.* **1999**, *40*, 425.

(100) Minami, T.; Esipenko, N. A.; Zhang, B.; Isaacs, L.; Anzenbacher, P. *Chem. Commun.* **2014**, *50*, 61.

(101) Liu, K.; Yao, Y.; Kang, Y.; Liu, Y.; Han, Y.; Wang, Y.; Li, Z.; Zhang, X. *Sci. Rep.* **2013**, *3*, 2372.

(102) Dsouza, R. N.; Pischel, U.; Nau, W. M. *Chem. Rev.* **2011**, *111*, 7941.

(103) Vázquez , J.; Remón , P.; Dsouza, R. N.; Lazar, A. I.; Arteaga, J. F.; Nau, W. M.; Pischel, U. *Chem. Eur. J.* **2014**, *20*, 9897.

(104) Montes-Navajas, P.; Baumes, L. A.; Corma, A.; Garcia, H. *Tetrahedron Lett.* **2009**, *50*, 2301.

(105) Mock, W. L.; Pierpont, J. *J. Chem. Soc., Chem. Commun.* **1990**, 1509.

(106) Jeon, Y. J.; Kim, H.; Jon, S.; Selvapalam, N.; Oh, D. H.; Seo, I.; Park, C.-S.; Jung, S. R.; Koh, D.-S.; Kim, K. *J. Am. Chem. Soc.* **2004**, *126*, 15944.

(107) Isobe, H.; Tomita, N.; Lee, J. W.; Kim, H.-J.; Kim, K.; Nakamura, E. *Angew. Chem. Int. Ed.* **2000**, *39*, 4257.

(108) Isobe, H.; Sato, S.; Lee, J. W.; Kim, H.-J.; Kim, K.; Nakamura, E. *Chem. Commun.* **2005**, 1549.

(109) Heitmann, L. M.; Taylor, A. B.; Hart, P. J.; Urbach, A. R. *J. Am. Chem. Soc.* **2006**, *128*, 12574.

(110) Hwang, I.; Baek, K.; Jung, M.; Kim, Y.; Park, K. M.; Lee, D.-W.; Selvapalam, N.; Kim, K. *J. Am. Chem. Soc.* **2007**, *129*, 4170.

(111) Pischel, U.; Uzunova, V. D.; Remon, P.; Nau, W. M. *Chem. Commun.* **2010**, *46*, 2635.

(112) Gao, C.; Silvi, S.; Ma, X.; Tian, H.; Venturi, M.; Credi, A. *Chem. Commun.* **2012**, *48*, 7577.

(113) Koner, A. L.; Ghosh, I.; Saleh, N. i.; Nau, W. M. *Can. J. Chem.* **2011**, *89*, 139.

(114) Koner, A. L.; Nau, W. M. *Supramol. Chem.* **2007**, *19*, 55.

(115) Buck, D. P.; Abeysinghe, P. M.; Cullinane, C.; Day, A. I.; Collins, J. G.; Harding, M. M. *Dalton Trans.* **2008**, 2328.

(116) Saleh, N. i.; Koner, A. L.; Nau, W. M. *Angew. Chem. Int. Ed.* **2008**, *47*, 5398.

(117) Zhao, Y.; Buck, D. P.; Morris, D. L.; Pourgholami, M. H.; Day, A. I.; Collins, J. G. *Org. Biomol. Chem.* **2008**, *6*, 4509.

(118) Ma, D.; Hettiarachchi, G.; Nguyen, D.; Zhang, B.; Wittenberg, J. B.; Zavalij, P. Y.; Briken, V.; Isaacs, L. *Nat. Chem.* **2012**, *4*, 503.

(119) Brewster, M. E.; Loftsson, T. *Adv. Drug Del. Rev.* **2007**, *59*, 645.

(120) Wheate, N. J.; Buck, D. P.; Day, A. I.; Collins, J. G. *Dalton Trans.* **2006**, 451.

(121) Biedermann, F.; Elmalem, E.; Ghosh, I.; Nau, W. M.; Scherman, O. A. *Angew. Chem. Int. Ed.* **2012**, *51*, 7739.

(122) Pais, V. F.; Carvalho, E. F. A.; Tomé, J. P. C.; Pischel, U. *Supramol. Chem.* **2014**, *26*, 642.

(123) Gadde, S.; Batchelor, E. K.; Weiss, J. P.; Ling, Y.; Kaifer, A. E. *J. Am. Chem. Soc.* **2008**, *130*, 17114.

(124) Montes-Navajas, P.; Corma, A.; Garcia, H. *ChemPhysChem* **2008**, *9*, 713.

(125) Mohanty, J.; Dutta Choudhury, S.; Upadhyaya, H. P.; Bhasikuttan, A. C.; Pal, H. *Chem. Eur. J.* **2009**, *15*, 5215.

(126) Wang, R.; Yuan, L.; Macartney, D. H. *J. Org. Chem.* **2006**, *71*, 1237.

(127) Jon, S. Y.; Ko, Y. H.; Park, S. H.; Kim, H.-J.; Kim, K. *Chem. Commun.* **2001**, 1938.

(128) Pattabiraman, M.; Natarajan, A.; Kaanumalle, L. S.; Ramamurthy, V. *Org. Lett.* **2005**, *7*, 529.

(129) Sindelar, V.; Cejas, M. A.; Raymo, F. M.; Chen, W.; Parker, S. E.; Kaifer, A. E. *Chem. Eur. J.* **2005**, *11*, 7054.

(130) Carvalho, C. P.; Dominguez, Z.; Da Silva, J. P.; Pischel, U. *Chem. Commun.* **2015**, *51*, 2698.

(131) Cong, H.; Li, C.-R.; Xue, S.-F.; Tao, Z.; Zhu, Q.-J.; Wei, G. *Org. Biomol. Chem.* **2011**, *9*, 1041.

(132) Wheate, N. J.; Day, A. I.; Blanch, R. J.; Arnold, A. P.; Cullinane, C.; Grant Collins, J. *Chem. Commun.* **2004**, 1424.

(133) Jin Jeon, Y.; Kim, S.-Y.; Ho Ko, Y.; Sakamoto, S.; Yamaguchi, K.; Kim, K. *Org. Biomol. Chem.* **2005**, *3*, 2122.

(134) Lei , W.; Zhou, Q.; Jiang , G.; Hou, Y.; Zhang, B.; Cheng, X.; Wang, X. *ChemPhysChem* **2011**, *12*, 2933.

(135) Nau, W. M.; Mohanty, J. *Int. J. Photoenergy* **2005**, *7*.

(136) Mohanty, J.; Pal, H.; Ray, A. K.; Kumar, S.; Nau, W. M. *ChemPhysChem* **2007**, *8*, 54.

(137) Mohanty, J.; Jagtap, K.; Ray, A. K.; Nau, W. M.; Pal, H. *ChemPhysChem* **2010**, *11*, 3333.

(138) Arunkumar, E.; Forbes, C. C.; Smith, B. D. *Eur. J. Org. Chem.* **2005**, *2005*, 4051.

(139) Wang, R.; Yuan, L.; Macartney, D. H. *Organometallics* **2006**, *25*, 1820.

(140) Gill, G. S.; Grobelny, D. W.; Chaplin, J. H.; Flynn, B. L. *J. Org. Chem.* **2008**, *73*, 1131.

(141) Wang, R.; Macartney, D. H. *Tetrahedron Lett.* **2008**, *49*, 311.

(142) Choi, S.; Park, S. H.; Ziganshina, A. Y.; Ko, Y. H.; Lee, J. W.; Kim, K. *Chem. Commun.* **2003**, 2176.

(143) Nilsson, J. R.; Parente Carvalho, C.; Li, S.; Da Silva, J. P.; Andréasson, J.; Pischel, U. *ChemPhysChem* **2012**, *13*, 3691.

(144) McInnes, F. J.; Anthony, N. G.; Kennedy, A. R.; Wheate, N. J. *Org. Biomol. Chem.* **2010**, *8*, 765.

(145) Wheate, N.; Vora, V.; Anthony, N.; McInnes, F. *J. Incl. Phenom. Macrocycl. Chem.* **2010**, *68*, 359.

(146) Schalley, C. A. *Analytical Methods in Supramolecular Chemistry*; Wiley-VCH: Weinheim, 2007.

(147) Wagner, B. D.; Fitzpatrick, S. J.; Gill, M. A.; MacRae, A. I.; Stojanovic, N. *Can. J. Chem.* **2001**, *79*, 1101.

(148) Wagner, B. D.; Stojanovic, N.; Day, A. I.; Blanch, R. J. *J. Phys. Chem. B* **2003**, *107*, 10741.

(149) Sindelar, V.; Cejas, M. A.; Raymo, F. M.; Kaifer, A. E. *New J. Chem.* **2005**, *29*, 280.

(150) Liu, S.; Ruspic, C.; Mukhopadhyay, P.; Chakrabarti, S.; Zavalij, P. Y.; Isaacs, L. *J. Am. Chem. Soc.* **2005**, *127*, 15959.

(151) Wiskur, S. L.; Ait-Haddou, H.; Lavigne, J. J.; Anslyn, E. V. *Acc. Chem. Res.* **2001**, *34*, 963.

(152) Martyn, T. A.; Moore, J. L.; Halterman, R. L.; Yip, W. T. *J. Am. Chem. Soc.* **2007**, *129*, 10338.

(153) Strickler, S. J.; Berg, R. A. *J. Chem. Phys.* **1962**, *37*, 814.

(154) Hennig, A.; Roth, D.; Enderle, T.; Nau, W. M. *ChemBioChem* **2006**, *7*, 733.

(155) Saleh, N. i.; Al-Soud, Y. A.; Al-Kaabi, L.; Ghosh, I.; Nau, W. M. *Tetrahedron Lett.* **2011**, *52*, 5249.

(156) Wyman, I. W.; Macartney, D. H. *Org. Biomol. Chem.* **2010**, *8*, 247.

(157) Wyman, I. W.; Macartney, D. H. *Org. Biomol. Chem.* **2010**, *8*, 253.

(158) Bhasikuttan, A. C.; Pal, H.; Mohanty, J. *Chem. Commun.* **2011**, *47*, 9959.

(159) Wang, R.; Yuan, L.; Macartney, D. H. *Chem. Commun.* **2005**, 5867.

(160) Shaikh, M.; Mohanty, J.; Singh, P. K.; Nau, W. M.; Pal, H. *Photochem. Photobiol. Sci.* **2008**, *7*, 408.

(161) Praetorius, A.; Bailey, D. M.; Schwarzlose, T.; Nau, W. M. *Org. Lett.* **2008**, *10*, 4089.

(162) Shaikh, M.; Dutta Choudhury, S.; Mohanty, J.; Bhasikuttan, A. C.; Nau, W. M.; Pal, H. *Chem. Eur. J.* **2009**, *15*, 12362.

(163) Bakirci, H.; Koner, A. L.; Schwarzlose, T.; Nau, W. M. *Chem. Eur. J.* **2006**, *12*, 4799.

(164) Dsouza, R. N.; Hennig, A.; Nau, W. M. *Chem. Eur. J.* **2012**, *18*, 3444.

(165) Wu, J.; Isaacs, L. *Chem. Eur. J.* **2009**, *15*, 11675.

(166) Shaikh, M.; Mohanty, J.; Bhasikuttan, A. C.; Uzunova, V. D.; Nau, W. M.; Pal, H. *Chem. Commun.* **2008**, 3681.

(167) Carvalho, C. P.; Uzunova, V. D.; Da Silva, J. P.; Nau, W. M.; Pischel, U. *Chem. Commun.* **2011**, *47*, 8793.

(168) Inouye, M.; Hashimoto, K.-i.; Isagawa, K. *J. Am. Chem. Soc.* **1994**, *116*, 5517.

(169) Chinai, J. M.; Taylor, A. B.; Ryno, L. M.; Hargreaves, N. D.; Morris, C. A.; Hart, P. J.; Urbach, A. R. *J. Am. Chem. Soc.* **2011**, *133*, 8810.

(170) Baumes, L. A.; Buaki Sogo, M.; Montes-Navajas, P.; Corma, A.; Garcia, H. *Chem. Eur. J.* **2010**, *16*, 4489.

(171) Baumes, L. A.; Buaki, M.; Jolly, J.; Corma, A.; Garcia, H. *Tetrahedron Lett.* **2011**, *52*, 1418.

(172) Baumes, L. A.; Sogo, M. B.; Montes-Navajas, P.; Corma, A.; Garcia, H. *Tetrahedron Lett.* **2009**, *50*, 7001.

(173) Nau, W. M.; Ghale, G.; Hennig, A.; Bakirci, H.; Bailey, D. M. *J. Am. Chem. Soc.* **2009**, *131*, 11558.

(174) Maddipatla, M. V. S. N.; Kaanumalle, L. S.; Natarajan, A.; Pattabiraman, M.; Ramamurthy, V. *Langmuir* **2007**, *23*, 7545.

(175) Koner, A. L.; Márquez, C.; Dickman, M. H.; Nau, W. M. *Angew. Chem. Int. Ed.* **2011**, *50*, 545.

(176) Smitka, J.; Lemos, A.; Porel, M.; Jockusch, S.; Belderrain, T. R.; Tesarova, E.; Da Silva, J. P. *Photochem. Photobiol. Sci.* **2014**, *13*, 310.

(177) Wu, X.-L.; Luo, L.; Lei; Liao, G.-H.; Wu, L.-Z.; Tung, C.-H. *J. Org. Chem.* **2008**, *73*, 491.

(178) Pemberton, B. C.; Singh, R. K.; Johnson, A. C.; Jockusch, S.; Da Silva, J. P.; Ugrinov, A.; Turro, N. J.; Srivastava, D. K.; Sivaguru, J. *Chem. Commun.* **2011**, *47*, 6323.

(179) Yang, C.; Mori, T.; Origane, Y.; Ko, Y. H.; Selvapalam, N.; Kim, K.; Inoue, Y. *J. Am. Chem. Soc.* **2008**, *130*, 8574.

(180) Biedermann, F.; Ross, I.; Scherman, O. A. *Polym. Chem.* **2014**, *5*, 5375.

Chapter 2

A Supramolecular Photoaddressable Model System for Drug Delivery

In this chapter, the phototriggered release of the Hoechst 33258 dye from a CB7 macrocycle upon a photo-induced pH jump is demonstrated. Although there are several examples of photo-triggered systems with macrocycles,[1-5] the novelty of this work is the use of light-induced pH changes to assemble or disassemble a CB*n*-drug complex.

Part of the supramolecular characterization was included in a previous Master thesis developed by the author.[6] In order to contextualize this doctoral thesis' new results and with the idea to provide a better understanding, a more detailed account of previous results is included in this chapter as well. Wherever indicated this is referenced accordingly.

2.1 Hoechst 33258

Hoechst 33258 (**H33258**; 2'-(4-hydroxyphenyl)-5-(4-methyl-1-piperazinyl)-2,5'-bi-1*H*-benzimidazole) is a commercially available heterocyclic dye containing two benzimidazole rings (bz) along with a phenol and a piperazine moiety as terminal units (Figure 2.1). This dye can have more than one conformation in solution due to various rotation sites.[7,8]

Since the early 1970s, **H33258** has been commonly used as a fluorescent probe, particularly for DNA staining. This application is possible because the dye is water-soluble, relatively non-toxic, exhibits membrane permeability, and becomes highly fluorescent upon a specific and strong binding to the minor groove of double-

stranded DNA.[9-13] It is also employed in DNA-intercalator displacement assays and in multi-color-labeling experiments, due to its relatively large Stokes shift.[14,15]

However, beside its application as staining agent **H33258** has also found entrance in several other important biochemical applications such as an anthelmintic drug for the treatment of infections by parasitic worms and protozoa.[16-18] It can also be used as a radioprotector and even shows anticancer activity.[19-23] Finally, the dye is known to inhibit the activity of helicase and topoisomerases and possibly interferes with other proteins involved in RNA transcription and protein translation.[24]

This interesting bio-relevant background of the dye and its variable photophysical properties, depending on the involved multiple potonation equilibria, motivated its selection for the herein performed study. The protonation states and corresponding pK_a values described for the dye are approximately 3.5 for the protonation of the bz2 ring, 5.5 for the analogous process involving the bz1 ring, 8.5 for the hydroxyl group of the phenol, and 9.8 for the lateral nitrogen atom of the piperazine ring (Figure 2.1).[7,25-27]

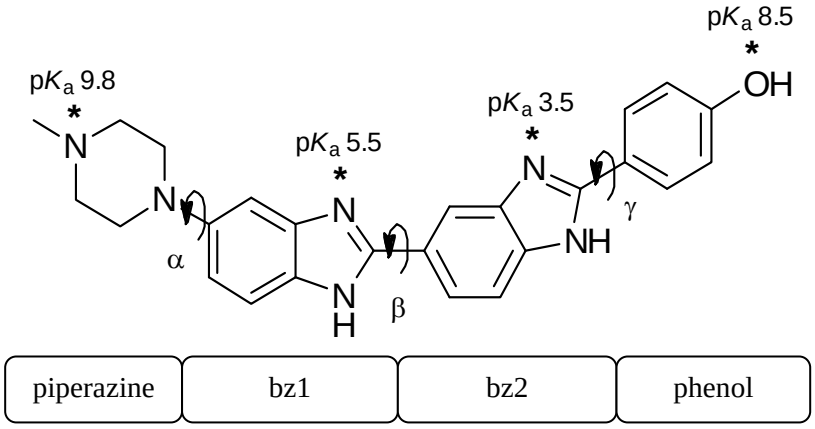

Figure 2.1– Molecular structure and protonation equilibria of **H33258**. The dye is composed by four structural units: a piperazine ring, two bz rings (bz1 and bz2), and a phenol ring. The torsional angles are indicated by α, β, and γ.

The photophysical properties of **H33258** vary not only with pH but also with the solvent medium, as represented in Table 2.1. The relatively large Stokes shift of the dye is likely caused by intramolecular proton and/or charge-transfer processes in the excited state.[10,15,26] In addition, the molar absorption coefficient of **H33258** varies with the medium, being established as (4.1-4.2) × 10^4 M^{-1} cm^{-1} at pH 7 in aqueous solution and *ca*. 15% higher at pH 3 or 10.[27,28]

Table 2.1 – Literature-known absorption and fluorescence maxima, Stokes shift, and fluorescence quantum yield of **H33258** in different media.[a]

Medium	λ_{abs} (nm)	λ_{fl} (nm)	Stokes shift (nm)	Φ_f
DMF	344	480	136	0.4
Ethanol	340	475	135	0.5
Water (pH 2)	344	485	141	0.05
Water (pH 4)	340	485	145	0.4
Water (pH 7)	337	490	153	0.02
Water (pH 10)	348	485	137	0.03

[a] Adapted from references[8,10,15,27]

Another significant feature of **H33258** is the ability to self-aggregate. Several studies indicate this feature, but do not determine clearly the critical concentration for this process.[14,27] Indeed, this phenomenon has to be taken into account for the explanations given in the literature with the intention to understand the steady-state and time-resolved fluorescence behavior of the dye at distinct pH values.[8]

H33258 is a perfect candidate for CB*n* host-guest chemistry (see below), where robust and pH-dependent photophysical changes are expected upon encapsulation in the hydrophobic cavity of the host.

2.2 Experimental Approach

The detailed experimental procedures used in this study are described in Chapter 7. Here I will limit myself to a brief methodological summary.

In order to investigate the manipulation of drug delivery through a supramolecular assembly with a phototriggered pH jump, a suitable guest-host pair has to be selected. First, it was desired to adjust the fluorescence properties of an organic fluorescent drug in aqueous solution, using a CB*n* as host. To this end, CB7 was the most promising candidate, due to its water solubility, low toxicity, and size, all of which contribute to the assembly of complexes with a wide range of organic guest molecules (see Chapter 1). Moreover, the complexation with CB7 is partially driven by cation-π interactions and thus, a variation of the binding affinity in dependence on the protonation status of the guest is expected. Invariably, when basic guests are investigated, their affinity increases at low pH and decreases at high pH. When coupled with a photoinduced pH jump it should be possible to exploit this known dependence to affect either the binding or release of the guest.

H33258 was the selected model guest, not only because of it is using in a vast array of applications, but also because it has the desirable structural and photophysical features in aqueous media. The dye exhibits various protonation states and shows a pH-dependent fluorescence response which should report directly on the pH jump. Besides, the guest fluorescence changes significantly upon macrocyclic complexation by CB7,[6] such that the guest uptake and release can be conveniently monitored.

To this end, spectroscopic techniques (optical spectroscopy, NMR spectroscopy) are not only useful to investigate the photophysical properties of the **H33258**, but also to get insight into the formation of the supramolecular host-guest complex between the dye and CB7.[6] With this knowledge, the ultimate objective of switching this assembly by a photoinduced pH jump was approached. The challenge in this case was to select a photoactive component that could generate a pH adjustment from neutral to basic without displacing itself the guest or interfering with the fluorescence monitoring of the guest release from the complex. Among the available photobases, malachite green leucohydroxide (MGOH) was selected.[29] Its irradiation with UV light efficiently produced the malachite green cation (MG^+) as well as hydroxide ions, leading to the desired pH jump (Scheme 2.1).

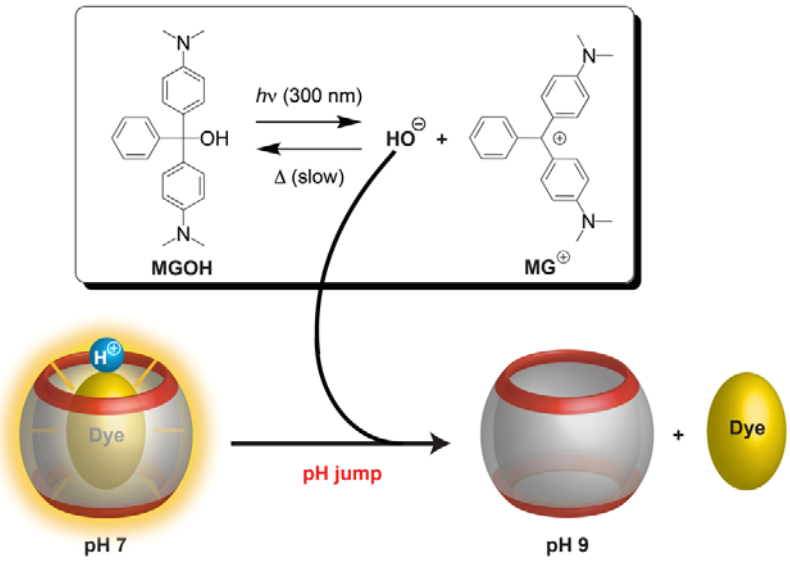

Scheme 2.1 – Switching of the **H33258**/CB7 complex by a photoinduced pH jump. Note that only one bz residue is actually immersed inside the cavity, and not the entire dye, see below.

2.3 Drug and CB7-Drug Complex Characterization

The **H33258** dye is known to form aggregates at higher concentrations in aqueous solutions.[8] Taking this into account, the behavior of the dye under the specific experimental conditions was analyzed and it was determined that it does not self-aggregate significantly below 30 μM. This was confirmed by the linearity of the Lambert-Beer plot in the corresponding concentration window (see Figure 2.2).[6] At pH 7 the slope of the Lambert-Beer plot for the absorption maximum was determined and the resulting molar absorption coefficient was found to be in good agreement with those reported previously (ε = 42300 M^{-1} cm^{-1} at 339 nm, see Figure 2.2).[14,27,28,30]

The photophysical properties of the dye at distinct pHs, in presence and absence of the CB7 macrocycle, were evaluated.[6] To that end, first the published data should be taken into account, showing that **H33258** has a large Stokes shift (*ca*. 130 nm at pH 7, see Figure 2.3), and that the absorption and emission properties are dependent on the pH.[6,8,27,31]

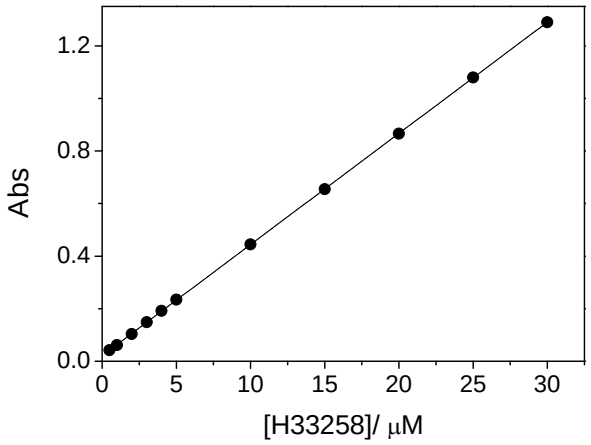

Figure 2.2 – Aggregation assay of **H33258** at pH 7 with a concentration maximum of 30 μM. The data are an average result of three assays.

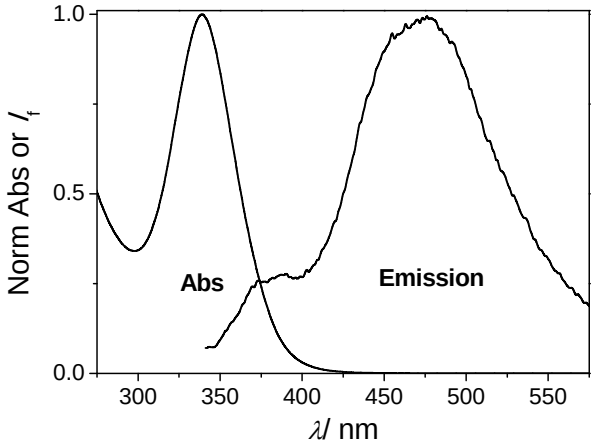

Figure 2.3 – Normalized absorption and fluorescence spectra of **H33258** dye in water at pH 7.

The pH titrations of **H33258** and **H33258**/CB7 were done in the pH range from 2.5 to 11. However, for an easier interpretation of the corresponding spectral alterations, only selected data are represented. In Figures 2.4 and 2.5 it is shown that the absorption and fluorescence spectra of the free dye underwent pH-dependent shifts.[6] On the one hand, from pH 2.5 to 7 a decrease of the absorption signal was accompanied by a hypsochromic shift from 345 to 339 nm. On the other hand, from pH 7 to 11 the opposite behavior was verified, showing a bathochromic shift to 354 nm. For the emission spectra, the fluorescence intensity increased

from pH 2.5 to 4.5 without spectral displacement. From pH 4.5 to 8 a fluorescence decrease was observed, accompanied by a hypsochromic shift (492 to 480 nm). Finally, from pH 8 to 10.5, the fluorescence intensity increased again and a bathochromic shift to 503 nm resulted. These changes are indicative of significant alterations in the electronic and structural properties of the dye, corresponding to the different protonation states.

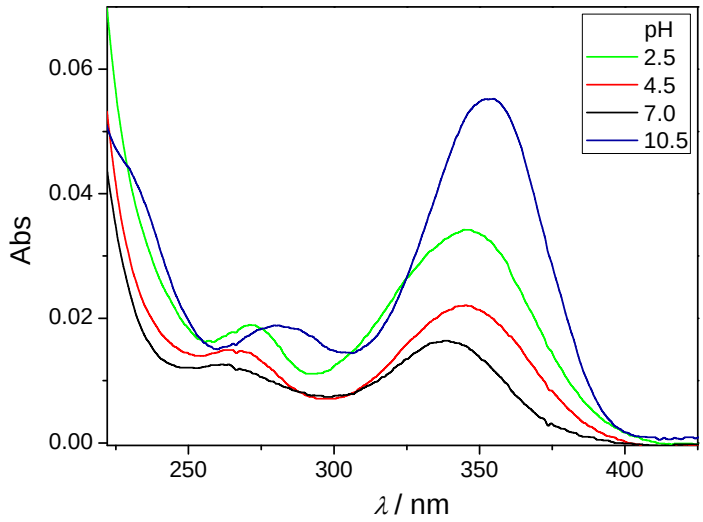

Figure 2.4– Absorption spectra of **H33258** in water. The dye concentration was 1 μM and the pH varied from 2.5 to 10.5.

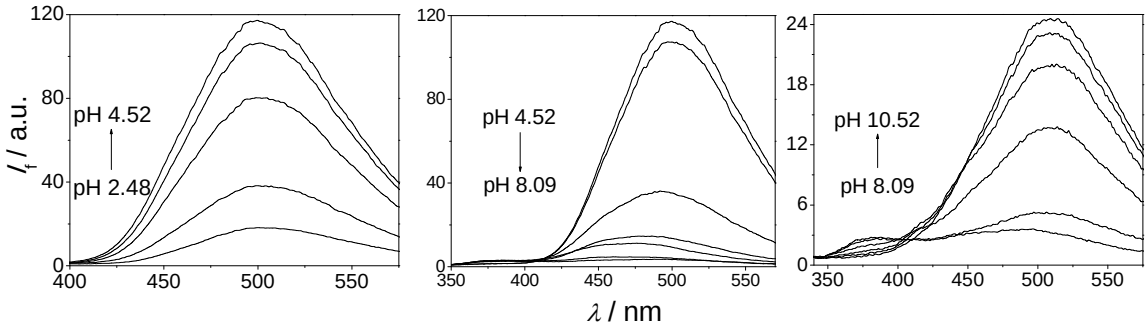

Figure 2.5 – Fluorescence spectra of **H33258** dye in water. The dye concentration was 1 μM and the pH varied from 2.5 to 10.5, λ_{exc} = 295 nm.

In view of the significant variations of the absorption and fluorescence spectra upon changes of the pH, the ground state pK_a was evaluated.[6] Table 2.2 shows the

several dissociation constants of the **H33258** dye, obtained by fluorescence titration experiments. These values are similar to the ones determined by the Clegg group.[14] On the other hand, the calculated pK_a values from UV/vis absorption pH titration were 4.1 and 8.8 (not shown in Table 2.2), which correspond to the values reported by the Zoete group for **H33258**$^{3+}$ and **H33258**.[7]

Table 2.2 – Acidity dissociation constants of **H33258** dye, where D represents the dye.

Protonation equilibrium	**pK_a**			
	from literature [a]	**from literature** [a]	**from literature** [b]	**this work***
$D^{3+} \rightarrow D^{2+} + H^+$	3.5	4.2	3.5	3.4
$D^{2+} \rightarrow D^{+} + H^+$	5.7	5.8	5.5	5.8
$D^{+} \rightarrow D + H^+$	8.0	7.9	8.5	9.1
$D \rightarrow D^{-} + H^+$	8.9	8.8	9.8	
$D^{-} \rightarrow D^{2-} + H^+$	11.7	12.5		

[a] According to reference[7]; [b] According to reference[14]; *Measured by fluorescence.

It is expected that dye encapsulation by CB7 hinders the intramolecular torsional motion of the bz moieties, which will affect the photophysical excited state deactivation mechanisms. Similar to the free dye, the **H33258**/CB7 complex (1 µM/30 µM) also underwent pH-dependent spectral shifts (Figures 2.6 and 2.7).[6] The absorbance at the maximum wavelength decreased and a small hypsochromic shift (351 to 349 nm) resulted from pH 2.5 to 7.5. Further increasing the pH until 11 led to an increase of the absorbance and a small bathochromic shift to 352 nm took place. The emission studies revealed the same pattern as for the free dye. From pH 2.5 to 6.5 the fluorescence intensity increased, accompanied by a hypsochromic shift (485 to 471 nm), and from pH 6.5 to 11 the fluorescence intensity decreased and underwent a further hypsochromic shift to 465 nm. Clearly, these pronounced spectral shifts suggest that the CB7 hydrophobic cavity provides a distinct microenvironment.

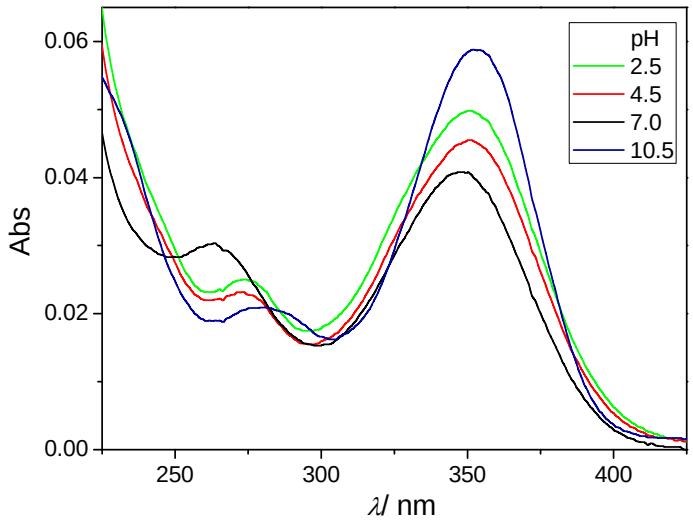

Figure 2.6 – Absorption spectra of **H33258**/CB7 complex in water. The concentrations were 1 μM **H33258**/30 μM CB7 and the pH varied from 2.5 to 10.5.

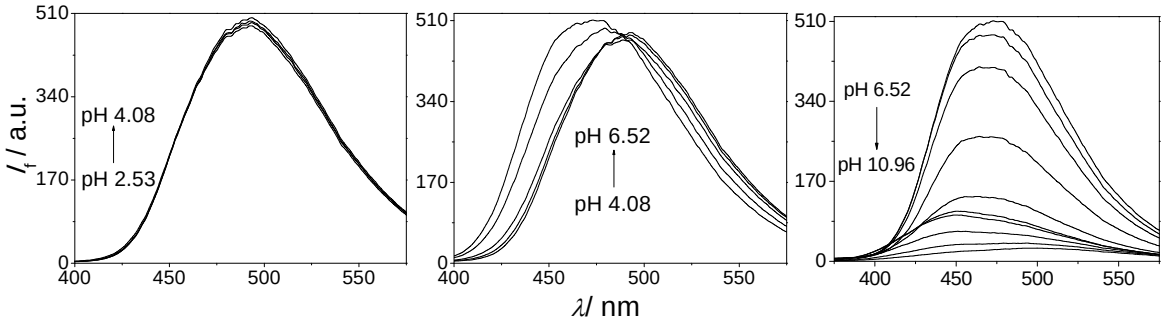

Figure 2.7 – Fluorescence spectra of **H33258**/CB7 complex in water. The concentrations were 1μM **H33258** to 30μM CB7 and the pH varied from 2.5 to 11, λ_{exc} = 295 nm.

The pH titration profiles are summarized in Figure 2.8, being in accordance with previous reports.[6,8] The free dye was very weakly fluorescent at pH 7 (*ca*. Φ_f = 0.01) and reached its maximum emission near pH 4.5 (Φ_f = 0.29), where the doubly protonated form **H33258**$^{2+}$ is known to be the most abundant (pK_a *ca*. 5.8).[8,31] On addition of 30 μM CB7 at pH 7 (> 95% dye complexation; see binding constants below), a remarkable fluorescence enhancement (*ca*. Φ_f = 0.74) was observed. Consequently, the pK_a values shifted by *ca*. 2.2 units, due to dye confinement in the nonpolar CB7 cavity and the concomitant host-assisted protonation of **H33258**, see Chapter 1. The pK_a shifts are evident in the traces plotted in Figure 2.8.[6]

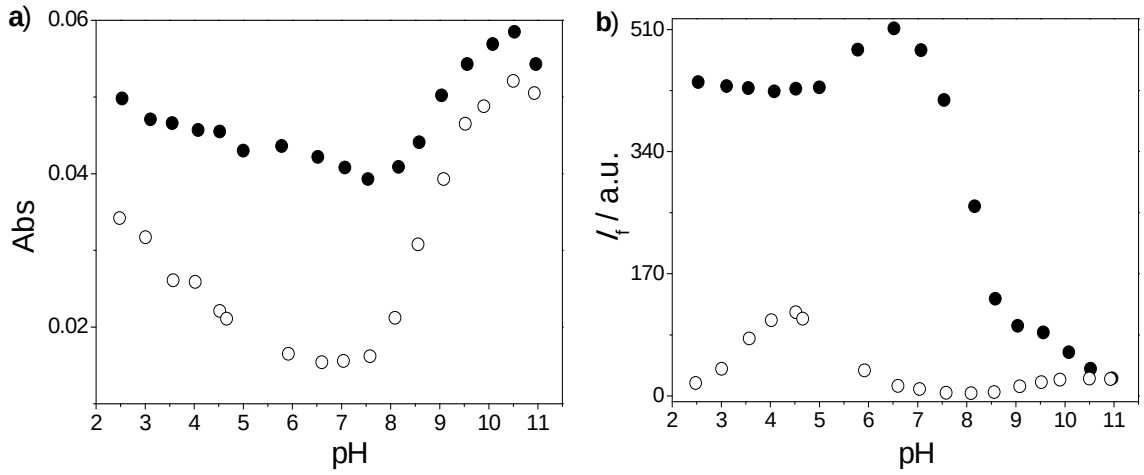

Figure 2.8 – pH Titration curve for the a) absorption and b) fluorescence spectra of **H33258** (1.0 μM) in the absence (empty circles) and presence (filled circles) of CB7 (30 μM) at selected wavelengths, and λ_{exc} = 295 nm. For free dye a) λ_{obs} = 345 nm, b) λ_{obs} = 497 nm; and in with macrocycle) λ_{obs} = 350 nm b) λ_{obs} = 473 nm.

Expectably, the fluorescence lifetime of **H33258**/CB7 is longer than for the free dye. However, the observation of a shorter lifetime component in the fluorescence decay curve of the free dye at pH 7 [τ_1 = 4.03 ns (33%) and τ_2 = 0.34 ns (67%)], is due to the occurrence of dye aggregation at the applied dye concentrations (100 μM). The short lifetime component disappears upon dye encapsulation with CB7 (τ = 4.47 ns).[6]

The striking effects upon addition of CB*n* observed for the fluorescence quantum yield, the fluorescence lifetime, and the absorption/fluorescence spectral properties are a direct consequence of the inclusion complex formation (see Chapter 1). The Job's continuous variation method (Figure 2.9) unambiguously confirmed a 1:1 stoichiometry, which was also supported by the ^{1}H NMR spectroscopy and ESI mass spectrometry studies (see below).[6] This observation is in line with a literature report for the Hoechst 34580 dye derivative and its host-guest complex with CB7.[32]

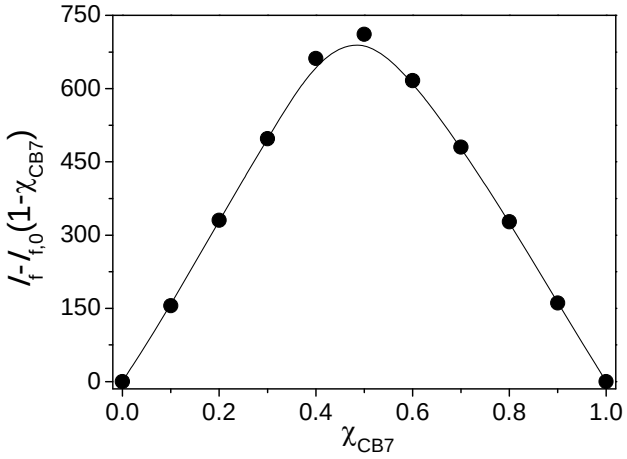

Figure 2.9 – Job's plot for binding of **H33258** by CB7 at pH 7 (1 mM phosphate buffer). The total concentration of both components was fixed at 10 μM. The formation of a 1:1 complex is evident by the maximum at 0.5.

To determine the binding mode of the dye in the 1:1 complex, an acidic solution (10 mM or 50 mM DCl) was used for ^{1}H and 2D COSY NMR experiments, because the peaks of the free dye are better resolved under these conditions than at neutral pH.[6,33] Higher concentrations were needed (mM) for these experiments and the rather broad aromatic signals produced by **H33258** are a direct consequence of its self-aggregation (6.3-7.4 ppm, see Figure 2.10).[6] The peak assignments of **H33258** were done according to the literature and the corresponding COSY spectrum (Figure 2.11).[33]

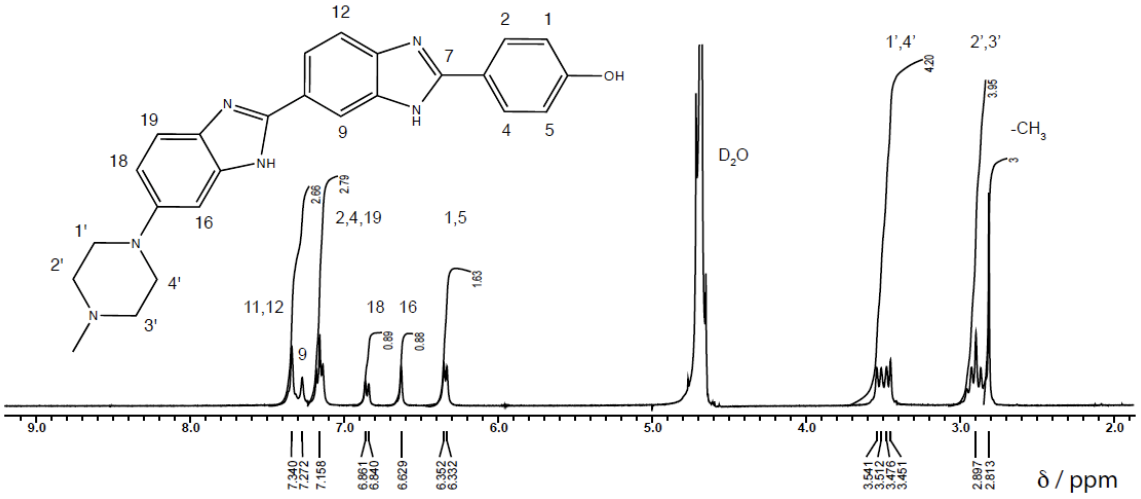

Figure 2.10 –^{1}H NMR spectrum of **H33258** dye (5 mM) in 50 mM DCl. Peak assignments were made according to reference and corresponding COSY spectrum (see Figure 2.11).[33]

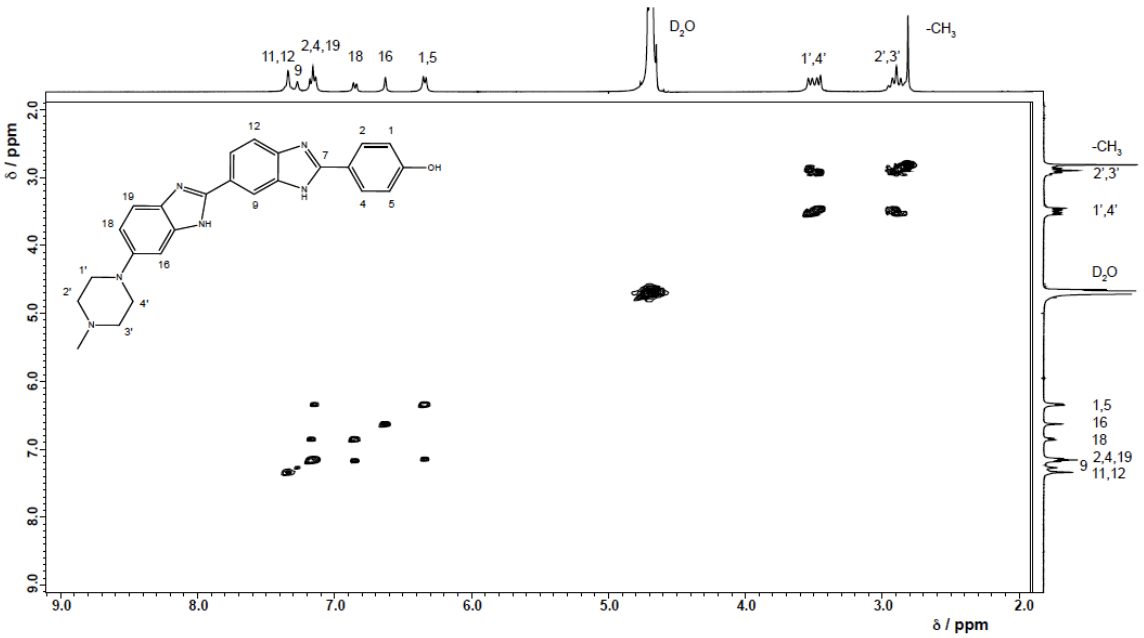

Figure 2.11 –COSY spectrum of **H33258** dye (5 mM) in 50 mM DCl.

The proposed structure of the **H33258**/CB7 complex is derived from the COSY data and the observation that upfield shifts correspond to protons immersed in the macrocycle cavity (Figure 2.12 and 2.13).[6] These upfield shifts are noted for the protons of the piperazine and the ones of the neighboring bz1 (see Figure 2.1). Furthermore, the complex showed fast exchange on the NMR time-scale, accompanied by an apparent symmetry distortion of the CB7 methylene protons at *ca.* 5.5-5.6 ppm, which align inside of the portals.[34] From the known structural characteristics and cavity size of the CB7, the encapsulation of the piperazinyl terminus of the dye was expected to occur in a 1:1 stoichiometry, as previously shown by Bhasikuttan group.[31]

As demonstrated in Figure 2.12, the addition of 1 equivalent of CB7 to the free **H33258** led to rather well-resolved NMR proton signals of the dye,[6] showing the corresponding up- and down-field shifts according to the above discussed binding mode of the dye. Again, as observed in the fluorescence lifetime measurements (see above), the addition of CB7 caused de-aggregation of the dye and confirmed host-guest complex formation. A second equivalent of macrocycle at neutral pH led to no further significant signal shifts, supporting the idea of a 1:1 complex formation (see Figure 2.14).

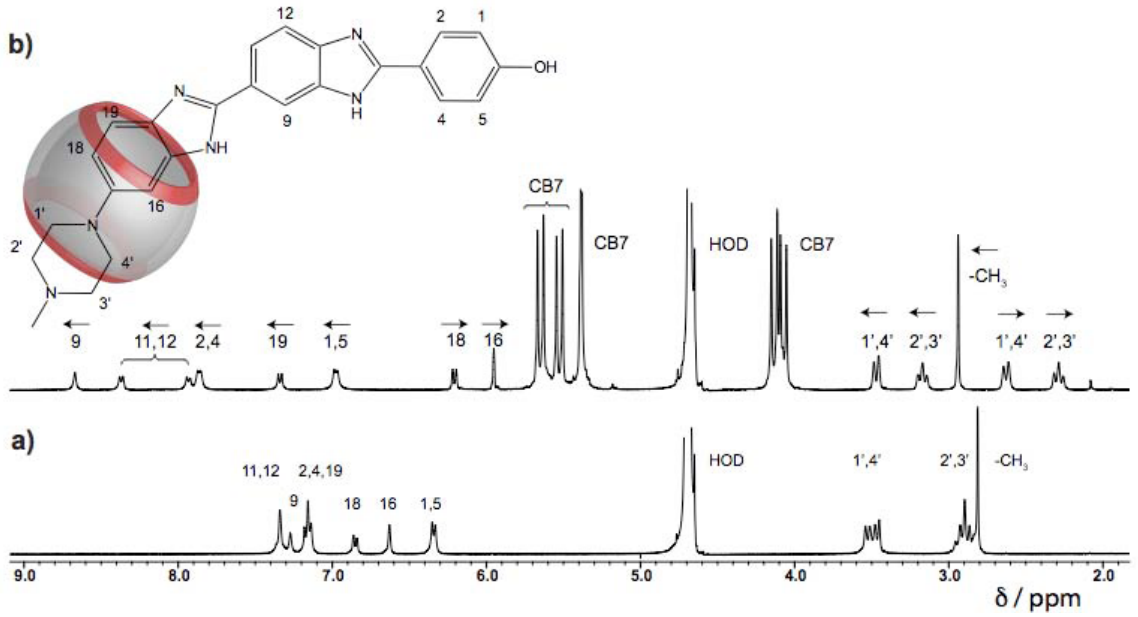

Figure 2.12 –Comparison of ^{1}H NMR spectra of a) **H33258** dye (5 mM) in its free form in 50 mM DCl and b) **H33258** dye (3 mM) in presence of CB7 (3 mM) in 10 mM DCl. Characteristic complexation-induced shifts are highlighted with arrows. In the proposed structure of the complex, the CB7 macrocycle is represented as a barrel.

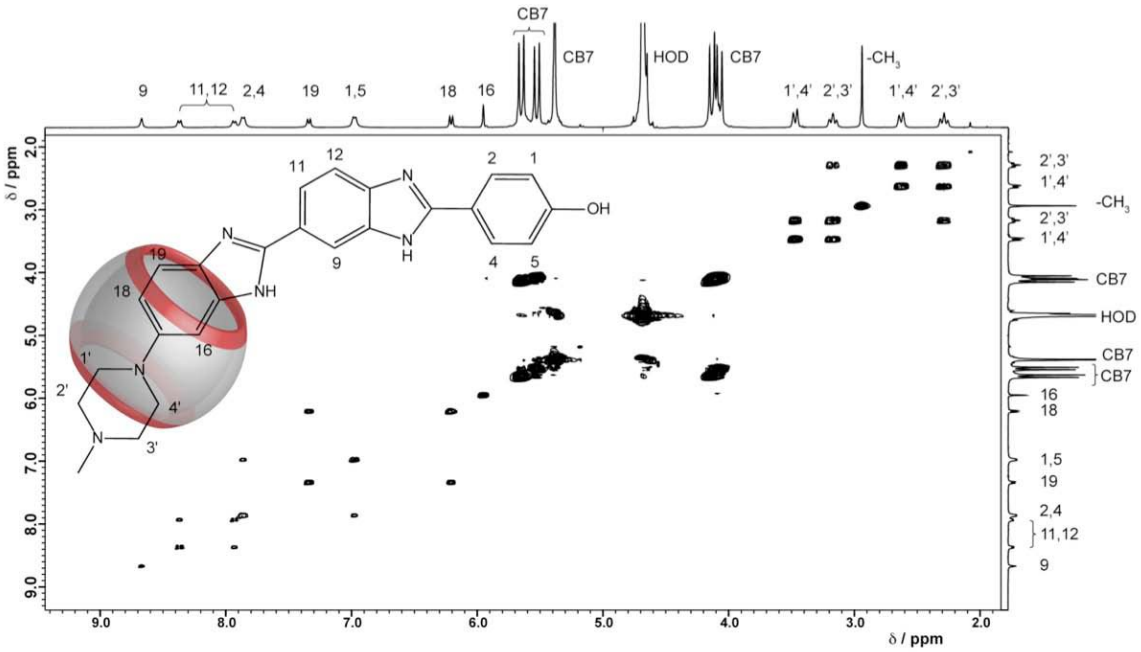

Figure 2.13 –COSY spectrum of **H33258** dye (3 mM) in presence of CB7 (3 mM) in 10 mM DCl.

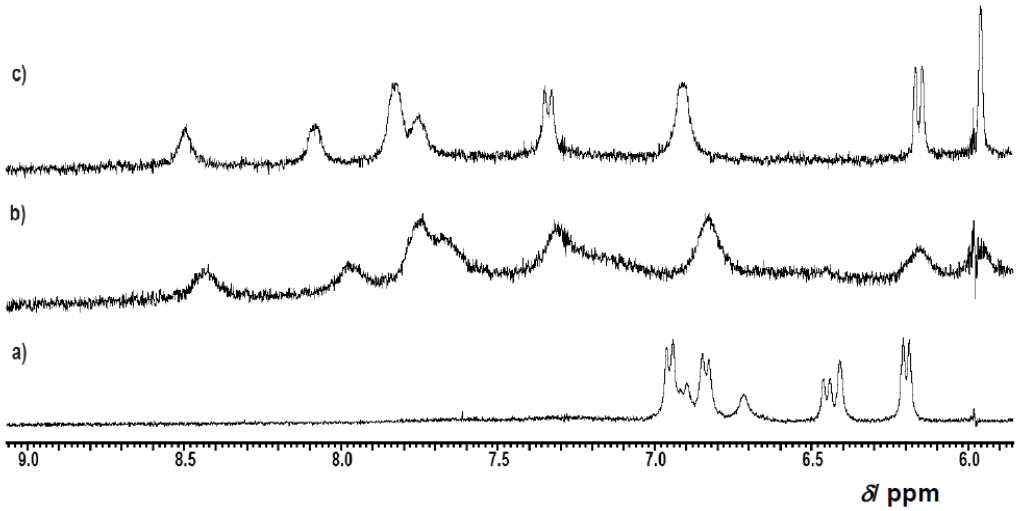

Figure 2.14 – ^{1}H NMR spectra at pH 7 of a) **H33258** (0.5 mM), b) the free dye (0.5 mM) in the presence of 1 eq. CB7 (0.5 mM), and c) **H33258** (0.5 mM) in the presence of 2 eq. CB7 (1.0 mM).

ESI-MS studies allowed to gain a deeper insight into the encapsulation of **H33258** by CB7.[6] As shown in Figure 2.15, different 1:1 complexes with two or three positive charges, containing H^+ or K^+, were observed (see assignments in the figure caption). MS/MS studies can be used to assist the peak assignment (Figure 2.16 to 2.18).

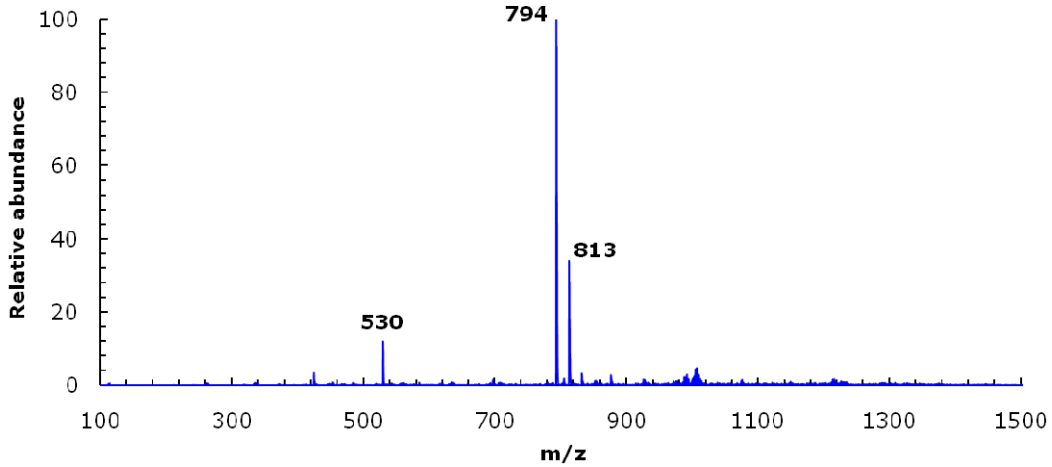

Figure 2.15 – ESI-MS spectrum of **H33258**/CB7complexes at pH 4.5. Assignments: m/z 530: [CB7 + **H33258**+ 2H]$^{3+}$; 794: [CB7 + **H33258**+ H]$^{2+}$; 813: [CB7 + **H33258**+ K]$^{2+}$.

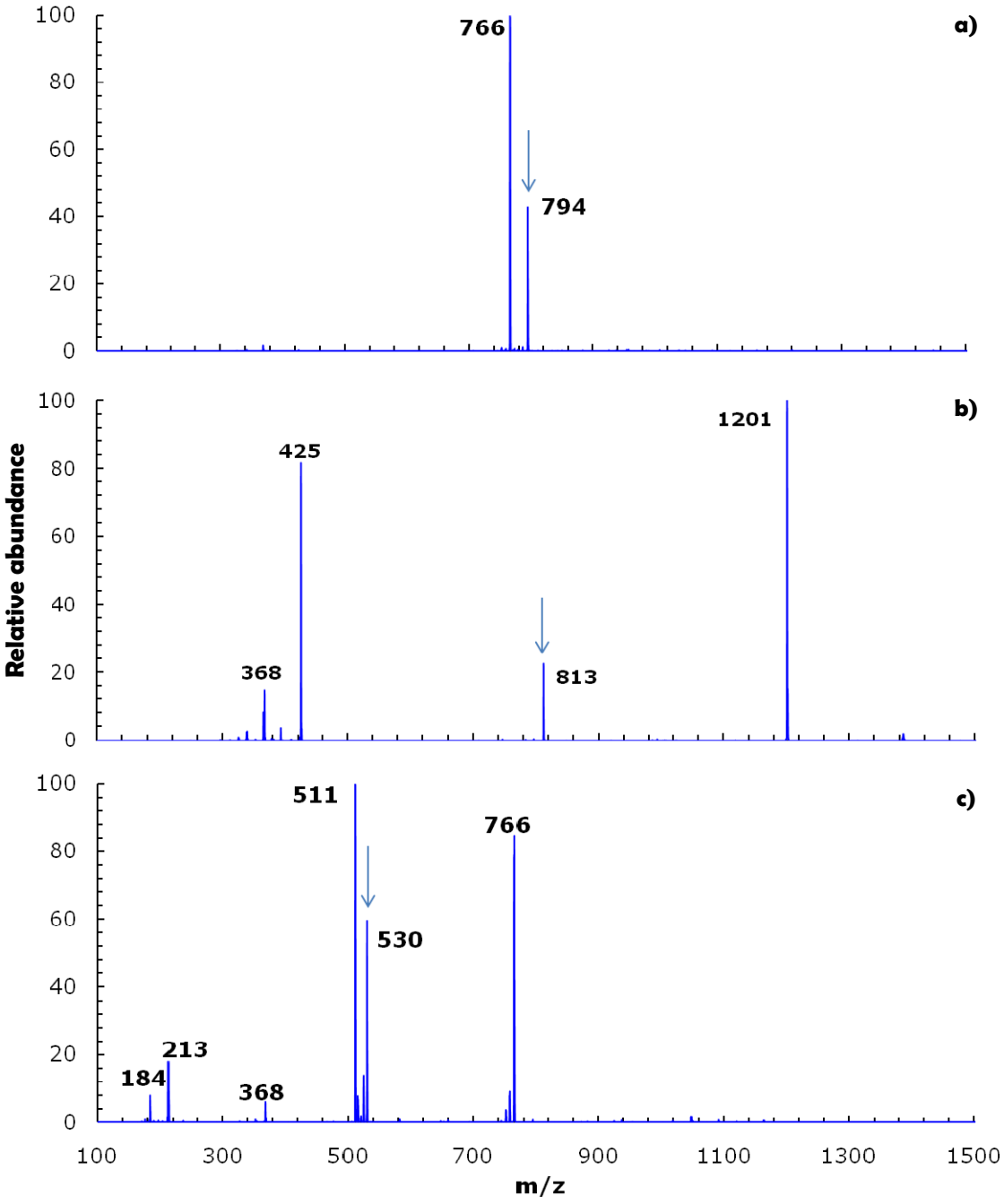

Figure 2.16 – Fragmentation (MS^2) of the distinct peaks from the ESI-MS spectrum of **H33258**/CB7 complex (see Figure 2.15). The arrows indicate the fragmented peak. a) *m/z* 794; Assignments: *m/z* 794: [CB7 + **H33258** + H]$^{2+}$; 766: [CB7 + **H33258** (-56) + H]$^{2+}$.b) *m/z* 813; Assignments: *m/z* 813: [CB7 + **H33258** + K]$^{2+}$; 1201: [CB7 + K]$^{+}$; 425: [**H33258**]$^{+}$; 368: [**H33258** (-56)]$^{+}$. c)*m/z* 530; Assignments: *m/z* 530: [CB7 + **H33258** + 2H]$^{3+}$; 766: [CB7 + **H33258** (-56) + H]$^{2+}$; 511: [CB7 + **H33258** (-56) + 2H]$^{3+}$; 368: [**H33258** (-56)]$^{+}$; 213: [**H33258** + H]$^{2+}$; 184: [**H33258** (-56) + H]$^{2+}$.

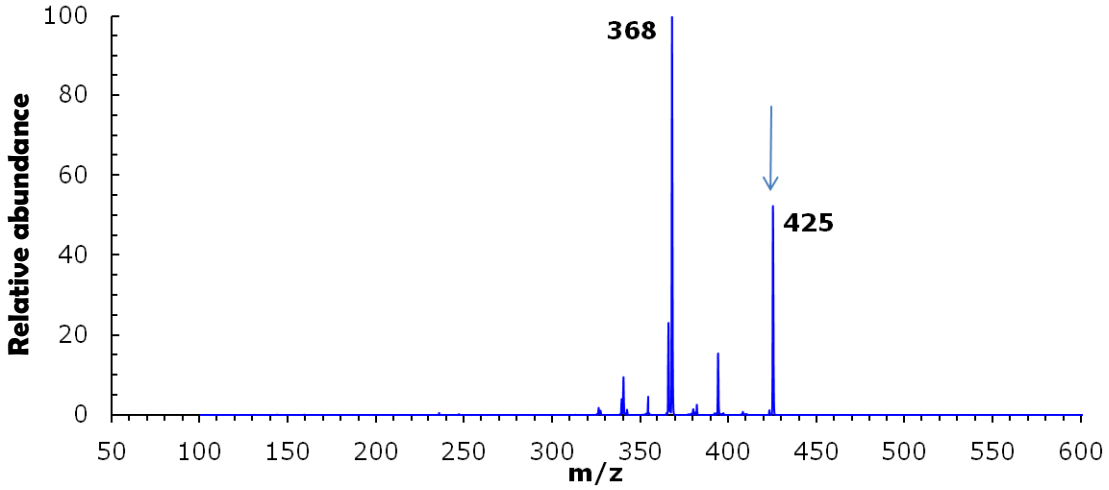

Figure 2.17 – Fragmentation (MS^2) of m/z 425 (free **H33258** dye at pH 7). The arrow indicates the fragmented peak. Assignments: m/z 425: [**H33258**]$^+$; 368: [**H33258**(-56)]$^+$.

The fragmentation (MS^2) of m/z 794 ([CB7 + **H33258** + H]$^{2+}$) gave a signal at m/z 766 (Figure 2.16 a), which corresponds to a mass loss of 56, also observed for the fragmentation of the free guest (Figure 2.17). Actually, such guest fragmentation inside a CB*n* has been recently reported.[35] The strength of the complex is underlined by the failure to disassemble it into the guest and host components. The situation was different for the fragmentation of the ion corresponding to m/z 813 (Figure 2.16 b), which gave the free host (m/z 1201, [CB7 + K]$^+$) and the free guest (m/z 425, [**H33258**]$^+$). In addition, the ion corresponding to the fragmented free guest (m/z 368, [**H33258**(-56)]$^+$), resulting from the same neutral mass loss 56 as noted for the CB7 complex, was observed. These results indicate that the m/z 813 ion is the complex [CB7 + **H33258** + K]$^{2+}$. The fragmentation pattern of this ion hints on a less stable supramolecular complex as compared to m/z 794. The ion at m/z 530 was assigned to the triply charged species [CB7 + **H33258** + 2H]$^{3+}$. Fragmentation of this peak (Figure 2.16 c) yielded m/z 511 and 766, which correspond to a triple and double protonated complex, respectively, with the partially fragmented guest **H33258**(-56) inside the CB7macrocycle (Figure 2.18).

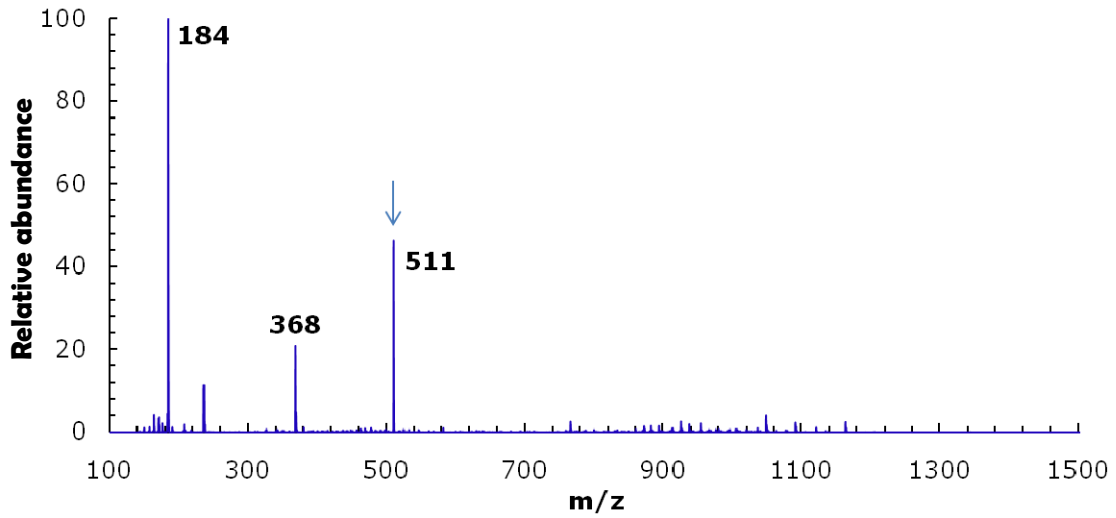

Figure 2.18– Consecutive fragmentation (MS^3) of *m*/*z* 511 (530→511; see Figure 2.16). The arrow indicates the fragmented peak. Assignments: *m*/*z* 511: [CB7 + **H33258**(-56) + 2H]$^{3+}$; 368: [**H33258**(-56)]$^{+}$; 184: [**H33258** (-56) + H]$^{2+}$.

The binding constant can be evaluated by monitorization of dye absorption spectra or fluorescence spectra upon addition of CB7. The UV/vis titration of **H33258** dye in its monocationic form (pH 7) with CB7 showed an initial decrease of the absorbance (until *ca.* 0.5 eq. CB7), followed by the growth of a broad and red shifted absorption signal band on further addition of CB7 (see Figure 2.19). As discussed above, the CB7 fluorescence titration of the dye at a constant pH of 7 displayed a significant enhancement (*ca*. 80 fold) in emission intensity. However, no spectral shifts were observed, except for the first addition (Figure 2.19).

The fluorescence changes upon successive addition of CB7 allowed the calculation of the effective 1:1 binding constant of the **H33258**/CB7 complex, which was K_b = 1.7 × 10^6 M^{-1} at pH 7.2 (see Figure 2.20). This values is 10 times greater than the one reported in an independent study (K_b = 1.5 × 10^5 M^{-1}).[31] This corresponds to the value fitted for the smallest employed dye concentration (0.2 μM), which is preferable for high affinity binding. Fluorescence and UV/vis titrations at higher dye concentrations (4 μM) yielded similar binding constants (K_b = 1.5 × 10^6 M^{-1} and K_b = 8.5 × 10^5 M^{-1}, respectively).

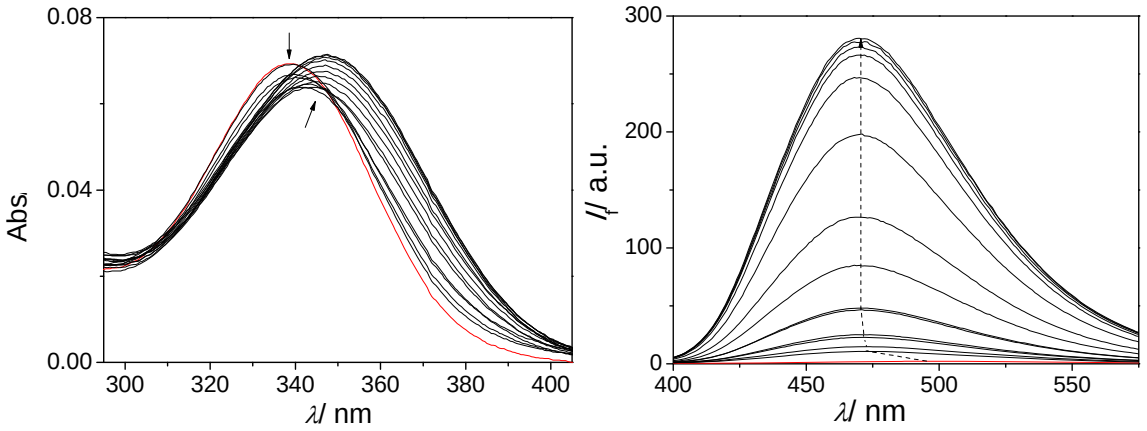

Figure 2.19– Absorption and fluorescence spectrum of **H33258** dye (2 μM) at pH 7 upon successive addition of CB7, until a maximum of 13 μM. The red solid line represents the dye in absence of CB7, and the arrows follow the shift in the maximum, and λ_{exc} = 295 nm.

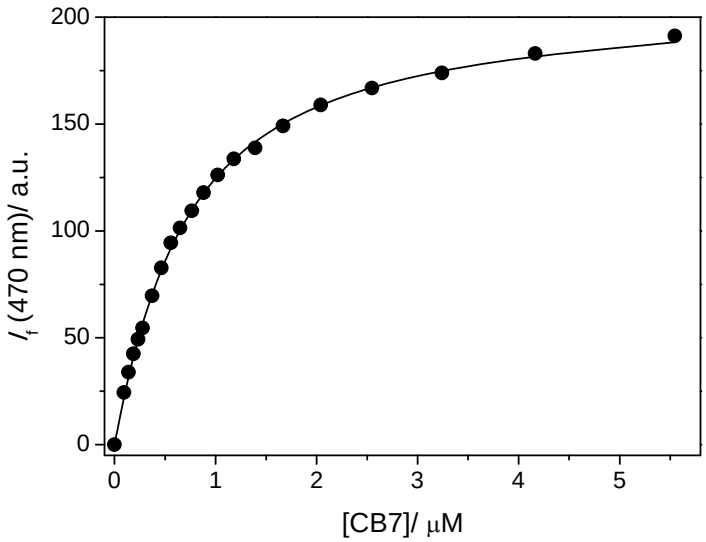

Figure 2.20 – Fluorescence titration of 0.2 μM of **H33258** with CB7 at pH 7.2 (10 mM phosphate buffer); λ_{exc} = 295 nm. The effective binding constant was determined as K_b = 1.7 × 10^6 M^{-1}, and the solid line represents the fitting.

In basic solution (pH >8.5) it is reasonable to assume that the dye is present in a zwitterionic form with a protonated piperazine unit and deprotonated phenol group.[30,31] The binding constant at pH 8.7 dropped by two orders of magnitude, to K_b = 2.8 × 10^4 M^{-1} (see Figure 2.21). Effectively, these results support a partial release of the guest as the pH is increased.

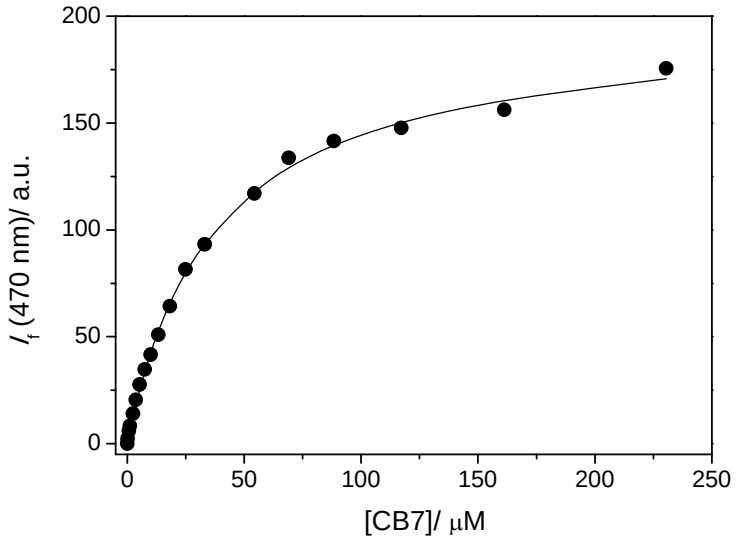

Figure 2.21 – Titration of 1 μM **H33258** with CB7 at pH 8.7 (10 mM phosphate buffer). λ_{exc} = 295 nm. The effective binding constant was determined as $K_b = 2.8 \times 10^4$ M^{-1}, and the solid line represents the fitting.

2.4 Photoinduced pH Jump

With the fluorescence variation of the dye in dependence on pH and the complexation by CB7 being established, the main objective of switching the assembly by a photoinduced pH jump was approached. As shown in Scheme 2.1, it was expected that a pH change from neutral to basic (from pH 7 to 9) would trigger the release of the dye from the complex, which could in turn be monitored through a decrease in fluorescence (as the free dye is much less fluorescent than the complexed one). The pH jump was achieved by photolysis of malachite green leucohydroxide (see Scheme 2.1, top) with 302 nm UV light.

When irradiated with UV light, the MGOH photobase can efficiently produce the malachite green cation and hydroxide ions (see Figure 2.22), the latter being responsible for the pH jump.[29] MG^+ has absorption windows near 340 and 470 nm, which allow selective excitation of **H33258**, and exclude inner filter effects when monitoring the dye fluorescence (Figure 2.22 and 2.23).

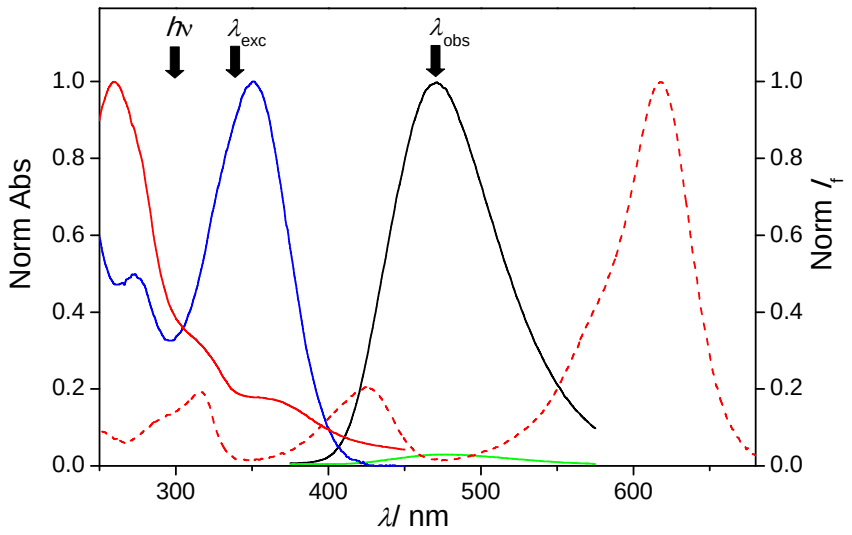

Figure 2.22 – Normalised absorption spectra of **H33258**/CB7 (1/30 μM) complex (blue line), MGOH (red line), and MG^+ (red dashed line) as well as relative fluorescence spectra of **H33258** dye (green line) *versus* **H33258**/CB7 (black line), all at pH 7. Note the selective dye excitation and the absence of competitive absorption at the observation wavelength (λ_{exc} = 340 nm and λ_{obs} = 370 nm). The irradiation wavelength to induce the photoinduced pH jump is indicated with $h\nu$.

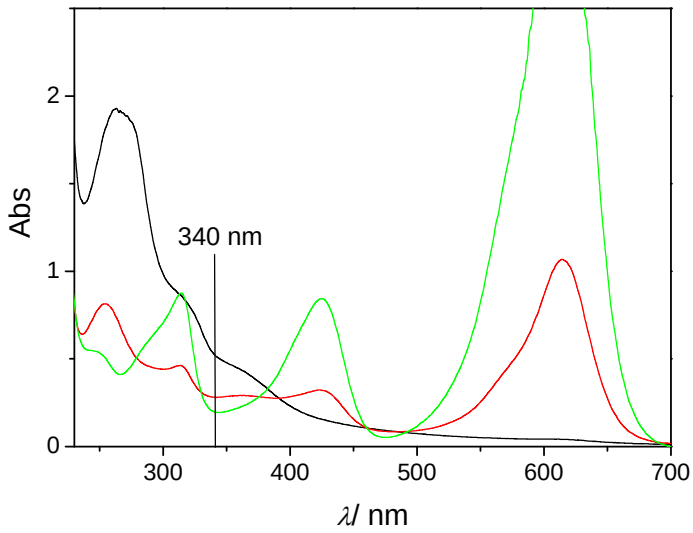

Figure 2.23 – UV/vis absorption spectra of the solutions containing 1 μM **H33258**, 30 μM CB7, and 100 μM MGOH: a) immediately after addition of MGOH (black line), b) after equilibration for *ca*. 1.5 hours (red line), and c) after photolysis with UV light for 10 min (green line). *ca*. 20 μM MGOH are converted to MG^+ under these conditions; estimated from the nascent absorption band.

While the photophysical prerequisites for this multicomponent system presented a challenge, one must recall that they are actually not required from the point view of drug release, which could be effected independent on the spectral properties of the drug itself. Nonetheless, any interference of the malachite green cation on **H33258**/CB7 complex stability has to be minimal. However, based on the relatively small binding constant of the closely related brilliant green cation with CB7 (K_b = 1.7 × 10^4 M^{-1})[36] a competition of MG^+ with **H33258** dye can be safely excluded.

The pH jump experiment was carried out by irradiating for 10 minutes after thermal equilibration of the reaction mixture for 90 minutes (Figure 2.24). Indeed, the dye fluorescence dropped dramatically as the pH increased to 8.7. Control experiments demonstrated that the fluorescence decrease was a genuine consequence of the pH jump. Most importantly, an experiment performed under similar conditions, but in a phosphate-buffered solution (pH 7.2), showed no significant pH or fluorescence response upon irradiation or prolonged standing (Figure 2.25).

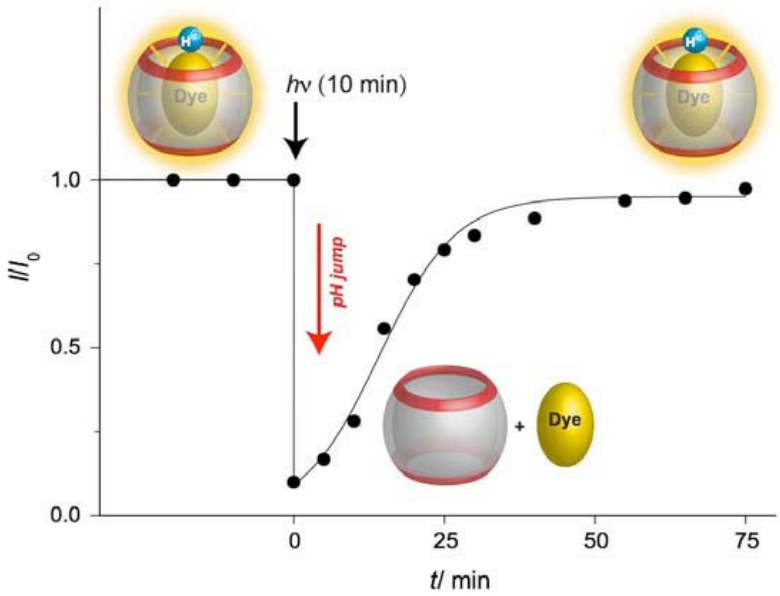

Figure 2.24 – Fluorescence response of the **H33258**/CB7 (1/30 μM) complex in the presence of 100 μM MGOH and irradiation at 300 nm for 10 minutes in aqueous solution with an initial pH of 7. λ_{exc} = 340 nm.

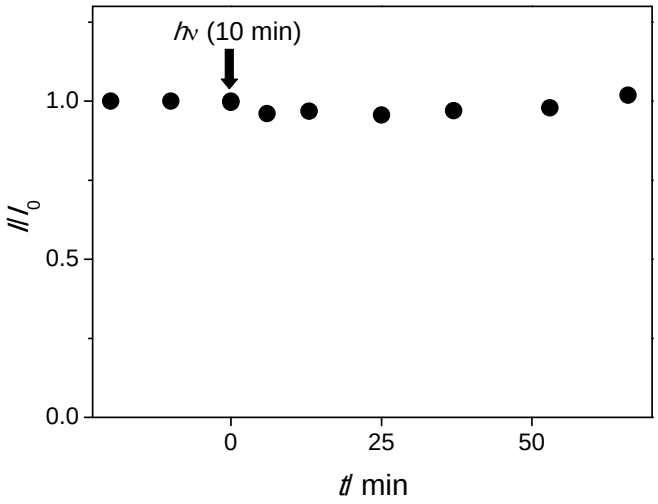

Figure 2.25 – Fluorescence response of the **H33258**/CB7 (1/30 μM) complex in the presence of 100 μM MGOH and irradiation at 300 nm for 10 minutes in 10 mM phosphate buffer solution, pH 7.2 (negative control experiment). λ_{exc} = 340 nm.

Within *ca*. 60 minutes after irradiation, the fluorescence recovered again to its initial levels, due to the slow recombination of MG^+ and hydroxide ions. This was accompanied by the restoration of the initial neutral pH value (Figure 2.26). This thermal reversibility of the photoinduced host-guest complex dissociation establishes a special example of a photochromic effect. In contrast to the very robust azobenzene and diarylethene switches, MGOH undergoes secondary irreversible photoprocesses,[37] which prevented our system to "cycle" through repetitive dissociation-association cycles. In fact, the fluorescence response was greatly reduced already in the second cycle (to *ca*. 20% of the initial value). However, one needs to recall that a potential application in a targeted photoinduced drug delivery system would neither require a reversible uptake of the drug nor a multiple release. Indeed, photocaged compounds, which are used for the selective triggering of biochemical processes, are invariably based on irreversible photoreactions.[38]

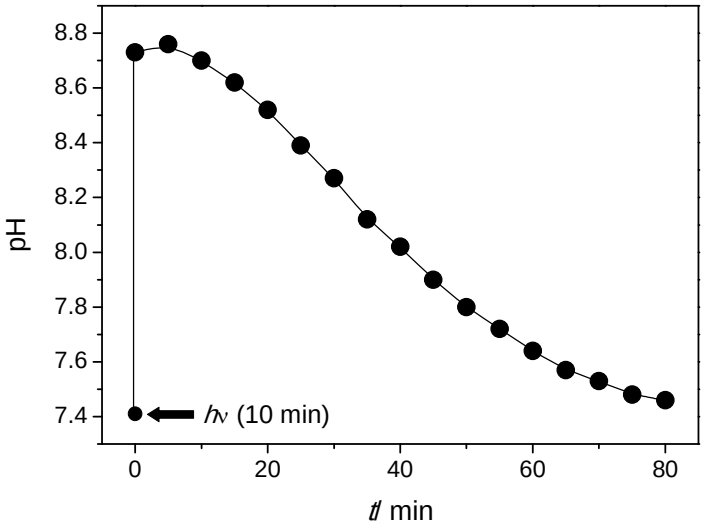

Figure 2.26 – Temporal development of pH after photoinduced pH jump of a solution containing 1 µM **H33258**, 30 µM CB7, and 100 µM MGOH.

2.5 Conclusion

In this work, it was shown that the dissociation of a host-guest complex between CB7 and **H33258** can be manipulated by a photo-induced pH jump. The increase in pH from 7 to 9 lowers the guest binding constant by two orders of magnitude, allowing an immediate (on the time scale of the photolysis) release of dye. Such phenomenon was conveniently signaled by fluorescence modulations of the guest dye and model drug. This approach opens new perspectives for photo-controlled drug release, exploiting cucurbituril host-guest chemistry. The transfer of the method to actual biological systems may not be straightforward, especially in view of their natural buffering capacity and the herein required use of UV light. However, pH jumps have been observed in living cells,[39] which highlights their potential applicability in complex biological systems.

References

(1) Ueno, A.; Takahashi, K.; Osa, T. *J. Chem. Soc., Chem. Commun.* **1981**, 94.

(2) Ueno, A.; Tomita, Y.; Osa, T. *Tetrahedron Lett.* **1983**, *24*, 5245.

(3) Mulder, A.; Jukovic, A.; Lucas, L. N.; van Esch, J.; Feringa, B. L.; Huskens, J.; Reinhoudt, D. N. *Chem. Commun.* **2002**, 2734.

(4) Molard, Y.; Bassani, D. M.; Desvergne, J.-P.; Horton, P. N.; Hursthouse, M. B.; Tucker, J. H. R. *Angew. Chem. Int. Ed.* **2005**, *44*, 1072.

(5) Schäfer, C.; Eckel, R.; Ros, R.; Mattay, J.; Anselmetti, D. *J. Am. Chem. Soc.* **2007**, *129*, 1488.

(6) Parente Carvalho, C., MSc Thesis, Universidade do Algarve, 2010.

(7) Ladinig, M.; Leupin, W.; Meuwly, M.; Respondek, M.; Wirz, J.; Zoete, V. *Helv. Chim. Acta* **2005**, *88*, 53.

(8) Barooah, N.; Mohanty, J.; Pal, H.; Sarkar, S. K.; Mukherjee, T.; Bhasikuttan, A. C. *Photochem. Photobiol. Sci.* **2011**, *10*, 35.

(9) Arndt-Jovin, D. J.; Jovin, T. M. In *Methods Cell Biol.*; Taylor, D. L., Yu-Li, W., Eds.; Academic Press: 1989; Vol. Volume 30, p 417.

(10) Cosa, G.; Focsaneanu, K. S.; McLean, J. R. N.; McNamee, J. P.; Scaiano, J. C. *Photochem. Photobiol.* **2001**, *73*, 585.

(11) Latt, S. A.; Stetten, G. *J. Histochem. Cytochem.* **1976**, *24*, 24.

(12) Yelian, F. D.; Dukelow, W. R. *Andrologia* **1992**, *24*, 167.

(13) Bontemps, J.; Houssier, C.; Fredericq, E. *Nucleic Acids Res.* **1975**, *2*, 971.

(14) Loontiens, F. G.; Regenfuss, P.; Zechel, A.; Dumortier, L.; Clegg, R. M. *Biochemistry* **1990**, *29*, 9029.

(15) Kakkar, R.; Garg, R.; Suruchi *J. Mol. Struct. (Theochem)* **2002**, *579*, 109.

(16) Lämmler, G.; Herzog, H.; Saupe, E.; Schütze, H. R. *Bull. W.H.O.* **1971**, *44*, 751.

(17) Denham, D. A.; Suswillo, R. R.; Rogers, R.; McGreevy, P. B.; Andrews, B. J. *J. Helminthol.* **1976**, *50*, 243.

(18) Ginsburg, H.; Nissani, E.; Krugliak, M.; Williamson, D. H. *Mol. Biochem. Parasitol.* **1993**, *58*, 7.

(19) Wong, S. S. C.; Sturm, R. A.; Michel, J.; Zhang, X. M.; Danoy, P. A. C.; McGregor, K.; Jacobs, J. J.; Kaushal, A.; Dong, Y.; Dunn, I. S.; Parsons, P. G. *Biochem. Pharmacol.* **1994**, *47*, 827.

(20) Kraut, E. H.; Fleming, T.; Segal, M.; Neidhart, J. A.; Behrens, B. C.; MacDonald, J. *Invest. New Drugs* **1991**, *9*, 95.

(21) Denison, L.; Haigh, A.; D'Cunha, G.; Martin, R. F. *Int. J. Radiat Biol.* **1992**, *61*, 69.

(22) Adhikary, A.; Bothe, E.; Jain, V.; Von Sonntag, C. *Int. J. Radiat Biol.* **2000**, *76*, 1157.

(23) Chaudhury, N. K.; Bhardwaj, R. *Curr. Sci.* **2004**, *87*, 1256.

(24) Soderlind, K. J.; Gorodetsky, B.; Singh, A. K.; Bachur, N. R.; Miller, G. G.; Lown, J. W. *Anticancer Drug Des.* **1999**, *14*, 19.

(25) Alemán, C.; Adhikary, A.; Zanuy, D.; Casanovas, J. *J. Biomol. Struct. Dyn.* **2002**, *20*, 301.

(26) Kalninsh, K. K.; Pestov, D. V.; Roshchina, Y. K. *J. Photochem. Photobiol. A: Chem.* **1994**, *83*, 39.

(27) Görner, H. *Photochem. Photobiol.* **2001**, *73*, 339.

(28) Jin, R.; Breslauer, K. J. *Proc. Natl. Acad. Sci. U. S. A.* **1988**, *85*, 8939.

(29) Irie, M. *J. Am. Chem. Soc.* **1983**, *105*, 2078.

(30) Umetskaia, V. N.; Rozanov Iu, M. *Biofizika* **1990**, *35*, 399.

(31) Barooah, N.; Mohanty, J.; Pal, H.; Bhasikuttan, A. C. *PCCP* **2011**, *13*, 13117.

(32) Lei , W.; Zhou, Q.; Jiang , G.; Hou, Y.; Zhang, B.; Cheng, X.; Wang, X. *ChemPhysChem* **2011**, *12*, 2933.

(33) Parkinson, J. A.; Barber, J.; Buckingham, B. A.; Douglas, K. T.; Morris, G. A. *Magn. Reson. Chem.* **1992**, *30*, 1064.

(34) Buschmann, H. J.; Wego, A.; Zielesny, A.; Schollmeyer, E. *J. Incl. Phenom. Macrocycl. Chem.* **2006**, *54*, 85.

(35) Saleh, N. i.; Meetani, M. A.; Al-Kaabi, L.; Ghosh, I.; Nau, W. M. *Supramol. Chem.* **2011**, *23*, 650.

(36) Bhasikuttan, A. C.; Mohanty, J.; Nau, W. M.; Pal, H. *Angew. Chem. Int. Ed.* **2007**, *46*, 4120.

(37) Liu, H.; Xu, Y.; Li, F.; Yang, Y.; Wang, W.; Song, Y.; Liu, D. *Angew. Chem. Int. Ed.* **2007**, *46*, 2515.

(38) Pelliccioli, A. P.; Wirz, J. *Photochem. Photobiol. Sci.* **2002**, *1*, 441.

(39) Meng, H.; Xue, M.; Xia, T.; Zhao, Y.-L.; Tamanoi, F.; Stoddart, J. F.; Zink, J. I.; Nel, A. E. *J. Am. Chem. Soc.* **2010**, *132*, 12690.

Chapter 3

Upgrading Photoswitches

In this chapter, the improvement of the photochromic performance of a spiropyran by developing a novel strategy based on the use of an anchor-substituted photoswitch and its encapsulation in CB7 is demonstrated.

3.1 Spiropyrans

The reversible photocontrol of the structure and electronic properties of organic molecules is a fascinating challenge with wide applications in a variety fields such as materials chemistry, catalysis, and chemical biology.[1-3] Nowadays it is well established that such compounds undergo reversible transformations (some or all of them being photoinduced) between two (or sometimes more) distinct forms, each one with its correspondent absorption spectrum (Scheme 3.1). This phenomenon is commonly termed as photoswitching and is accompanied by a change in physicochemical properties, including refractive index, dielectric constant, oxidation/reduction potential, absorption spectra, fluorescence, and geometrical structure.[4,5]

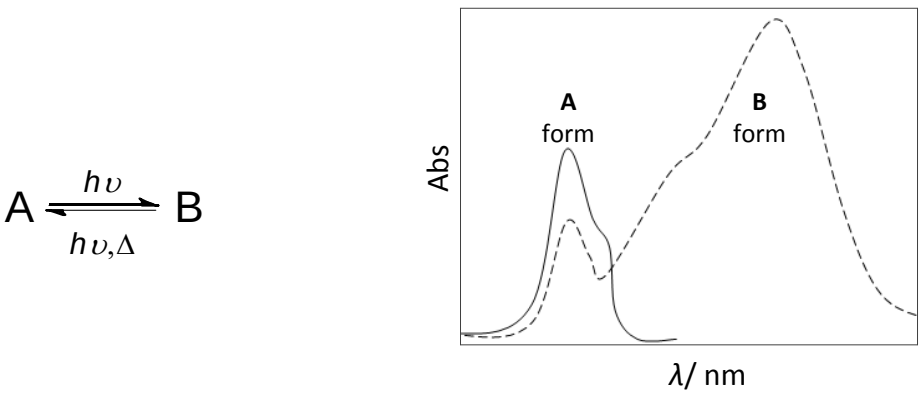

Scheme 3.1 – Typical phototransformation reaction of a two-state photoswitch, and the corresponding absorption spectra of the implied forms.

There are many families of photochromic compounds such as azobenzenes, fulgides/fulgimides, diarylethenes, and spiropyrans.[5] The latter, being also the class of choice for this work, which has been exploited for a number of technologically important applications. These include dynamic materials, photocontrol of biological systems, nanomachines, "smart" receptors, drug delivery, and imaging of cancer cells, just to cite a few examples.[3,6-10]

Spiropyrans are composed by two heterocyclic parts, a benzopyran, and an indole moiety, joined at a spiro centre. The two "halves" of the molecule are located on two perpendicular planes, leading to an UV/vis optical spectrum with two localized transitions (~270-300 nm band from the π*-π* electronic transition of the indole part, and ~320-350 nm corresponding to transitions of the benzopyran moiety).[11,12] Upon UV irradiation, the colorless thermodynamically stable spiro form (SP, **a** of Scheme 3.2) is converted into a metastable colored merocyanine form that is best described by zwitterionic and quinoidal resonance forms (MC, **b** and **c** of Scheme 3.2, respectively).[13] This photodissociation reaction of the C_{spiro}-O bond leads to completely different optical spectra, characterized by the appearance of a strongly shifted absorption band in the visible region (λ_{max} ≈ 500-600 nm),[6] spanning a wide optical range between 300 and 600 nm.[14]

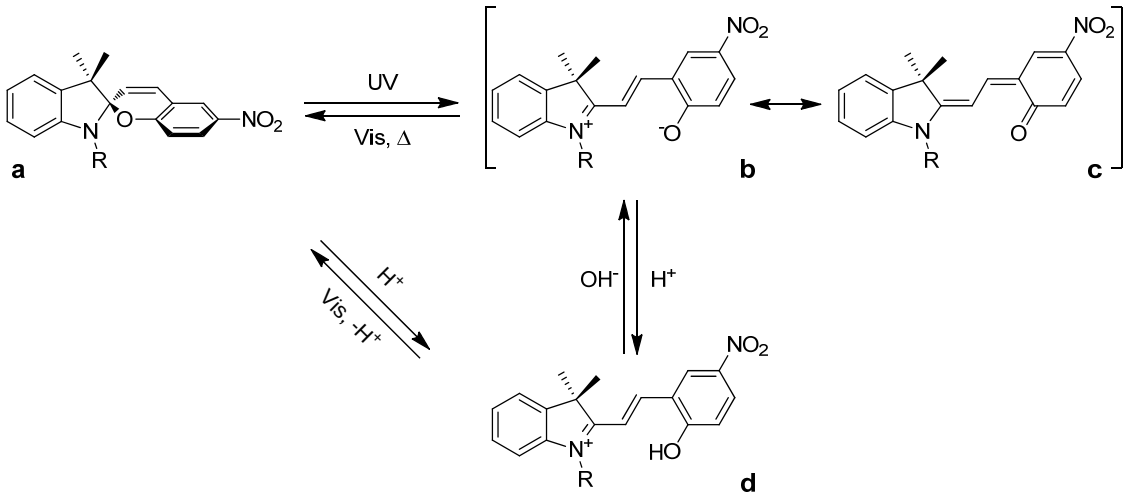

Scheme 3.2 – Reversible photochromism, thermochromism and acidochromism transformation between the three states: SP (**a**), MC (**b** and **c**), and MCH (**d**)

Interestingly, the extended π-conjugated system of the MC leads to a significant increase of the ground state dipole moment of the species, from *ca*. 4D for SP to 18D for MC.[15] Another distinguishable difference between these two states is their emission behavior, where only the open form exhibits some weak fluorescence.[3,16] Moreover, the pH-dependent nature of MC leads to a third possible state, the protonated MC form (MCH, **d** of Scheme 3.2), with a characteristic band at approximately 420 nm.[17]

Light, solvent, metal ions, acids and bases, temperature, redox processes, and mechanical force can control the reversible transformations between the spiropyran forms.[3] The reverse isomerization of MC to the stable SP can be accomplished thermally or photochemically by irradiation with visible light (>400 nm).[1,3]

The photoisomerization of spiropyran is often accompanied by side reactions that may generate by-products.[4] The gradual degradation with an increasing number of switching cycles ("fatigue") has been described by many authors, not only in water, where the MC form gradually decomposes by hydrolysis (see below), but also in non-polar solvents.[4,6,18] In this context, many attempts have been made to overcome the drawbacks of using spiropyrans in aqueous solutions. These include the use of antioxidants,[19] micelles,[20] immobilization onto/within macromolecular supports or inorganic scaffolds,[3] and employment of supramolecular systems.[16,21,22] This work combines two complementary strategies, where a simple synthetic approach is used to achieve spyropiran-derivative supramolecular assemblies with CB*n*, to improve the hydrolytic properties of spiropyrans, while maintaining their photochromic performance.

3.2 Experimental Approach

The experimental procedure used in this study is described in detail in Chapter 7. Here a brief account of some experimental planning together with some general considerations about the design will be given.

In order to overcome the drawbacks of using spiropyran switches in aqueous solution, namely avoiding the decomposition by hydrolysis, a supramolecular approach was developed. In collaboration with the Professor Andréasson group, from the Chalmers University of Technology in Gothenburg (Sweden), novel spiropyrans with a cadaverine-derived anchor were designed.[16] It was expected that the encapsulation of the anchor by a macrocycle would improve the thermal and hydrolytic stability of the merocyanine form. The supramolecular assemblies and the non-complexed photoswitches were characterized with respect to the thermally induced ring-opening isomerization of the spiro form, the hydrolytic stability of the merocyanine form, and the photoinduced ring closure.

Encapsulation of organic dyes by macrocyclic host compounds can dramatically alter their photophysical and chemical properties, due to changes in the microenvironment, confinement effects, or host-induced guest protonation (see Chapter 1). With this in mind, the approach was to apply a water-soluble macrocycle, known to interact with positive charges (as formed in the ring opening process). This, in turn, would improve the hydrolytic stability of the MC form. An obvious choice for the organic macrocycle was CB7, known for its water solubility, and efficient binding of cationic guests.

The host-guest complexation of the anchor by the CB7 was then studied by UV/vis absorption titrations, NMR spectroscopy, and mass spectrometry (ESI-MS). The importance of an adequate molecular design of the anchor was demonstrated by including model compounds with variations in the anchors structure or total lack of such structural feature.

3.3 Anchored-Spiropyran and Supramolecular Interaction with CB7

3.3.1 Characterization of the Spiropyran

Spiropyrans **1**-**3**, represented in Scheme 3.3, were synthesized and provided by Professor Andréasson's group (Chalmers University, Gothenburg, Sweden).[16] The focus of this work is on compound **1**, while **2** and **3** were included for the purpose of comparison. The derivates **1** and **2** contain the photochromic 3',3'-dimethyl-6-nitrospiro[2*H*-1-benzopyran-2,2'-indoline] moiety and an *N*,*N*-dimethylaminoalkyl-derived anchor but differ in the number of methylene units contained in the anchor (**1** has five CH_2 units, whereas **2** has only three CH_2 units). Because the terminal dimethylamino function can be protonated, both derivatives show sufficient water solubility at neutral and acidic pH. On the other hand, spiropyran **3** is different from the others because it contains no anchor and an electron-withdrawing amidinium substituent in the 6-position (instead of nitro).

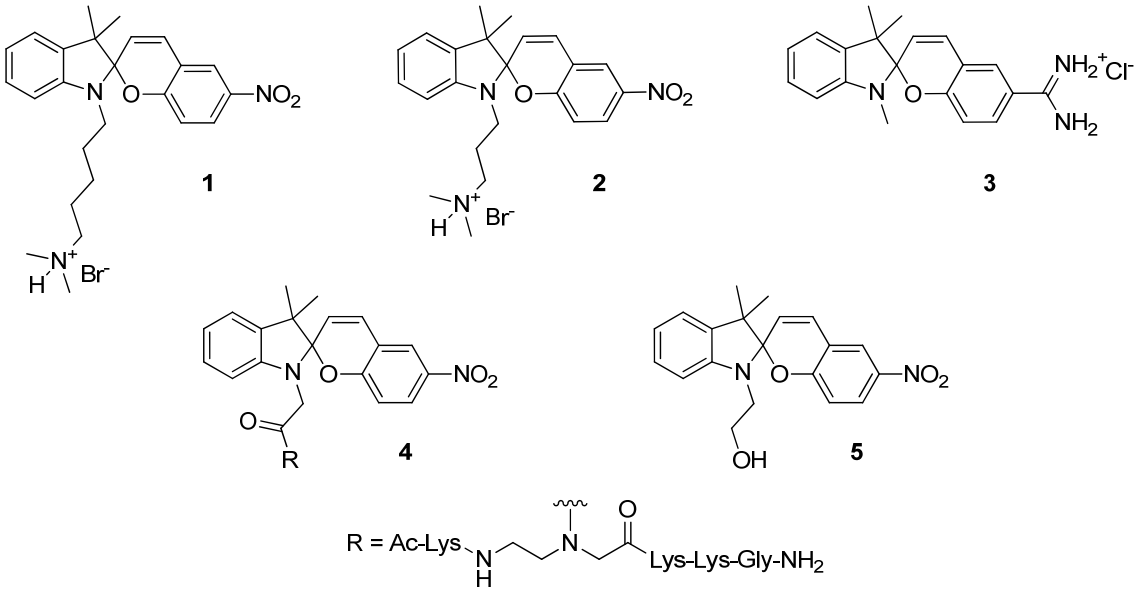

Scheme 3.3 - Structures of spiropyrans used in this study (**1**-**3**), in theirs SP isoform. The spiropyrans **4** and **5** are related structures from previous studies.[18,21]

The anchor design of **1** was motivated by the strong binding of protonated cadaverine by CB7 (K_b = 2.0 × 10^7 M^{-1}, see Figure 7.2), which was expected to apply similarly for the twice positively charged anchor in the MC form.

The acido- and photo-chromic switching behavior and possible hydrolytic degradation of spiropyran **1** are resumed in Scheme 3.4.

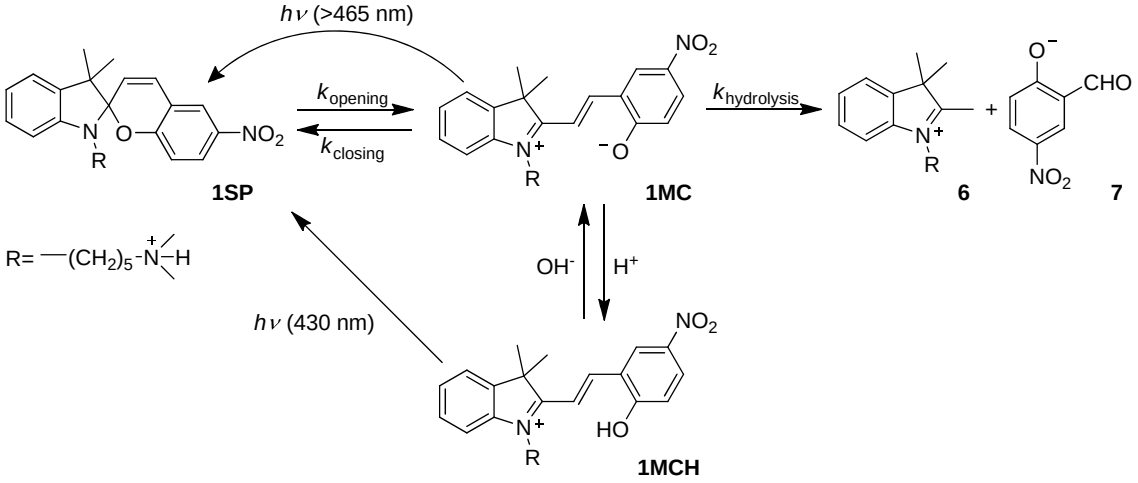

Scheme 3.4 – Photochromic and acidochromic interconversion between the three different forms of **1** (**1SP**, **1MC**, and **1MCH**) and the structures of the hydrolysis products (**6** and **7**).

The absorption spectra of the different forms of **1** agree widely with the general features observed for spiropyrans (see spectra in Figure 3.1). In aqueous solution at pH 7 (10 mM phosphate buffer), the spiro form (**1SP**) showed an absorption maximum at 353 nm (ε = 7800 M^{-1} cm^{-1}). This form converted thermally in a ring-opening process to the MC form (**1MC**) with a maximum conversion of about 90%, as verified by ^{1}H NMR spectroscopy.

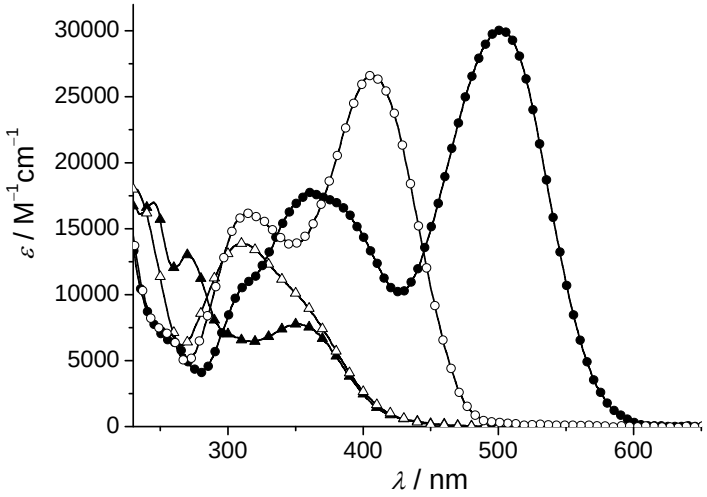

Figure 3.1 – Absorption spectra of **1SP** (▲), **1SPH** (△), **1MC** (●), **1MCH** (○).

Predictably, the functional characteristics of the free photochrome were not altered significantly by the length of the anchor, and were thus very similar for compounds **1**-**3** (see Table 3.1). Kinetic stability data were extracted by exponential fitting of the time-dependent absorbance of MC, observed at its absorption maximum (e.g., for **1MC:** 501 nm, ε = 30100 M^{-1} cm^{-1}; Figure 3.2). Similar kinetics with biexponential "rise and decay" behavior have been reported for related spiropyrans.[18,20] In this study, the fitting yielded a rise time constant of τ_1 = 6.5 h, corresponding to a rate constant of k_1 = 4.3 × 10^{-5} s^{-1}. In a first approximation,[16] this rate constant corresponds to the sum of the rate constants for ring opening (**1SP→1MC**) and closing (**1MC→1SP**), $k_{opening}$ and $k_{closing}$, respectively (Scheme 3.4). The decay time constant τ_2 = 47.4 h (k_2 = 5.3 × 10^{-6} s^{-1}) corresponds mainly to the hydrolytic decomposition of **1MC**. This process was significantly slower for **1** than that recently reported for nitrospiropyran **4**, for which $\tau_2 \approx$ 7 h was determined at pH 7.[18]

Table 3.1 – Rate constants for the rise (k_1) and decay (k_2) of the MC forms of **1**, **2**, and **3** in 10 mM phosphate buffer (pH 7) at 293 K.

Compound	k_1 [s^{-1}]	k_2 [s^{-1}]	k_1 (CB7)* [s^{-1}]	k_2 (CB7)* [s^{-1}]
1	4.3 × 10^{-5}	5.3 × 10^{-6}	3.2 × 10^{-3}	0
2	5.5 × 10^{-5}	7.2 × 10^{-6}	3.8 × 10^{-4}	1.8 × 10^{-6}
3	2.7 × 10^{-5}	2.2 × 10^{-6}	7.0 × 10^{-5}	1.6 × 10^{-6}

*In presence of 20 equivalents of CB7.

As mentioned above, the generally observed hydrolytic instability of spiropyrans is an important limiting factor for their applications in aqueous medium.[18,20] For example, this may be a problem for the storage capability of the MC form during long-term experiments in water. Hydrolysis is known to be initiated by nucleophilic attack at the ene–iminium cation followed by a retro-aldol reaction, which results in Fischer's base (**6**) and 4-nitrosalicylaldehyde (**7**) (Scheme 3.4).[18] One way to avoid this problem in our system is by lowering the pH, where no signs of hydrolysis are observed within 24 h. At pH≤3, the **1MC** form is transformed into the stable protonated form **1MCH**, which is accompanied by a hypsochromic shift of the long-wavelength absorption maximum (λ_{max} = 405 nm, ε = 26600 M^{-1} cm^{-1}, pK_a = 4.2; Figure 3.2 and 3.3). However, in biological studies such acidic pH is not desirable.

The irradiation of **1MCH** at 430 nm or **1MC** at 503 nm induced ring closure to yield **1SP**. Under the chosen irradiation conditions, the time constants for these photoprocesses are in the order of a few seconds (see the Experimental Procedure in the Chapter 7): 5.0 s for **1MC** and 5.1 s for **1MCH**. Noteworthy, for **1MC** the competing hydrolysis process is considerably slower (see Table 3.1 for the rate constants). The quantum yield for the photoinduced **1MC→1SP** ring closure was determined to be $\Phi_{\mathbf{1MC\rightarrow 1SP}}$ = 0.03, whereas the conversion of **1MCH→1SP** proceeded with $\Phi_{\mathbf{1MCH\rightarrow 1SP}}$ = 0.04.

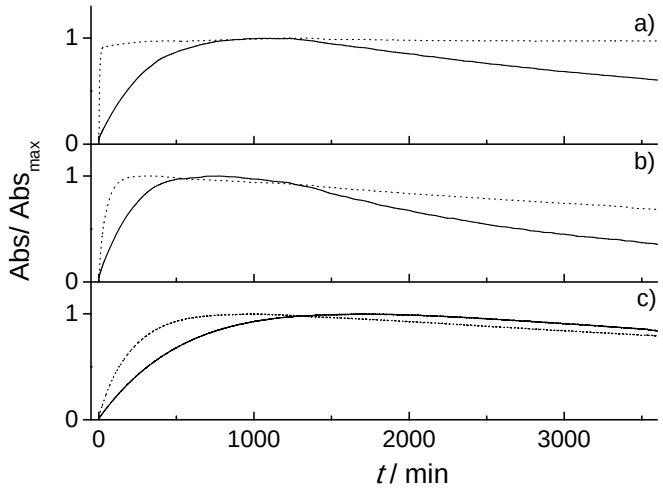

Figure 3.2 – Kinetic traces (monitored at the respective UV/vis absorption maxima) of a) **1**, b) **2**, c) **3**, reflecting the thermal ring opening of the SP form and subsequent hydrolysis of the MC form in the absence (—) and presence (···) of CB7 (20 equivalents). All traces were measured at 293 K.

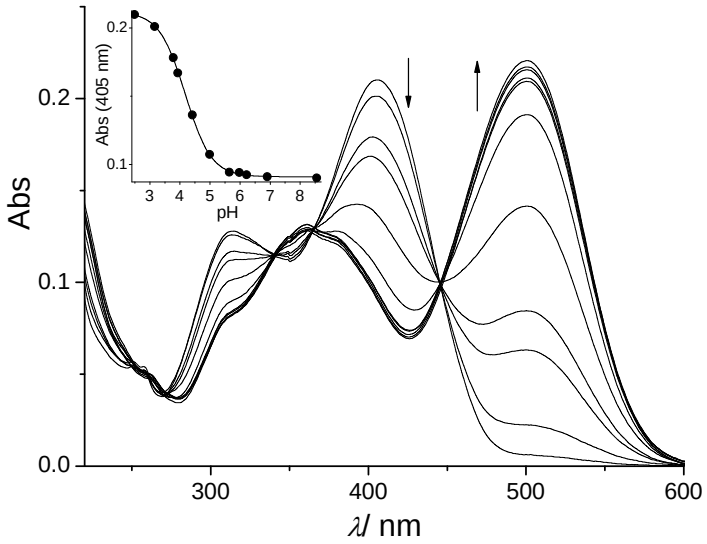

Figure 3.3 – Absorption spectra of 10 µM **1MCH** from pH 2.5 to 8.6 (**MCH→MC**, acidochromic interconversion, isosbestic point at 446 nm). The inset shows the corresponding pH titration curve at λ_{obs} = 405 nm.

3.3.2 Characterization of the Supramolecular Spiropyran-CB7 Assembly

In the presence of CB7, the spiro form **1SP** rapidly converted into **1MC**. This hampered our attempts to obtain clear-cut data for the binding efficiency of this form. In attempt to overcome this obstacle, continuous irradiation with visible light (465 nm long-pass filter) was employed during the titration procedure. In this way, **1MC** was steadily converted back to **1SP**. This enabled us to follow at least some spectral changes in the UV/vis absorption spectrum on addition of the CB7 macrocycle (at pH 7). As a result a bathochromic shift of about 13 nm (λ_{max} = 365 nm for **1SP**/CB7) was observed, which lent some qualitative support to the possible complexation by CB7.

On the other hand, the inherently stable protonated form **1MCH** allowed the convenient monitoring of the UV/vis absorption titration with CB7 at pH 2.5 (see Figure 3.4 a). The titration could be divided in two phases. First an initial decrease of the absorption band at 405 nm accompanied by a slight hypsochromic shift by

about 2–3 nm was observed. This was followed by the growth of a bathochromically shifted band with a maximum at 420 nm, accompanied by an isosbestic point at about 409 nm. The global fitting according to the consecutive complexation of two CB7 macrocycles by **1MCH** yielded the following binding constants: K_{b1} = 7.9 × 10^5 M^{-1} and K_{b2} = 1.3 × 10^3 M^{-1}. Constant K_{b1} is tentatively assigned to the binding of the anchor by CB7. The second binding constant, K_{b2}, may be associated with the rather hindered formation of an *exo* complex with the indolenium part of the molecule. Also the **1MC** form was stable enough on the timescale of an UV/vis absorption titration experiment (Figure 3.4 b). A similar behavior to that noted for **1MCH** was observed. Namely, the long-wavelength band decreased and shifted bathochromically by about 4 nm in the first phase of the titration. This was followed by a further shift of the absorption maximum to 526 nm and which was accompanied by a hyperchromic effect. The global fitting (consecutive formation of 1:1 and 1:2 complexes) yielded K_{b1} = 1.2 × 10^5 M^{-1} and K_{b2} = 8.6 × 10^3 M^{-1} for **1MC**. The somewhat lower binding constant K_{b1} in comparison to that of **1MCH** reflects the negative charge at the supposedly nearby phenolate oxygen, which interferes the carbonyl-laced CB7 portals. Job's plots for both ring-open forms at a total concentration of 10 μM yielded a maximum at 0.5, which corroborated the formation of a 1:1 complex in a low-concentration regime (see Figure 3.5).

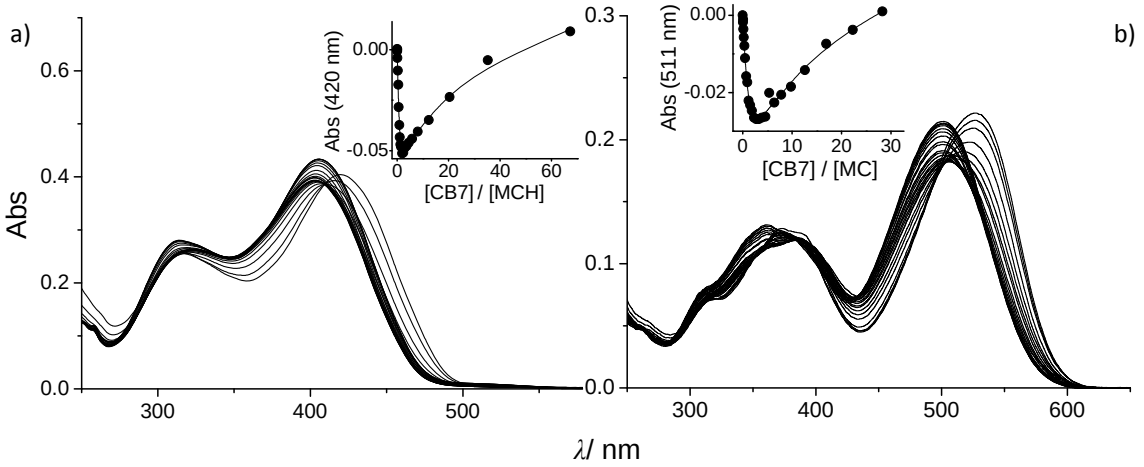

Figure 3.4 – Absorption titration of a) **1MCH** (*ca.* 16 μM) at pH 2.5, and b) **1MC** (*ca.* 9 μM) at pH 7, with CB7. The insets show the corresponding Absorption changes at a) 420 nm, b) 511 nm upon CB7 addition. The solid line illustrates the fit in according to consecutive complexation of two macrocycles.

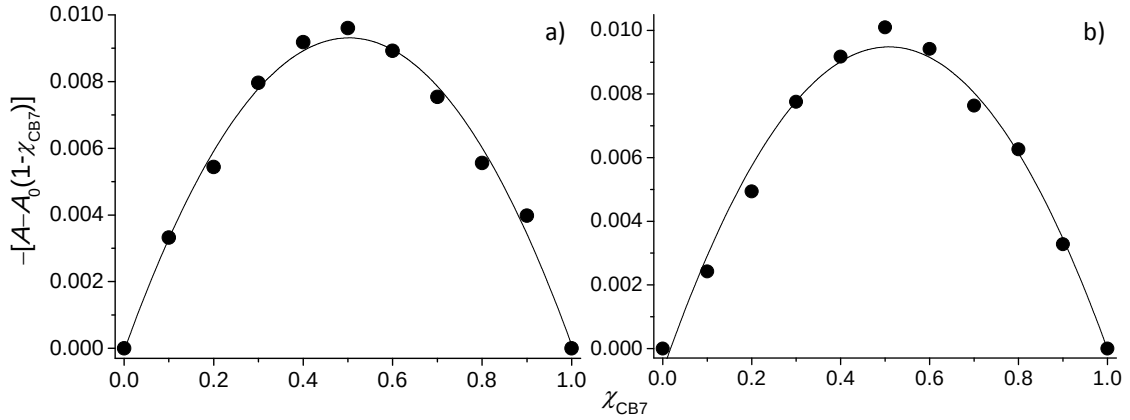

Figure 3.5 – Job's Plot for a) **1MC**/CB7 (pH 7.5) with λ_{obs} = 501 nm, and b) **1MCH**/CB7 (pH 2.6) with λ_{obs} = 406 nm. The total concentration of both components was fixed at 10 μM. The formation of a 1:1 complex is evident by the maximum at 0.5.

Complementary evidence for the formation of a complex between the anchor and CB7 was obtained by ^{1}H NMR spectroscopy (Figure 3.6 and 3.7). For this experiment, the **1MC** form was used. Of particular interest are the protons of the anchor (H_f–H_k) and the aromatic protons of the indolenium ring (H_m–H_p, see Scheme 3.5 for letter codes). The terminal methylene protons of the anchor were observed as isolated triplets at δ = 4.48 and 3.09 ppm for H_f and H_j, respectively. The ammonium methyl protons (H_k) were assigned to a singlet at δ = 2.82 ppm. The aromatic protons H_m–H_p appeared as a group of multiplets in the range of δ = 7.5 – 7.8 ppm. In agreement with the encapsulation of the anchor by the CB7 cavity a signal broadening and substantial upfield shifts of the protons H_f–H_k were noted on adding CB7. For example, the H_j and H_k protons underwent clear upfield shifts by 0.72 and 0.81 ppm, respectively. Interestingly, signal broadening was much less evident for the aromatic H_m–H_p protons and no upfield shifts were observed. This lends some support to the interpretation that the anchor constitutes the preferential CB7 complexation site.

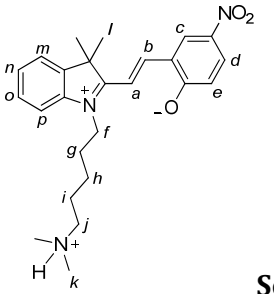

Scheme 3.5 – Structure of **1MC** and letter code for ^{1}H NMR studies.

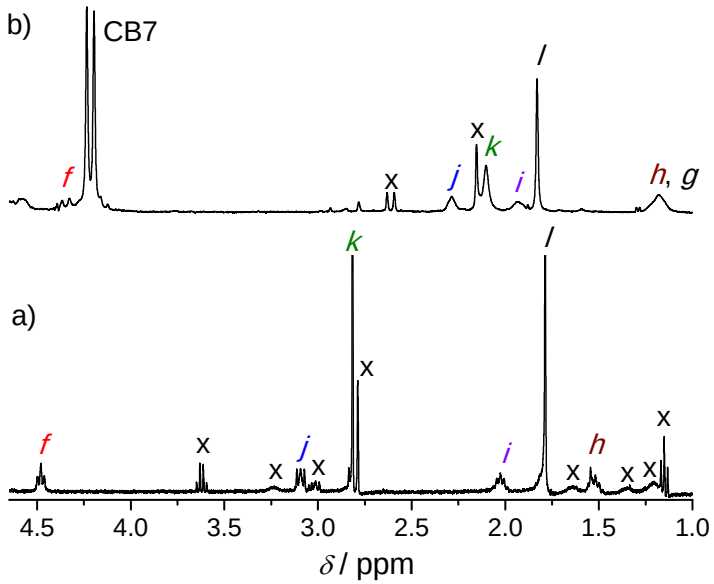

Figure 3.6 – Aliphatic region of the ^{1}H NMR spectrum of **1MC** (with *ca*. 10% **1SP**) in a) absence and b) presence of excess CB7. The signals marked with x refer to residual ethanol and **1SP** signals (spectrum a) or to minor impurities (spectrum b, e.g., the signal at *ca*. 2.2 ppm is commonly ascribed to encapsulated acetone resulting from the purification of the CB7 sample). The minor signals of **1SP** in spectrum a) disappeared in presence of CB7 due to an efficient conversion to **1MC**. Proton H_g in spectrum a) was difficult to assign and is very likely hidden under the signal at *ca.* 1.8 ppm.

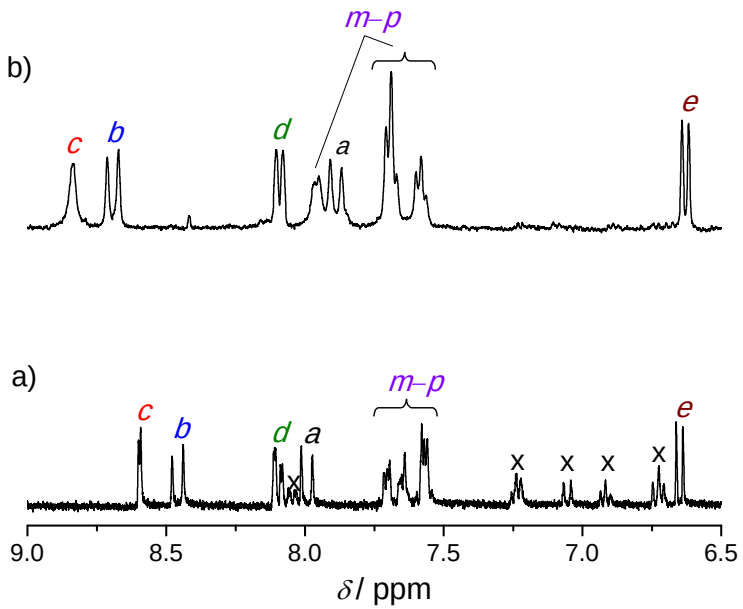

Figure 3.7 – Aromatic region of the ^{1}H NMR spectrum of **1MC** (with *ca*. 10% **1SP**) in a) absence and b) presence of excess CB7. The signals marked with x refer to residual **1SP** (a).

The mass spectrometric characterization (ESI-MS) of free **1MCH** and its complex with CB7 yielded further interesting insights in support of complex formation in the gas phase. The free guest showed signals at m/z 422 and 211, with isotope pattern spacings (Δm) of 1.0 and 0.5, consistent with singly and doubly charged ions, respectively (Figure 3.8 a). Therefore these signals were assigned to **1MC** and **1MCH**, respectively, indicating partial deprotonation of **1MCH** upon ionization. The fragmentation of the ion with m/z 422 yielded major peaks at m/z 325 and 160 (Figure 3.9 a). These data underline the formation fragments corresponding to 4-nitro-2-vinylphenol and the *N*,*N*-dimethylaminoalkyl-derived anchor (Scheme 3.6). The fragmentation of the m/z 211 ion was more complex and far less conclusive (Figure 3.9 b).

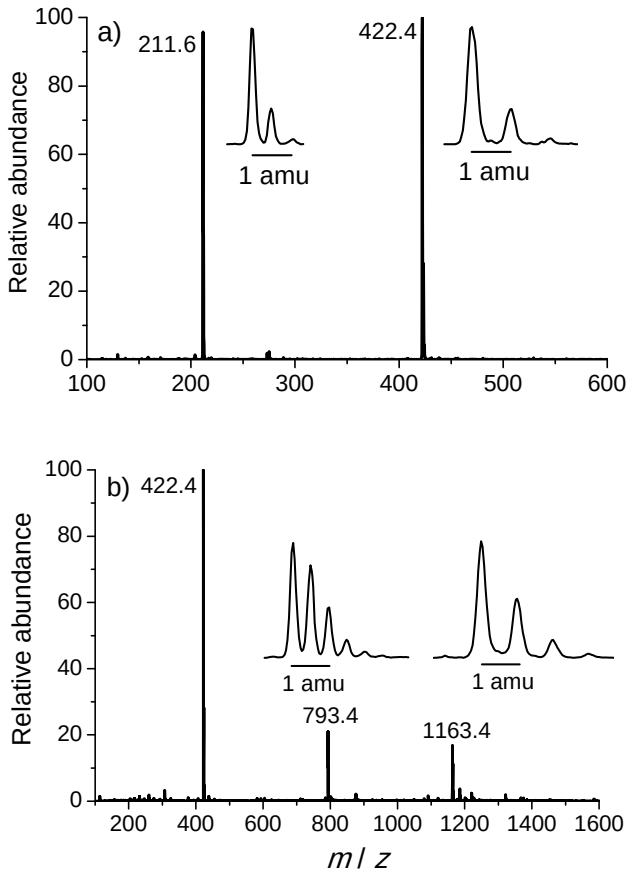

Figure 3.8 - ESI-MS spectra (full scans) of a) free **1MCH** and b) **1MCH/**CB7 at pH 2.5. The insets show the corresponding isotope patterns. Assignments with charge indication: m/z: 211.6 [**1MCH** + H]$^{2+}$, 422.4 [**1MC**]$^{+}$, 793.4 [**1MCH** + CB7 + H]$^{2+}$, 1163.4 [CB7 + H]$^{+}$.

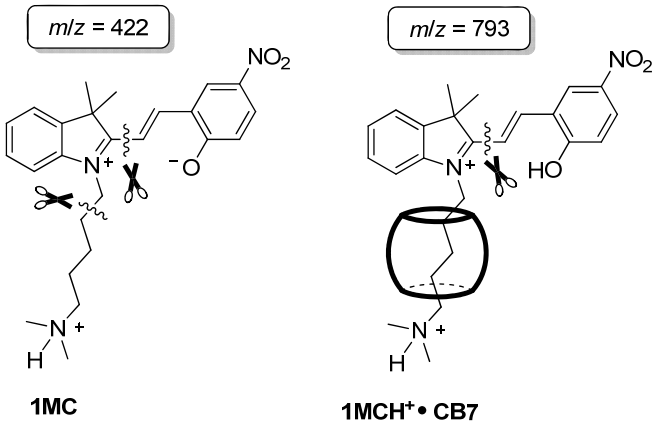

Scheme 3.6 – Proposed fragmentations of **1MC** and **1MCH**/CB7 in the gas phase.

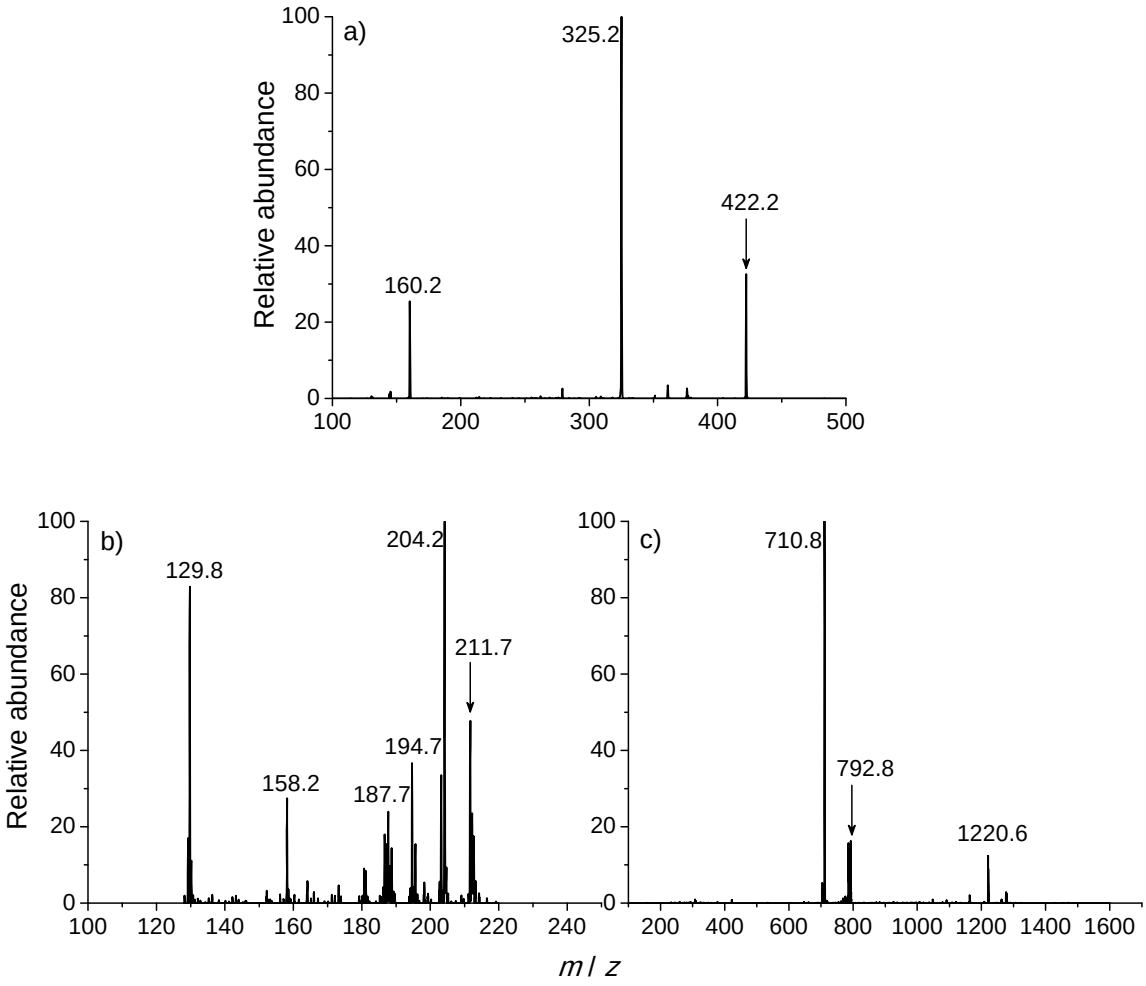

Figure 3.9 – Fragmentation of a) [**1MC**]$^{+}$ (m/z 422.2), b) [**1MCH** + H]$^{2+}$ (m/z 211.7), and c) [**1MCH +** CB7 + H]$^{2+}$ (m/z 792.8). The arrows indicate the fragmented peaks.

The presence of CB7 changed the ESI-MS spectrum significantly (Figure 3.8 b). The free deprotonated guest **1MC** (m/z 422) was present together with ions at m/z 1163 and 793. The former ion was readily assigned to the singly protonated CB7,[23] while the doubly charged ion (Δm = 0.5) at m/z 793 belongs to the 1:1 complex between **1MCH** and CB7. The merocyanine guest prevails as the MCH form in the complex, most likely due to a disfavored deprotonation. The MS^2 of the ion at m/z 793 yielded a main peak at m/z 711 (Figure 3.9 c), which indicated the loss of the 4-nitro-2-vinylphenol moiety. However, no fragmentation at the anchor was seen, which indicated a protective effect exerted by the CB7 macrocycle in the gas phase.

As described previously (see Chapter 1), CB*n* complexation of organic guests with functions that can be protonated is known to impose changes of the protonation constants, known as host-assisted guest protonation.[24] In the present study, the phenolic moiety has a pK_a value of 4.2 for the uncomplexed guest **1MCH**, which shifted to pK_a' = 5.0 for the CB7 complex, that is, ΔpK_a = 0.8 (Figure 3.10). The increased basicity of the phenolic oxygen is in agreement with the somewhat stronger binding of **1MCH** by CB7 (see above). Additional evidence for the role of the CB7 macrocycle in the shift of protonation equilibria can be obtained by the application of the four-state thermodynamic cycle shown in Scheme 3.7,[24] which yields Equation 3.1. With the CB7 binding constants of **1MC** and **1MCH**, a pK_a shift of 0.8 units was predicted, which was in agreement with the experimentally verified shift.

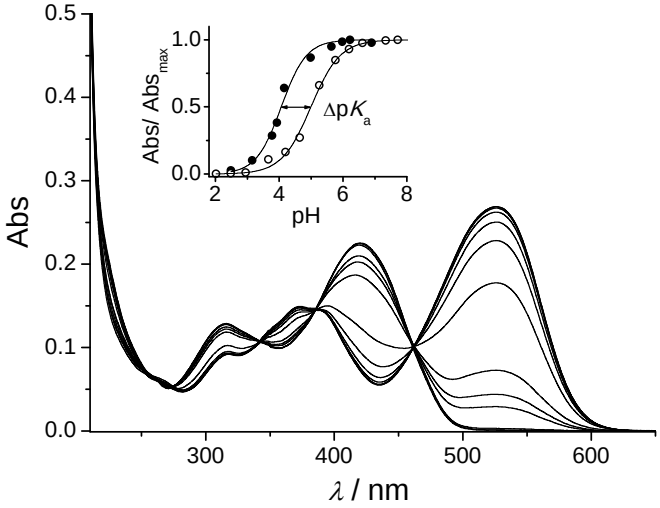

Figure 3.10 – pH Titration of **1MC** in the presence of CB7 (20 equivalents). The inset shows the titration curves for the MC absorption maximum in presence (○) and absence (●) of CB7.

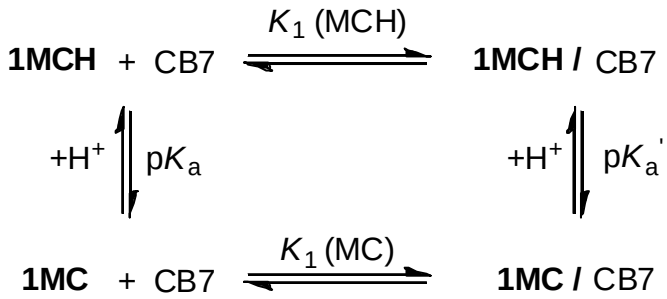

Scheme 3.7 – Four-state model for the complexation of **1MC** and **1MCH** by CB7. Note that only 1:1 complexation with the anchor moiety was considered.

$$\frac{K_1(\mathrm{MCH})}{K_1(\mathrm{MC})} = 10^{\Delta \mathrm{p}K_a} \qquad \textbf{Equation 3.1}$$

The indoline nitrogen of **1SP** can be protonated as well.[25] However, the pH titrations of **1SP** were complicated by the thermal ring opening (**1SP**→**1MC**) in presence of CB7. Therefore, the experiments had to be performed under steady irradiation with visible light (λ > 465 nm), as described above. Under these conditions protonation constants of pK_a = 1.4 and pK_a' = 3.2 were determined in the absence and presence of CB7, respectively (Figure 3.11). The decrease in pH resulted in the disappearance of the typical absorption of the SP form at around 350 nm and the buildup of a new band with a maximum at 310 nm, which is ascribed to the protonated spiro form **1SPH**.[25] The pK_a shift of almost two units corroborates the close interaction between the protonated indoline nitrogen and one of the CB7 portals. Thus, it can be assumed that the CB7 ring is capable of slipping completely over the anchor, accommodating one protonated nitrogen on each portal. Furthermore, it is reasonable to speculate that for two positively charged nitrogen atoms (indolenium and ammonium) in the ring-opened forms, **1MC** and **1MCH**, the same scenario applies. This lends indirect support to the assumption of complete immersion of the anchor into the CB7 cavity.

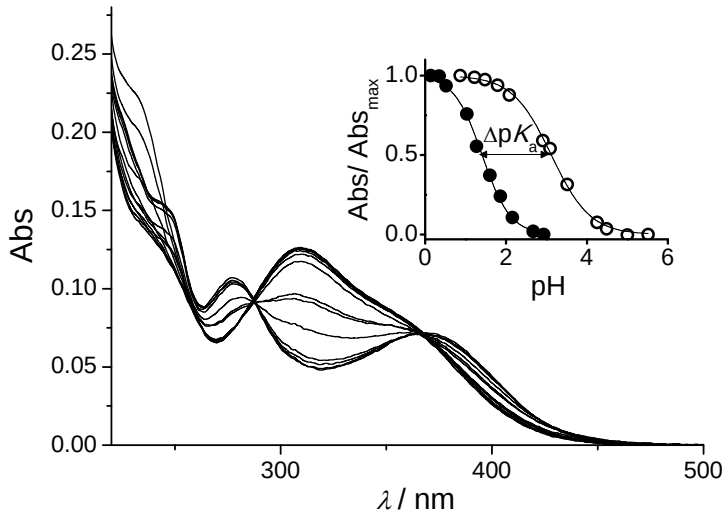

Figure 3.11 – pH titration of **1SP** in the presence of 20 equivalents CB7 under steady illumination with visible light (λ > 465 nm). The inset shows the titration curves for the SP in the presence (○) or absence (●) of CB7, respectively.

3.4 Photoinduced and thermal reactions in presence of CB7

The previously discussed CB7 complexation of the spiropyran anchor has interesting consequences for the thermally induced ring opening of **1SP** and the hydrolytic stability of **1MC** form. Importantly, the hydrolytic stability of the MC form is a crucial precondition for potential applications of spiropyrans in aqueous media.[4,6,18]

In the presence of CB7 (20 equivalents), **1SP**→**1MC** ring opening was considerably accelerated (Figure 3.2 a). The rise time constant for the appearance of the MC form was obtained from simple monoexponential fitting, τ_1 = 5.2 min (see rate constants in Table 3.1), due to the absence of hydrolysis of **1MC** in the presence of CB7 (see below). This was about 70 times faster than in the absence of CB7 (see Table 3.2). This rate-acceleration effect has been noted in related contexts of CB*n* chemistry.[21,26] However, for spiropyran **5**, no kinetic effect of CB7 on thermal ring opening at acidic pH was observed in a recent study.[22] This underlines the importance of the anchor for the observation of catalyzed ring opening. The composition of the equilibrium mixture was determined by ^{1}H NMR spectroscopy

as [**1MC**/CB7]/[**1SP**/CB7]> 95/5, corresponding to the absence of the SP form. The acceleration of **1MC** formation is explained by the presence of the positively charged indolenium nitrogen as an integral part of the anchor. This positive charge likely already partially develops in the transition state of the ring opening, which hence, experiences acceleration in the presence of CB7. This argument was underpinned by temperature-dependent kinetic measurements of the conversion of **1SP** into **1MC**. Arrhenius type data analysis (Figure 3.12) yielded an apparent activation energy, E_a, of 109 kJ mol^{-1} (preexponential factor A = 1.4 × 10^{15} s^{-1}; T = 293.15 – 320.15 K, 6 points, r^2 = 0.998) in the absence of CB7, in line with previous studies.[27] However, in the presence of CB7 (20 equivalents), the activation energy was considerably lower: E_a = 88 kJ mol^{-1} (pre-exponential factor A = 1.2 × 10^{13} s^{-1}; T = 293.15 – 315.15 K, 5 points, r^2 = 0.999). These complementary data support the observed kinetic effects of CB7 in the thermally induced formation of **1MC**.

Table 3.2 - Rate ratios from values in Table 3.1.

Compound	k_1 **(CB7)**/k_1	k_2 **(CB7)**/ k_2
1	73.00	≈ 0
2	7.00	0.26
3	2.60	0.72

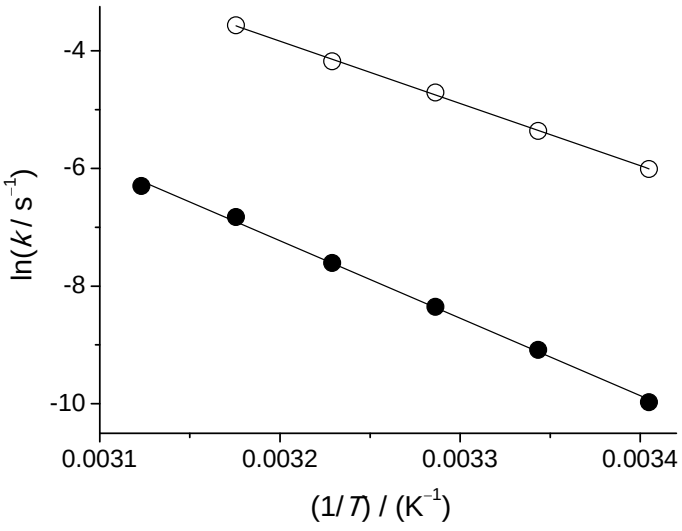

Figure 3.12 - Arrhenius plot of **1SP** thermal ring opening in the presence (○) and absence (●) of 20 equivalents CB7 at pH 7.

The beneficial effects of CB7 complexation extend further to a dramatically increased stability of the MC form against undesired hydrolysis. While, as discussed above, the **1MC** underwent considerable degradation in hours, the **1MC**/CB7 complex showed impressive long term stability. In practice, no decay of the characteristic MC absorption was observed after 2.5 days at 293 K (Figure 3.2). In contrast, in the same time period, already about 40% of uncomplexed **1MC** was irreversibly hydrolyzed. Noteworthy, the known long-term thermal stability of the protonated MC form (**1MCH** in our case) was not altered by CB7. Independently of the absence or presence of CB7 host macrocycle, practically no change occurred in the **1MCH** absorption over 24 h.

To show that the supramolecular complexation with CB7 caused the observed effects stabilization effects on **1MC**, a control experiment with an efficient competitor for the macrocycle was performed. The well-reported preference of CB7 for cadaverine (K_b = 2.0 × 10^7 M^{-1} in water at pH 7; see Figure 7.2) was used to remove the macrocycle from the anchor in a competitive displacement. As shown in Figure 3.13, the release of the photochrome resulted in increased vulnerability toward hydrolysis, which followed a similar kinetics as observed for **1MC** in the absence of CB7. Importantly, cadaverine itself had no influence on the decomposition kinetics of uncomplexed **1MC**.

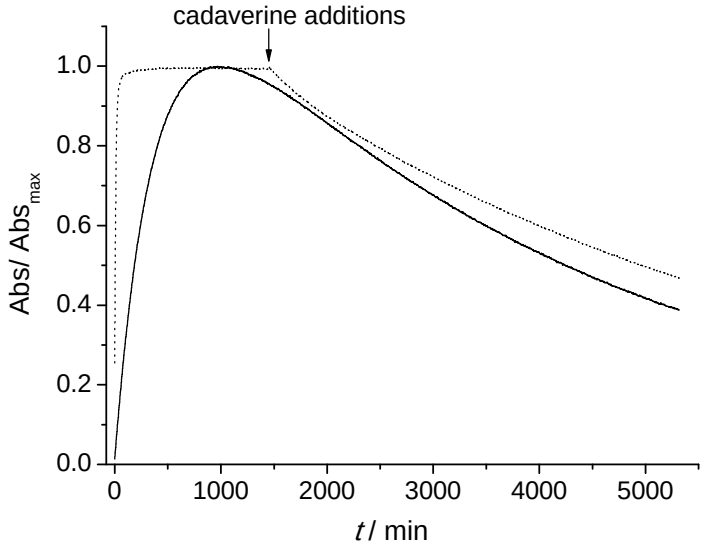

Figure 3.13 – Thermal ring opening of **1SP** in the presence (solid line), and absence of CB7 (20 equivalents, dashed line). At *t* = 24 h, cadaverine (100 equivalents) was added to both samples.

The importance of the anchor design was further evaluated by including the spiropyrans **2** and **3** in the study. In compound **2**, the anchor is shortened by two methylene groups. Based on reported data for the complexation of 1,*n*-bisammoniumalkanes by the homologous CB6, it can be anticipated that n = 5 – 6 is an ideal situation for strong complexation, whereas n = 3 will lead to complexes with inferior stability.[28] Hence, different effects based on a weaker supramolecular interaction with CB7 may be expected for compound **2** (Table 3.1 and Figure 3.2). The rise time constant for MC formation (τ_1 = 5 h) of the uncomplexed photochrome was very similar to that observed for spiropyran **1**. However, in comparison to **1**, the addition of CB7 (20 equivalents) to spiropyran **2** led to a less pronounced rate acceleration (factor of just 7) for MC formation (τ_1 = 44 min), see also rate constants in Table 3.2. In addition, the hydrolytic stability of **2** in the presence of CB7 was inferior (τ_2 = 36.5 h). Note that for **1MC**/CB7 the hydrolysis time constant τ_2 is practically infinite. Spiropyran **3**, which contains no anchor but a positively charged amidinium group in the 6-position, showed a slightly increased rate for **3MC** formation upon addition of CB7 (factor of *ca.* 2.6) and a practically unchanged hydrolysis rate (see rate constants in Table 3.2 and kinetic traces in Figure 3.2). These control experiments corroborated that the observed effects were related to the supramolecular encapsulation of the anchor. It is interesting to note that the recently reported partial encapsulation of spiropyran **5** by CB8 yielded a sixfold slower hydrolysis rate than that of the uncomplexed photochrome.[21] This corresponds roughly to the effects observed herein for photochrome **2** with a moderately efficient anchor. Based on these data, it becomes clear that the described molecular design based on an anchor approach constitutes a viable strategy for extraordinary MC stabilization.[20,21,29]

To test the influence of anchor complexation on the photoreactivity of the open forms (**1MC** and **1MCH**), samples of uncomplexed and CB7-complexed guests were irradiated under identical conditions. **1MC** and **1MCH** in their complexes showed the same efficient photoreaction as in the absence of CB7. The time constants for the photoinduced ring closing of **1MC** and **1MCH** in the presence of CB7 were determined to be $\tau \approx$ 3.5 and 6.0 s, respectively, which was very comparable to the kinetics observed for the uncomplexed guests (see section 3.3.1). In the presence of CB7, the photoreaction was characterized by the following quantum yields:

$\Phi_{\mathbf{1MC/CB7 \rightarrow 1SP/CB7}}$ = 0.06 and $\Phi_{\mathbf{1MCH/CB7 \rightarrow 1SPH/CB7}}$ = 0.04, also very similar to the behavior of the non-complexed photochrome. These results are in sharp contrast to the reported behavior of the CB8 complex of the MC form of **5**, for which a confinement effect considerably slowed down the photochromic ring closing.[21] This drawback was eliminated by the anchor approach adopted herein, which does not impose any confinement effect because the photochromic unit is not directly encapsulated in the CB7 cavity. It should be noted that a recent study showed that the partial CB7 inclusion of the MCH form of **5** even led to a slightly enhanced photoisomerization rate to the SP form under acidic conditions.[22] Irradiation of **1MC**/CB7 produced the typical absorption spectrum of the SP form as a photoproduct (see Figure 7.1). However, the irradiation of **1MCH**/CB7 yielded a product absorption spectrum (λ_{max} = 310 nm) that corresponded to the protonated spiro form (**1SPH**). According to the protonation constant of the free **1SPH** (pK_a = 1.4), the photoirradiation of **1MCH** at pH 2.5 in the absence of CB7 yielded the unprotonated **1SP**. On the other hand, the phototransformation of **1MCH**/CB7 at pH 2.5 resulted in CB7-complexed **1SPH** (pK_a = 3.2).

After demonstrating that the photochromic properties were maintained in the complexes, it was finally aimed to show that the CB7-modulated fast thermal SP to MC conversion and the photoinduced back reaction could be recycled repeatedly. The result of these experiments is shown in Figure 3.14. The thermal **1SP→1MC** transformation in the presence of CB7 (20 equivalents) was run for 30 min, which was sufficient to reach the maximum conversion to **1MC**. Then, visible-light irradiation (λ > 465 nm, 1.67 Wcm^{-2}) was applied for 40 s, which yielded the **1SP** form. Remarkably, in ten cycles no fatigue effect of the photochromic system was noted, which was the result of a clean thermal ring opening, the high hydrolytic stability of the MC, and an efficient photoinduced back isomerization.

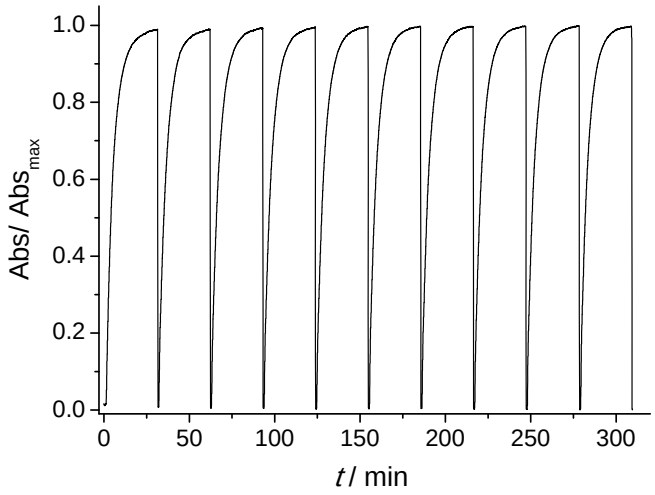

Figure 3.14 – Reversible switching between **1SP** and **1MC** in presence of CB7 (20 equivalents). Thermal **1SP→1MC** conversion run for 30 min, while **1MC→1SP** was achieved by irradiation at λ > 465 nm for 40 s. The absorbance was monitored at 526 nm.

3.5 Conclusion

In this study an improved supramolecular strategy to upgrade the switching and stability properties of spiropyrans was devised. This approach led to an impressive rate-accelerated formation and long-term protection of the MC form (**1MC**) against hydrolytic degradation. Furthermore, a fast, clean, and fatigue-resistant photoinduced ring closure back to the spiro form was observed for the MC-CB7 complex.

The observed kinetic and thermodynamic effects can be rationalized based on the strong binding of the macrocycle to the cadaverine-derived anchor of **1**. The importance of an adequate anchor design is underlined by the much less pronounced benefits for **2**, containing a shorter anchor. The absence of an anchor, as in **3**, turns the system into a spiropyran with commonly observed hydrolytic instability. Contrary to other efforts to stabilize the MC form by inclusion in supramolecular macrocycles, the photoinduced back conversion to the SP form was not negatively affected by the presence of the host macrocycle.

The remarkable hydrolytic stability and the robust photoswitching performance of the supramolecular assembly may provide a new drive for the further application of spiropyrans in aqueous solutions.

References

(1) Szymański, W.; Beierle, J. M.; Kistemaker, H. A. V.; Velema, W. A.; Feringa, B. L. *Chem. Rev.* **2013**, *113*, 6114.

(2) Mal, N. K.; Fujiwara, M.; Tanaka, Y. *Nature* **2003**, *421*, 350.

(3) Klajn, R. *Chem. Soc. Rev.* **2014**, *43*, 148.

(4) Minkin, V. I. *Chem. Rev.* **2004**, *104*, 2751.

(5) Durr, H.; Bouas-Laurent, H. *Photochromism: Molecules and systems*; 2nd ed.; Elsevier: Amsterdam, 2003.

(6) Kamiya, Y.; Asanuma, H. *Acc. Chem. Res.* **2014**, *47*, 1663.

(7) Natali, M.; Giordani, S. *Chem. Soc. Rev.* **2012**, *41*, 4010.

(8) Barachevskii, V. A.; Karpov, R. E. *High Energ. Chem.* **2007**, *41*, 188.

(9) Tong, R.; Hemmati, H. D.; Langer, R.; Kohane, D. S. *J. Am. Chem. Soc.* **2012**, *134*, 8848.

(10) Zhu, M.-Q.; Zhang, G.-F.; Li, C.; Aldred, M. P.; Chang, E.; Drezek, R. A.; Li, A. D. Q. *J. Am. Chem. Soc.* **2011**, *133*, 365.

(11) Tyer, N. W.; Becker, R. S. *J. Am. Chem. Soc.* **1970**, *92*, 1289.

(12) Moniruzzaman, M.; Sabey, C. J.; Fernando, G. F. *Polymer* **2007**, *48*, 255.

(13) Swansburg, S.; Buncel, E.; Lemieux, R. P. *J. Am. Chem. Soc.* **2000**, *122*, 6594.

(14) Gorner, H. *PCCP* **2001**, *3*, 416.

(15) Bletz, M.; Pfeifer-Fukumura, U.; Kolb, U.; Baumann, W. *J. Phys. Chem. A* **2002**, *106*, 2232.

(16) Nilsson, J. R.; Parente Carvalho, C.; Li, S.; Da Silva, J. P.; Andréasson, J.; Pischel, U. *ChemPhysChem* **2012**, *13*, 3691.

(17) García, A. A.; Cherian, S.; Park, J.; Gust, D.; Jahnke, F.; Rosario, R. *J. Phys. Chem. A* **2000**, *104*, 6103.

(18) Stafforst, T.; Hilvert, D. *Chem. Commun.* **2009**, 287.

(19) Li, X.; Li, J.; Wang, Y.; Matsuura, T.; Meng, J. *J. Photochem. Photobiol. A: Chem.* **2004**, *161*, 201.

(20) Li, R.; Santos, C. S.; Norsten, T. B.; Morimitsu, K.; Bohne, C. *Chem. Commun.* **2010**, *46*, 1941.

(21) Miskolczy, Z.; Biczók, L. *J. Phys. Chem. B* **2011**, *115*, 12577.

(22) Miskolczy, Z.; Biczók, L. *Photochem. Photobiol.* **2012**, *88*, 1461.

(23) Da Silva, J. P.; Jayaraj, N.; Jockusch, S.; Turro, N. J.; Ramamurthy, V. *Org. Lett.* **2011**, *13*, 2410.

(24) Marquez, C.; Nau, W. M. *Angew. Chem. Int. Ed.* **2001**, *40*, 3155.

(25) Wojtyk, J. T. C.; Wasey, A.; Xiao, N.-N.; Kazmaier, P. M.; Hoz, S.; Yu, C.; Lemieux, R. P.; Buncel, E. *J. Phys. Chem. A* **2007**, *111*, 2511.

(26) Saleh, N. i.; Koner, A. L.; Nau, W. M. *Angew. Chem. Int. Ed.* **2008**, *47*, 5398.

(27) Shiraishi, Y.; Itoh, M.; Hirai, T. *PCCP* **2010**, *12*, 13737.

(28) Mock, W. L.; Shih, N. Y. *J. Org. Chem.* **1986**, *51*, 4440.

(29) Piantek, M.; Schulze, G.; Koch, M.; Franke, K. J.; Leyssner, F.; Krüger, A.; Navío, C.; Miguel, J.; Bernien, M.; Wolf, M.; Kuch, W.; Tegeder, P.; Pascual, J. I. *J. Am. Chem. Soc.* **2009**, *131*, 12729.

Chapter 4

Supramolecular Control of Enzymatic Reactions

In this chapter, the inhibition enzymatically catalyzed restrictions of circular and linear DNA by CB6 and CB7 will be demosntrated. This effect can be inverted by supramolecular masking of the macrocycles through competitive complexation with polyamines. These observations demonstrate the possibility of exerting supramolecular control over biocatalytic processes.

4.1 Enzymes and CB*n*

The ability to control and guide biological functions are of crucial importance for innumerous applications in biochemistry, biotechnology, and pharmaceutical industries. Thus, it is of great interest to understand the chemical and biological properties of enzymes. CB*n* macrocycles can in principle be used as a tool to control biological functions *via* reversible supramolecular interactions with (a) substrates, (b) inhibitors/promoters or (c) directly with biocatalysts (see Scheme 4.1).

According to the strategies (a) and (b), shown in Scheme 4.1, several approaches for biological control with CB*n* have been developed. For instance, CB7 is known to protect peptides from protease-catalyzed hydrolytic degradation, which is an example of substrate-related supramolecular control of biological functions by CB*n* (strategy (a)).[1,2] As an example for strategy (b), CB7 can complex inhibitors of bovine carbonic anhydrase or acetylcholinesterase and thereby trigger catalytic reactions through competitive displacement of the enzyme inhibitors.[3] In the context of enzymatic transformations of DNA substrates, it was shown that the spermidine/CB6 complex catalyzes the topoisomerization of supercoiled plasmid

DNA and that CB6 can invert the promoting effect of spermine in plasmid DNA restriction (strategy (b)).[4] To date, there is no report on the direct control of a biocatalytic process by macrocycle-enzyme interactions (path (c) in Scheme 4.1). It was speculated that this might be the consequence of generally weak interactions between proteins and CB*n*, even though it is well established that different amino acids and peptides bind to different supramolecular hosts with variable strength and selectivity.[5-10]

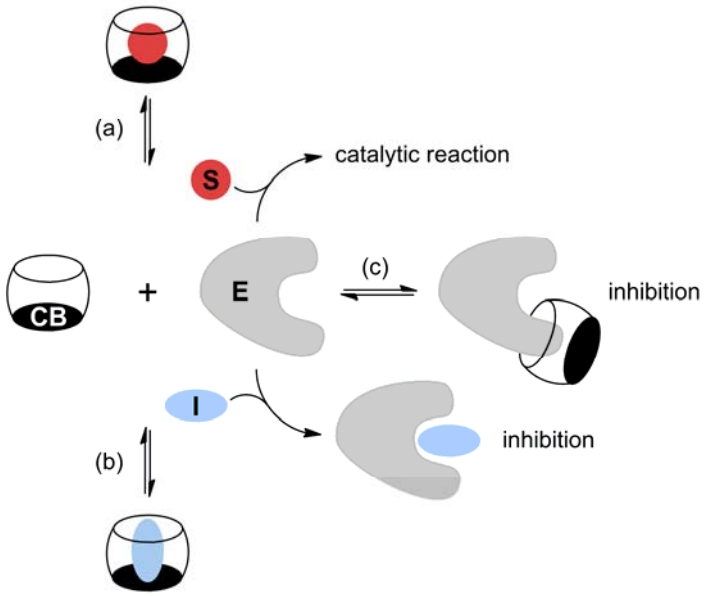

Scheme 4.1 – Supramolecular control of enzymatic catalysis by host macrocycles (e.g., CB*n*) *via* (a) substrate binding, (b) inhibitor binding, or (c) biocatalyst deactivation. E: enzyme, S: substrate, I: inhibitor.

In the course of this thesis work, an unprecedented inhibition of DNA restriction was unveiled, a process that plays a fundamental role in the defence of bacteria and archaea organisms against foreign DNA. This discovery, which will be discussed in the next section, is a nice example for strategy (c). It should be already noted at this point that the direct enzyme-CB*n* interaction is not straightforward to prove due to experimental limitations. However, host-guest binding of CB*n* with proteins such as human insulin and ubiquitins and with peptides was already described in the literature.[11-15]

4.2 Experimental Approach

The experimental procedure used in this study is described in detail in the experimental section of Chapter 7. Here, some aspects that an important for the understanding of the described results will be briefly outlined.

As model reaction, the enzymatic restriction of DNA was selected. Restriction assays are currently used to manipulate DNA for different scientific applications.[16-18] These assays constitute a good model to investigate how CB*n* can modulate enzyme activity because they are cost-effective, easy to manipulate, and allow for rapid monitoring using standard molecular biology tools. Endonucleases recognize and cleave specific DNA sequences (restriction sites), producing a number of smaller fragments.[19,20] Knowing the DNA template sequence, the number and size of these fragments can be accurately predicted. The resulting restriction pattern can be easily resolved by agarose gel electrophoresis, serving to monitor the enzymatic activity. For optimizing the assays and experimental approach, the enzyme and the appropriate DNA sequence had to be selected carefully. pGL3-Basic plasmid is a widely used vector and was chosen for this study (Scheme 7.1 and sequence in Chapter 7). This was also motivated by the fact that this template is well characterized and readily available.

In order to obtain the template DNA in high concentration and purity, pGL3-Basic plasmid was amplified in DH5α *E. coli* cells and subsequently purified with a commercially available kit. The amount of DNA in the assays was maintained constant, and both linearized and circular plasmid DNA were used. The linearized DNA was obtained from the circular form by employing a single-cut enzyme (*Pdm*I endonuclease).

To ascertain whether CB*n* macrocycles exert a generalized effect on restriction endonucleases, three different restriction enzymes were employed: *Kpn*I, *Sac*I, and *Xap*I. These type II restriction enzymes were chosen randomly for this proof of concept and it was made sure that each had their own amino acid sequence (shown in Chapter 7), restriction site (for different cutting positions), and even more than one cutting possibility. For this step, the online tools NEBcutter and

REBASE[21,22] were used to find matches for the previously chosen 4818 bp DNA sequence (pGL3-Basic plasmid).

In the next step the optimization of the restriction assays with *Kpn*I, *Sac*I, and *Xap*I enzymes for the different DNA substrates was accomplished. In the case of the presence of CB*n* the concentrations of the CB6 and CB7 macrocycles were adjusted to produce *ca*. 50% enzyme inhibition. The quantification of the degree of inhibition was performed by analysis of the resulting electrophoresis gels using the ImageJ tool.[23]

To determine if the inhibitory effect of CB*n* on the enzymatic activity is reversible, a competitor for the CB*n* cavity was introduced and its effects on the endonuclease activity were investigated. Cadaverine, putrescine, spermine, and spermidine are strongly binding CB*n* guests (e.g., K_b *ca*. 10^5-10^7 M^{-1} for CB7; see Scheme 4.2) and were used as the competitors. Furthermore, several control experiments were performed in an attempt to disclose the likely cause for the modulation of the enzyme activity by CB*n*; see below.

Putrescine
(K_b= 1.0 × 10^5 M^{-1} with CB7)

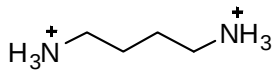

Cadaverine
(K_b= 2.0 × 10^7 M^{-1} with CB7)

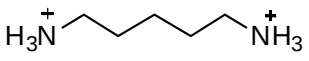

Spermine
(K_b= 4.1 × 10^8 M^{-1} with CB6)

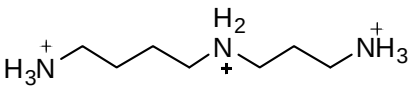

Spermidine
(K_b= 3.3 × 10^9 M^{-1} with CB6)
(K_b= 1.2 × 10^6 M^{-1} with CB7)

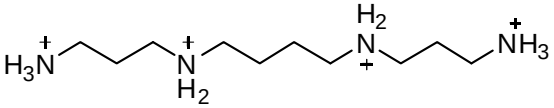

Scheme 4.2 – Structures and binding constants with CB6 or/and CB7 of the biogenic polyamines putrescine, cadaverine, spermidine, and spermine. K_b values with CB7 were calculated (see Figure 7.2), while CB6 values were taken from the literature.[24] Only binding constants that are of relevance for the performed study are given.

4.3 Modulation of Type II Endonuclease Activity

Taking advantage of molecular biology techniques it is possible to evaluate the hydrolysis of distinct DNA forms (circular and *Pdm*I-linearized) catalyzed by the endonucleases *Kpn*I, *Sac*I, and *Xap*I in the presence a CB*n* macrocycle and polyamines. As shown in Scheme 4.3, *Kpn*I and *Sac*I have one restriction site (GGTACC and GAGCTC, respectively), while *Xap*I has four [RAATTY; R is abbreviation for a purine (A or G), and Y to a pyrimidine (C or T)], resulting in distinct digestion patterns (see Scheme 4.4).

a)

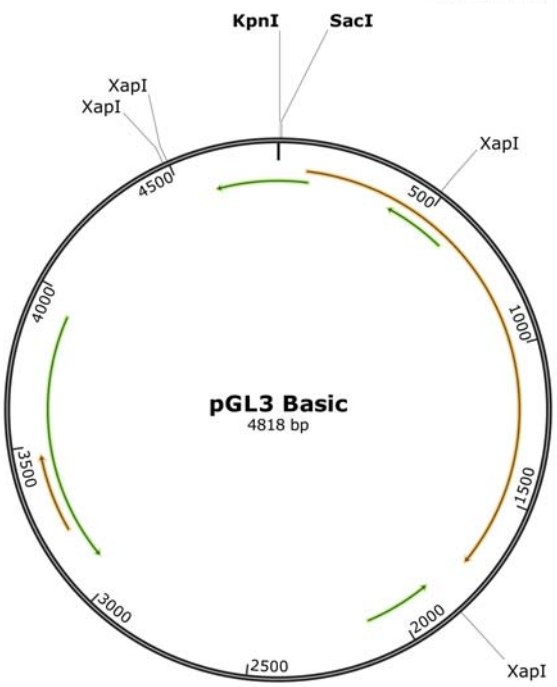

b)

Scheme 4.3 – Restriction map of pGL3-Basic DNA with the *Kpn*I, *Sac*I, and *Xap*I endonucleases, for the a) undigested plasmid (circular fragment), and b) *Pdm*I-digested plasmid (linear fragment).

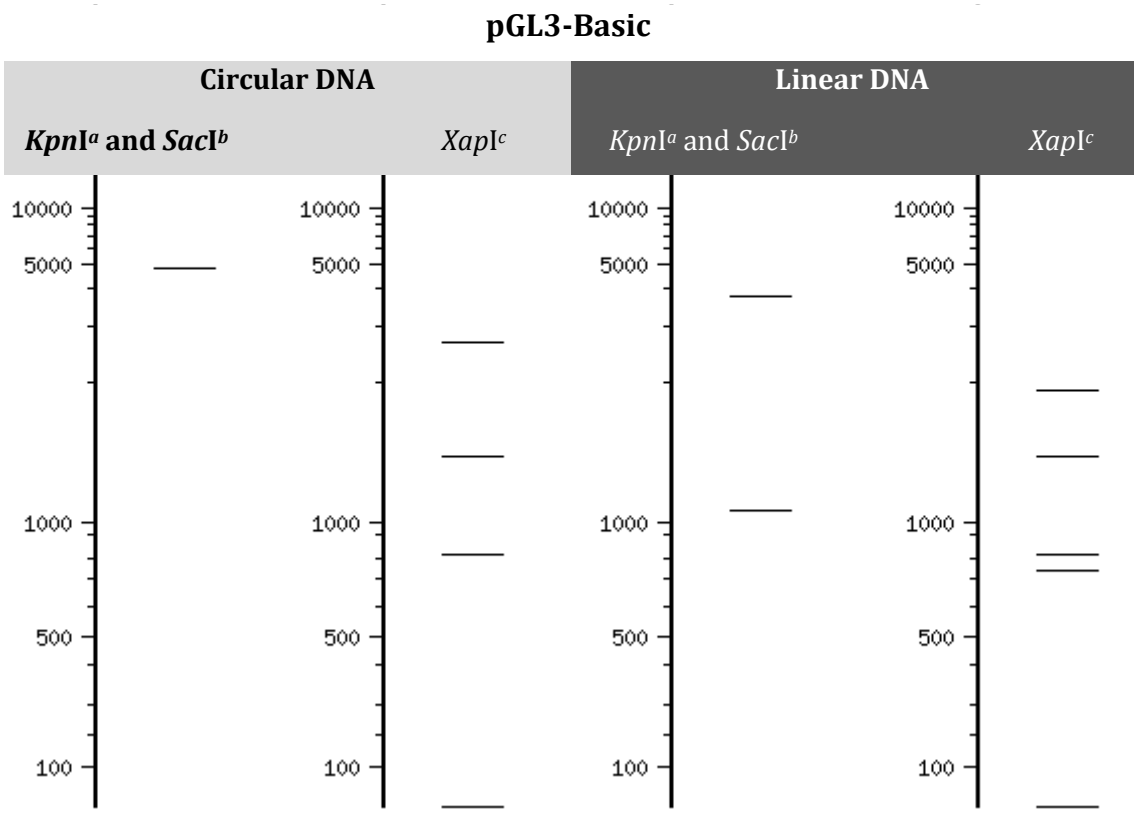

Scheme 4.4 –Theoretical digestion pattern of circular and *Pdm*I-linearized pGL3-Basic DNA (4818 bp) with *Kpn*I, *Sac*I and *Xap*I. [a] One restriction, creating a linear 4818 bp fragment for the circular DNA, while 3747 and 1071 bp fragments for the linearized. [b] One restriction, creating a linear 4818 bp fragment for the circular DNA, while 3741 and 1077bp fragments for the linearized. [c] Four restrictions, creating linear 2638, 1356, 813, 11 bp fragments for the circular, and 1905, 1356, 813, 733 and 11 bp fragments for the linearized DNA.

The hydrolysis of pGL3-Basic DNA catalyzed by the different endonucleases was conducted under identical conditions concerning pH, buffer composition, temperature, and digestion time (see Chapter 7). As first example, the hydrolysis of the DNA at GGTACC site by the endonuclease *Kpn*I (Figure 4.1) is described. The electrophoresis of the plasmid DNA alone evidenced its preferential presence in the supercoiled form (lane 1). Upon enzymatic hydrolysis of the plasmid DNA, the linear form appeared (lane 2). However, in the presence of 6 μM CB6 ([CB6]/[KpnI] = 4542, lane 3) the enzymatic reaction was significantly hindered leading to 47% inhibition with respect to the absence of the macrocycle. The

incomplete enzymatic reaction was confirmed by the observation of a substantial amount of non-restricted plasmid DNA in the electrophoresis. The restriction reaction can be re-activated by the addition of one equivalent of strongly competitive polycationic binders such as spermidine (K_b = 4.1 × 10^8 M^{-1}) and spermine (K_b = 3.3 × 10^9 M^{-1}),[24] lanes 5 and 8, respectively. In a control experiment, the enzymatic hydrolysis was performed in the presence of the amines but in the absence of CB6 (lane 4 and 7 *versus* lane 5 and 8, respectively). The result confirmed that the amine alone had no effect on the DNA restriction under the chosen experimental conditions.

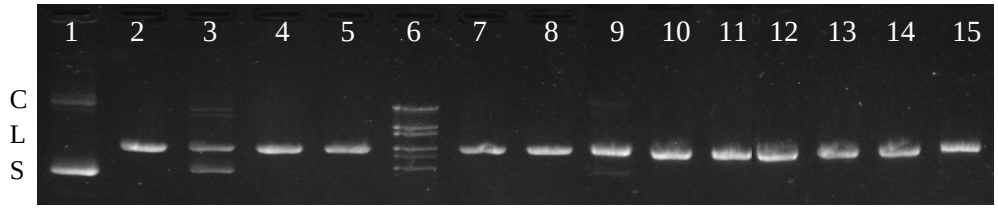

Figure 4.1 – Electrophoretic analysis of *Kpn*I enzymatic hydrolysis of plasmid pGL3-Basic DNA (lane 1: unrestricted DNA, lane 2: reaction in absence of other additives, lane 3: reaction in presence of CB6, lane 4: reaction in presence of spermidine, lane 5: reaction in presence of the complex spermidine/CB6, lane 6: λDNA/Eco91I (BstEII) marker, lane 7: reaction in presence of spermine, lane 8: reaction in presence of the complex spermine/CB6, lane 9: reaction in presence of CB7, lane 10: reaction in presence of spermidine, lane 11: reaction in presence of the complex putrescine/CB7, lane 12: reaction in presence of cadaverine, lane 13: reaction in presence of the complex cadaverine/CB7, lane 14: reaction in presence of putrescine, lane 13: reaction in presence of the complex putrescine/CB7; C = relaxed/nicked circular DNA, L = linear DNA, S = supercoiled DNA).

CB7 was also used as a supramolecular inhibitor of the restriction of circular or linearized pGL3-Basic DNA by the endonucleases. The results are resumed in Table 4.1 and shown in the Figures 4.1 to 4.6, where the macrocycle concentration (90-500 μM CB7) was adjusted to yield again *ca.* 50% inhibition. Furthermore, the polyamines putrescine, cadaverine, and spermidine were screened for their potential to fully re-activate the DNA restriction, which required 1-5 equivalents, depending on their relative affinity to the CB7 macrocycle.

Table 4.1 – Restriction assays (*Kpn*I, *Sac*I, and *Xap*I endonucleases) of circular and linear pGL3-Basic DNA sequence in the presence of CB7 macrocycle, and re-activation by the polyamines putrescine, cadaverine, and spermidine.

Components	Circular DNA			Linear DNA[a]		
	*Kpn*I[b]	*Sac*I[c]	*Xap*I[d]	*Kpn*I[b]	*Sac*I[c]	*Xap*I[d]
[CB7]/μM[e]	90	250	500	200	350	500
Inhibition (%)	32	42	54	48	52	58
[putrescine]/[CB7][f]	5	5	5	5	5	5
[cadaverine]/[CB7][f]	1	2	2	1	2	2
[spermidine]/[CB7][f]	2	1	1	2	1	1

[a] Obtained by total restriction of plasmid pGL3-Basic DNA with *Pdm*I endonuclease. [b] Restriction at GGTACC sites. [c] Restriction at GAGCTC sites. [d] Restriction at RAATTY sites. [e] Optimized CB7 concentration to achieve ca. 50% inhibition. [f] Optimized polyamine/macrocycle ratio for complete re-activation (< 5% inhibition); K_b / 10^{-6} M^{-1} with CB7 in water at pH 7 (see also Figure 7.2): 0.11 for putrescine, 20 for cadaverine, and 1.2 for spermidine.

In Figure 4.1, the behavior of circular pGL3-Basic DNA in the restriction reaction catalyzed by the *Kpn*I enzyme is resumed. Similar results as discussed for CB6 were obtained. In the following, the electrophoretic analysis of the *Kpn*I-induced hydrolysis of linear pGL3-Basic DNA, its inhibition by CB7, and the re-activation by addition of putrescine, cadaverine, or spermidine will be detailed (see Figure 4.2). The restriction reaction (lane 1) led to fragments with 3747 and 1071 bp, while in the presence of 200 μM CB7 (lane 2) the enzymatic hydrolysis was hindered (48% inhibition). The residual band of unrestricted DNA (4818 bp) reflected the latter conclusion. Adding different proportions of the amines putrescine, cadaverine, or spermidine ([putrescine]/[CB7] = 5; [cadaverine]/[CB7] = 1; [spermidine]/[CB7] = 2) sequestered the CB7 and thereby re-activated the process (lanes 4, 7, and 9). Controls in sole presence of the amines, but absence of CB7, showed no effect on the restriction (lanes 3, 6, and 8).

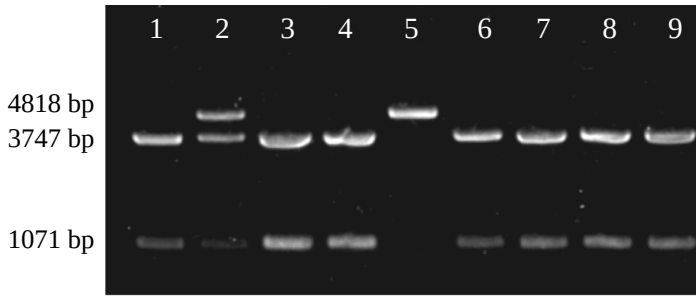

Figure 4.2 - Electrophoretic analysis of *Kpn*I enzymatic hydrolysis of linearized pGL3-Basic DNA (lane 1: reaction in absence of other additives, lane 2: reaction in presence of CB7 lane 3: reaction in presence of spermidine, lane 4: reaction in presence of the complex spermidine/CB7, lane 5: unrestricted DNA, lane 6: reaction in presence of cadaverine, lane 7: reaction in presence of the complex cadaverine/CB7, lane 8: reaction in presence of putrescine, lane 9: reaction in presence of the complex putrescine/CB7).

Similarly to the results observed for *Kpn*I, it was possible to reproduce the described effects of CB7 and polyamines for other endonucleases, see Table 4.1 and Figures 4.3 to 4.6. As predicted in Scheme 4.4, pGL3-Basic DNA has one recognition site (GAGCTC) for the *Sac*I enzyme. With circular DNA one linear fragment of 4818 bp was produced (Figure 4.3) and for the linearized DNA two linear fragments of 3741 and 1077 bp are obtained (Figure 4.4).

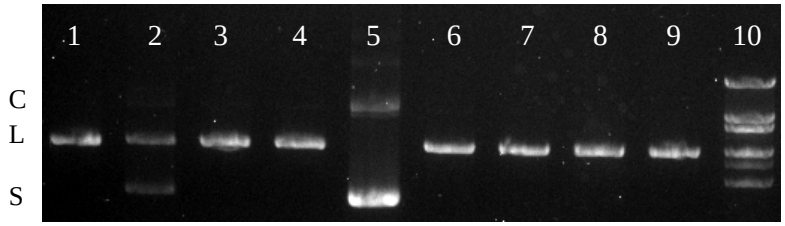

Figure 4.3 – Electrophoretic analysis of *Sac*I enzymatic hydrolysis of plasmid pGL3-Basic DNA (lane 1: reaction in absence of other additives, lane 2: reaction in presence of CB7 lane 3: reaction in presence of spermidine, lane 4: reaction in presence of the complex spermidine/CB7, lane 5: unrestricted DNA, lane 6: reaction in presence of cadaverine, lane 7: reaction in presence of the complex cadaverine/CB7, lane 8: reaction in presence of putrescine, lane 9: reaction in presence of the complex putrescine/CB7, lane 10: λDNA/Eco91I (BstEII) Marker; C = relaxed/nicked circular DNA, L = linear DNA, S = supercoiled DNA).

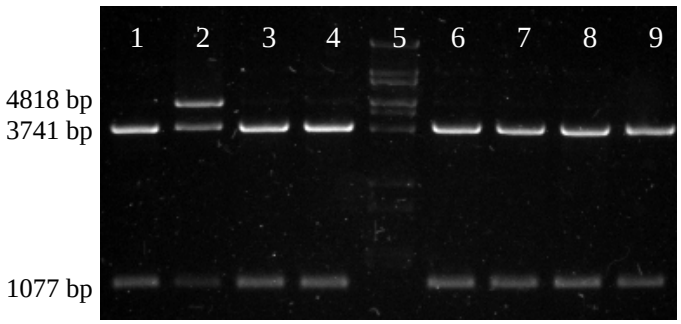

Figure 4.4 – Electrophoretic analysis of *Sac*I enzymatic hydrolysis of linearized pGL3-Basic DNA (lane 1: reaction in absence of other additives, lane 2: reaction in presence of CB7 lane 3: reaction in presence of spermidine, lane 4: reaction in presence of the complex spermidine/CB7, lane 5: λDNA/Eco91I (BstEII) Marker, lane 6: reaction in presence of cadaverine, lane 7: reaction in presence of the complex cadaverine/CB7, lane 8: reaction in presence of putrescine, lane 9: reaction in presence of the complex putrescine/CB7).

The restriction enzyme *Xap*I recognizes four RAATTY sites in the plasmid pGL3-Basic DNA sequence and originates four fragments (2638, 1356, 813, and 11 bp) as shown in Scheme 4.4. As shown in Figure 4.5 only three correspondent bands are visible, because the 11 bp fragment cannot be visualized under the selected experimental conditions. The restriction of linearized DNA originates five DNA fragments (1905, 1356, 813, 733, and 11 bp) (Figure 4.6). Again, the smallest fragment was not visible. In the experiments with *Xap*I in the presence of CB7 unselective restriction (star activity), yielding a multitude of fragments, was observed (lane 4 in Figure 4.5 and lane 2 in Figure 4.6). The reason for this star activity that was not observed for *KpnI* and *SacI* enzymes is not entirely clear. Figures 4.3 to 4.6 do not include the unrestricted DNA, which however, is the same as shown in lane 5 of Figure 4.2.

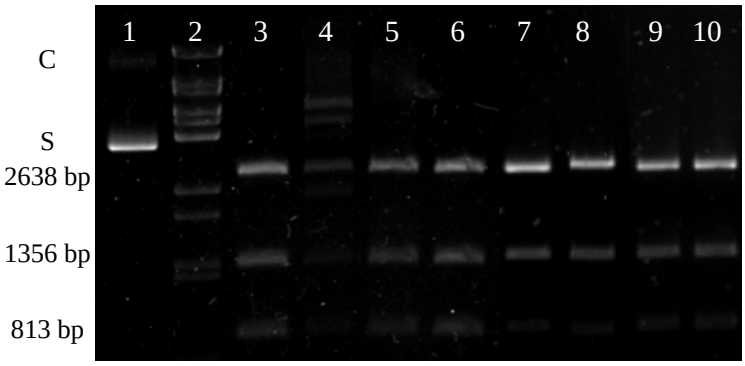

Figure 4.5 – Electrophoretic analysis of *Xap*I enzymatic hydrolysis of plasmid pGL3-Basic DNA (lane 1: unrestricted DNA, lane 2: λDNA/Eco91I (BstEII) Marker, lane 3: reaction in absence of other additives, lane 4: reaction in presence of CB7, lane 5: reaction in presence of spermidine, lane 6: reaction in presence of the complex spermidine/CB7, lane 7: reaction in presence of cadaverine, lane 8: reaction in presence of the complex cadaverine/CB7, lane 9: reaction in presence of putrescine, lane 10: reaction in presence of the complex putrescine/CB7; C = relaxed/nicked circular DNA, S = supercoiled DNA).

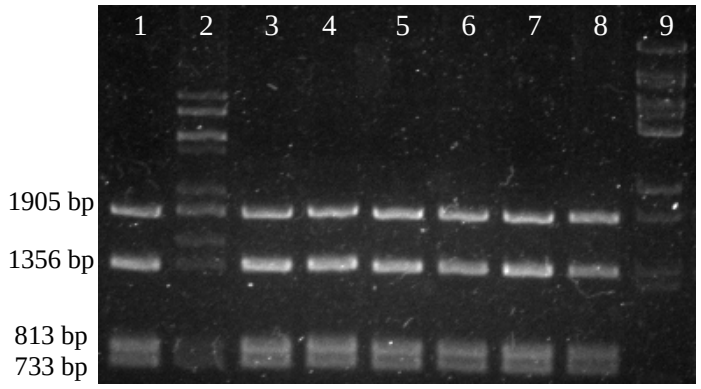

Figure 4.6 – Electrophoretic analysis of *Xap*I enzymatic hydrolysis of linearized pGL3-Basic DNA (lane 1: reaction in absence of other additives, lane 2: reaction in presence of CB7 lane 3: reaction in presence of spermidine, lane 4: reaction in presence of the complex spermidine/CB7, lane 5: reaction in presence of cadaverine, lane 6: reaction in presence of the complex cadaverine/CB7, lane 7: reaction in presence of putrescine, lane 8: reaction in presence of the complex putrescine/CB7, lane 9: λDNA/Eco91I (BstEII) Marker).

The variety of DNA conformations and endonucleases, for which the inhibition by CB*n* was observed, points to a general effect. However, in order to exclude other scenarios than the enzyme-CB*n* interaction, several control experiments and arguments had to be developed. These are discussed in the following paragraphs.

The apparent binding constants of the polyamines with DNA are ca. 1–2 orders of magnitude lower than the ones for the respective CB7 complexes (compared to the CB6 complexes they are even ca. 3–4 orders of magnitude lower).[4,24-27] This means that in presence of CB*n* polyamines prefer to form host-guest complexes instead of associating with DNA. This excludes *a priori* a competition between CB*n* and DNA for the added polyamines under the selected experimental conditions.

A previous report ruled out significant supramolecular interactions between CB*n* and DNA.[28] In accordance, also herein performed CD spectroscopic measurements did not reveal any sign of direct supramolecular interaction between model DNA and CB7 (see Figure 4.7). Additional support came from the observation of unchanged gel mobility of circular and linear pGL3-Basic DNA in the absence and presence of excess macrocycle (Figure 4.8). On this basis, an interaction with the DNA substrate is unlikely the reason for the inhibitory effect.

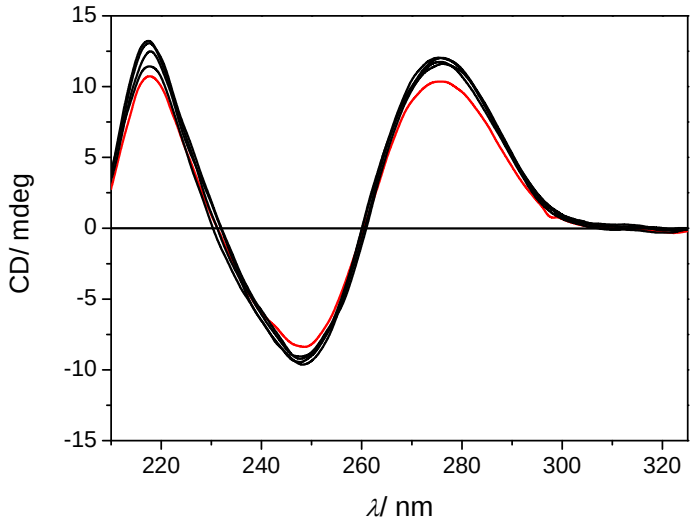

Figure 4.7 – CD spectra of salmon sperm DNA (597 μg ml^{-1}) in absence (red line) and in presence of CB7 (black lines, up to 500 μM).

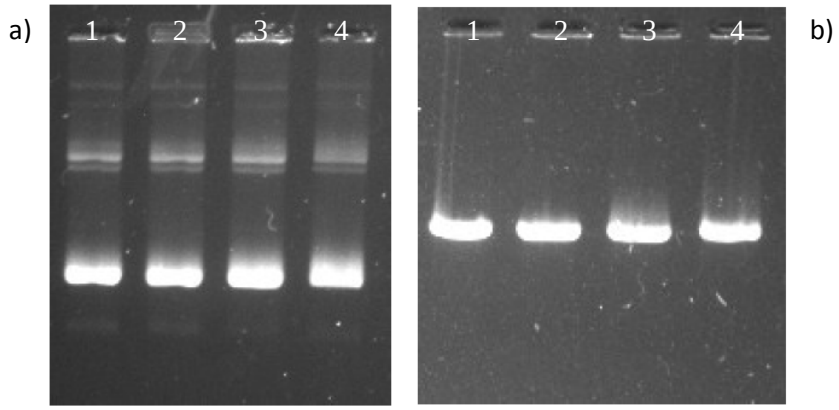

Figure 4.8 – Gel mobility of a) plasmid pGL3-Basic DNA (600 μg ml^{-1}) and b) linear pGL3-Basic DNA (300 μg ml^{-1}) in the absence (lane 1) and the presence of CB7 (lane 2: 500 μM, lane 3: 1 mM, lane 4: 1.5 mM).

The possibility of metal-ion sequestration from the buffer solution by CB*n* is another factor that deserved clarification.[29] In particular, magnesium ions (Mg^{2+}) are known to serve as an essential cofactor of the type II endonucleases employed herein.[20] A control experiment revealed that ethylenediaminetetraacetic acid (EDTA; 1 mM), a strong Mg^{2+} chelator, did not lead to *Xap*I inhibition (Figure 4.9). The EDTA concentration corresponds to double the CB7 concentration used for the experiments with this enzyme. These results exclude metal-ion sequestration as a cause of the observed inhibition, at least at the CB*n* concentrations used herein (maximum of 500 μM). It is noteworthy that bovine serum albumin (BSA) is often present in digestion reaction mixtures, fulfilling the role of a stabilizer and a protective agent against impurities that may be problematic for the restriction reaction. On the one hand, for the BSA concentration used in our assays (*ca.* 1.5 μM for *Kpn*I and *Xap*I; note that *Sac*I does not require BSA) no protection against the inhibitory action of CB7 was noted. Only at much higher BSA concentrations (>30 μM; tested for the example of the *Xap*I assay) the CB*n*-induced inhibition was suppressed. On the other hand, the inhibitory action of CB7 in the absence of BSA was maintained (see Figure 4.10 for the example of *Kpn*I in BSA-free reaction buffer). Thereby, the interaction of CB*n* with BSA could also be excluded as the underlying reason for the observed inhibition effect.

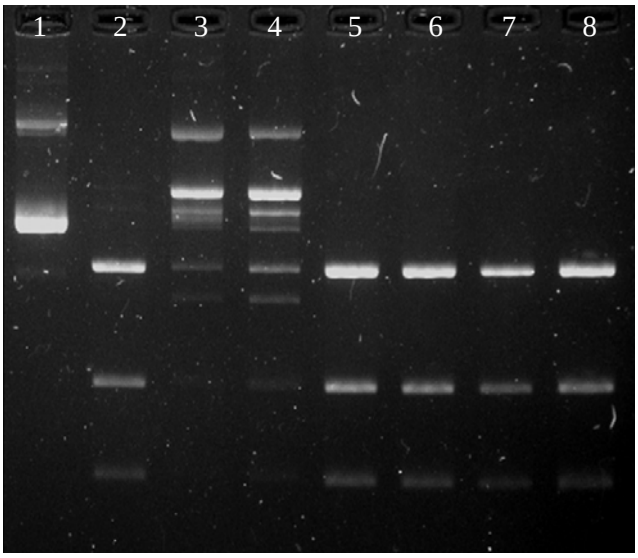

Figure 4.9 – Electrophoretic analysis of *Xap*I enzymatic hydrolysis of plasmid pGL3-Basic DNA (lane 1: DNA alone, lane 2: reaction in the absence of other additives, lane 3: reaction in the presence of 500 μM CB7, lane 4: reaction in the presence of 500 μM CB7 and 1 mM EDTA, lane 5: reaction in the presence of 1 mM EDTA, lane 6: reaction in the presence of 500 μM of CB7, 1mM EDTA, and 1mM cadaverine, lane 7: reaction in the presence of 500 μM of CB7 and 1mM cadaverine, lane 8: reaction in the presence of 1 mM cadaverine).

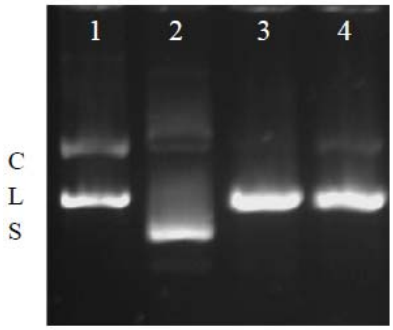

Figure 4.10 – Electrophoretic analysis of *Kpn*I (purchased in Sigma-Aldrich) enzymatic hydrolysis of plasmid pGL3-Basic DNA (lane 1: reaction in the presence of CB7 (500 μM), lane 2: unrestricted DNA, lane 3: reaction in the absence of additives, lane 4: reaction in presence of CB7 (250 μM); C = relaxed/nicked circular DNA, L = linear DNA, S = supercoiled DNA). These experiments were done in BSA-free formulations at 310 K; reaction buffer: 10 mM Tris-HCl buffer (pH = 7.5), 10 mM $MgCl_2$, 1 mM DTE.

There is ample evidence for host–guest interactions between CB*n* and peptides or proteins.[12,13,30] It is generally accepted that peptides with *N*-terminal aromatic amino acids (Trp, Phe, Tyr) or long alkylamino chains (Lys) can form strong complexes with CB7 or CB6, respectively.[7,9,13,31,32] However, also amino acids at the *C*-terminus and even internal ones can form complexes, albeit somewhat weaker.[7,9,11,32] The binding of proteins to CB*n* is naturally more complex and depends on the accessibility of the mentioned amino acids at the surface of the biomolecular structure. One example of an efficient CB*n*/protein interaction is that of insulin, which features an exposed Phe *N*-terminal residue.[14] For the restriction enzymes used in this study, predictions on accessible binding sites for CB*n* are not straightforward to make, especially because they are rich in amino acids displaying the required recognition motifs (Lys, Tyr, Trp, and Phe; see amino acid sequences of the enzymes in Chapter 7). Additionally, the inhibitory action of CB*n* could be caused by both binding near the DNA binding domain of the enzyme or through a more remote binding associated with an allosteric effect.[14]

Efforts to obtain direct experimental evidence (by UV-vis absorption spectroscopy, CD spectroscopy, MALDI-TOF mass spectrometry) for the interaction between the CB7 macrocycles and the enzymes were hampered by the presence of significant BSA concentrations and low enzyme concentrations in the commercially available samples. However, other possible reasons for the observed inhibitory effect, such as interactions with the substrate itself, metal–ion sequestration, or masking of buffer components were clearly excluded (see above). Hence, by joining all puzzle pieces of direct and indirect proof, the main hypothesis is that CB*n* is able to interact with the enzymes and that the supramolecular interaction is efficient enough to modulate the enzyme activity. Based on the data presented here and previous reports on CB*n*-protein interactions a mechanistic proposal as shown in Scheme 4.5 results.

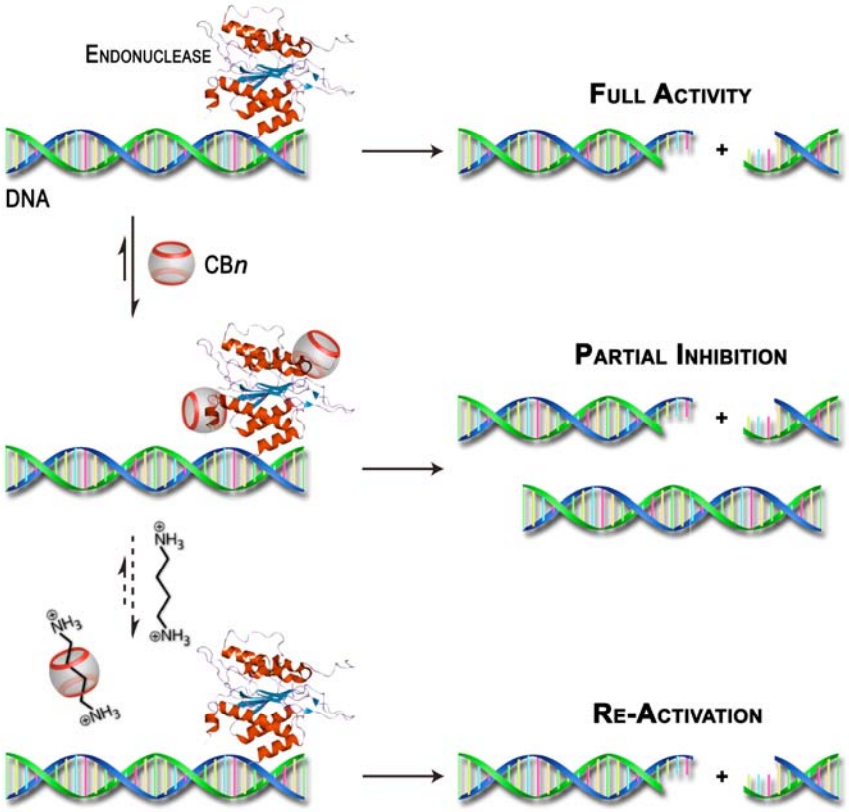

Scheme 4.5 – Schematic illustration of the postulated inhibition of DNA restriction enzymes by CB*n* hosts and their re-activation by competitive binding with polyamines.

4.4 Conclusion

In conclusion, it was demonstrated that CB*n* macrocycles can inhibit the enzymatic hydrolysis of DNA substrates. The reversible nature of the observed effects was underpinned by the successful re-activation of the type II endonuclease activity *via* addition of CB*n*-binding polyamines. The interaction between the enzyme and the macrocycle is likely responsible for the observed effects, causing abnormal protein folding or blocking of actives sites, which leads to at least partial loss of enzymatic activity. The observed effects are conveniently related to some "unconventional" supramolecular interactions. This phenomenon should be further investigated due to the increasing importance of CB*n* in biological studies. Furthermore, the described supramolecular methodology could find potential applications in molecular biology, where the use of restriction enzymes plays a crucial role.[19]

References

(1) Logsdon, L. A.; Urbach, A. R. *J. Am. Chem. Soc.* **2013**, *135*, 11414.

(2) Hennig, A.; Ghale, G.; Nau, W. M. *Chem. Commun.* **2007**, 1614.

(3) Ghosh, S.; Isaacs, L. *J. Am. Chem. Soc.* **2010**, *132*, 4445.

(4) Isobe, H.; Sato, S.; Lee, J. W.; Kim, H.-J.; Kim, K.; Nakamura, E. *Chem. Commun.* **2005**, 1549.

(5) Rajgariah, P.; Urbach, A. R. *J Incl Phenom Macrocycl Chem* **2008**, *62*, 251.

(6) Buschmann, H.-J.; Mutihac, L.; Mutihac, R.-C.; Schollmeyer, E. *Thermochim. Acta* **2005**, *430*, 79.

(7) Ghale, G.; Ramalingam, V.; Urbach, A. R.; Nau, W. M. *J. Am. Chem. Soc.* **2011**, *133*, 7528.

(8) Stancu, A.; Buschmann, H.-J.; Mutihac, L. *J Incl Phenom Macrocycl Chem* **2013**, *75*, 1.

(9) Rekharsky, M. V.; Yamamura, H.; Ko, Y. H.; Selvapalam, N.; Kim, K.; Inoue, Y. *Chem. Commun.* **2008**, 2236.

(10) Dang, D. T.; Nguyen, H. D.; Merkx, M.; Brunsveld, L. *Angew. Chem. Int. Ed.* **2013**, *52*, 2915.

(11) Sonzini, S.; Ryan, S. T. J.; Scherman, O. A. *Chem. Commun.* **2013**, *49*, 8779.

(12) Lee, J.; Heo, S.; Lee, S.; Ko, J.; Kim, H.; Kim, H. *J. Am. Soc. Mass Spectrom.* **2013**, *24*, 21.

(13) Urbach, A. R.; Ramalingam, V. *Isr. J. Chem.* **2011**, *51*, 664.

(14) Chinai, J. M.; Taylor, A. B.; Ryno, L. M.; Hargreaves, N. D.; Morris, C. A.; Hart, P. J.; Urbach, A. R. *J. Am. Chem. Soc.* **2011**, *133*, 8810.

(15) Heath, B.; Jockusch, R. *J. Am. Soc. Mass Spectrom.* **2012**, *23*, 1911.

(16) Tee, K. L.; Wong, T. S. *Biotechnol. Adv.* **2013**, *31*, 1707.

(17) Qi, H.; Lu, H.; Qiu, H.-J.; Petrenko, V.; Liu, A. *J. Mol. Biol.* **2012**, *417*, 129.

(18) Pingoud, A.; Wilson, G. G.; Wende, W. *Nucleic Acids Res.* **2014**, *42*, 7489.

(19) Chan, S.-H.; Stoddard, B. L.; Xu, S.-y. *Nucleic Acids Res.* **2011**, *39*, 1.

(20) Pingoud, A.; Jeltsch, A. *Nucleic Acids Res.* **2001**, *29*, 3705.

(21) Vincze, T.; Posfai, J.; Roberts, R. J. *Nucleic Acids Res.* **2003**, *31*, 3688.

(22) Roberts, R. J.; Vincze, T.; Posfai, J.; Macelis, D. *Nucleic Acids Res.* **2007**, *35*, D269.

(23) Schneider, C. A.; Rasband, W. S.; Eliceiri, K. W. *Nat Meth* **2012**, *9*, 671.

(24) Rekharsky, M. V.; Ko, Y. H.; Selvapalam, N.; Kim, K.; Inoue, Y. *Supramol. Chem.* **2007**, *19*, 39.

(25) Kabir, A.; Hossain, M.; Kumar, G. S. *J. Chem. Thermodyn.* **2013**, *57*, 445.

(26) Hennig, A.; Bakirci, H.; Nau, W. M. *Nat Meth* **2007**, *4*, 629.

(27) Bailey, D. M.; Hennig, A.; Uzunova, V. D.; Nau, W. M. *Chem. Eur. J.* **2008**, *14*, 6069.

(28) Isobe, H.; Tomita, N.; Lee, J. W.; Kim, H.-J.; Kim, K.; Nakamura, E. *Angew. Chem. Int. Ed.* **2000**, *39*, 4257.

(29) Pais, V. F.; Carvalho, E. F. A.; Tomé, J. P. C.; Pischel, U. *Supramol. Chem.* **2014**, *26*, 642.

(30) Biedermann, F.; Nau, W. M. *Angew. Chem. Int. Ed.* **2014**, *53*, 5694.

(31) Logsdon, L. A.; Schardon, C. L.; Ramalingam, V.; Kwee, S. K.; Urbach, A. R. *J. Am. Chem. Soc.* **2011**, *133*, 17087.

(32) Ghale, G.; Kuhnert, N.; Nau, W. M. *Nat. Prod. Commun.* **2012**, *7*, 343.

Chapter 5

Supramolecular Keypad Lock

In this chapter, a reversible photoswitch based on the anthracene [4+4] cyclodimerization, using the template effect of the CB8 macrocycle, is demonstrated. This example of supramolecular chemistry in water was harnessed to demonstrate the operation of a keypad lock device that is driven by means of light and chemicals as inputs.

5.1 Supramolecular Logic

The first molecular logic device was published by de Silva and co-workers in 1993, providing proof-of-principle that the universality of logic allows its implementation with bistable molecular systems and non-electrical input/output signals.[1] Since then, molecular logic has been extended in many directions and what started with basic logic gates like AND, OR, INH, and XOR has now reached a high level of complexity. The idea of using chemical systems to mimic logic operations, following binary coding principles (0 and 1) and Boolean language continues to receive wide attention among researchers.[2-4] Finding molecules that are able to perform a predetermined logic operation is a rising challenge for the application of molecular logic gates in sensing, drug delivery, theranostics, and materials chemistry.[5-11]

Surprisingly, there are not many examples of supramolecular logic gates in the literature. The up to now reported supramolecular molecular logic devices are based on the recognition of metal ion inputs by crown ethers,[1,12-15] supramolecular recognition of substrates by enzymes,[16,17] hydrogen-bonded supramolecular assemblies,[18,19] [2]pseudorotaxane- and [2]rotaxane-based switches,[20-24] and host-

guest complexes with cyclodextrins[25-27] and CB*n*[24,28]. A careful survey of the published reports unveils that a variety of supramolecular assemblies could be perceived has supramolecular logic devices.[2,29-31]

Among the different logic operations, those that imply memory function are among the most demanding in terms of their chemical design.[32] In this type of logic, known as sequential logic, the outputs are not only sensitive to the actual input combination, but also to the input history, i.e., the sequence in which the inputs were applied. Current research along these lines has a strong focus on flip-flops and molecular keypad locks.[33-37] Of particular interest is the keypad lock function, which is used daily in user identification and which was first demonstrated at the molecular level by the Shanzer group in 2007.[34] Given the correct input sequence, the output of the keypad lock is "switched ON" and opens the lock, authorizes the user, or initiates other processes of interest. Photochromic switches have been often exploited to demonstrate the keypad lock function,[38-41] but the development of a system recurring to CB*n* macrocycles is unprecedented.

CB*n* macrocycles were successfully used to demonstrate the reconfigurable and resettable operation of logic gates in aqueous solution.[42,43] As described in Chapter 1, these macrocycles are drawing much attention for their supramolecular application potential with a strong focus on biological and pharmacological contexts.[29,44-49] Therefore, the combination of molecular information processing with cucurbituril chemistry may open interesting paths for biological applications. Fairly it must be stated that the herein undertaken study does not surpass a proof-of-concept level.

5.2 Experimental Approach

The experimental procedure used in this study is described in detail in the experimental section of Chapter 7. Here, selected aspects of the experimental approach will be briefly discussed.

To develop this study, the anthracene derivative **ANT-D** (see Chapter 7, and Scheme 7.2),[50] which contains a positively charged tetraalkylammonium side

chain, was designed. The charged side chain was integrated to the improve water solubility and binding properties of the guest with the CB8 macrocycle. Unlike the smaller homologues CB6 and CB7, that commonly offer space for only one guest molecule, the larger CB8 macrocycle often accommodates two guests. The resulting complexes may feature new emission properties (e.g., excimer fluorescence) or lead to fluorescence self-quenching.[51-54] Additionally, the resulting pre-organization of the two guests will facilitate intracomplex photoreactions that would not happen at the dilute concentrations of the free dye molecules.[53,55,56] In the specific case of **ANT-D**, where the aromatic parts are expected to be immersed in the CB8 cavity, this pre-organization can give rise to a template effect in a [4+4] photodimerization.[56] This is a well-known photoreaction of anthracenes.[57] The ammonium arms are predicted to be oriented in opposite directions, occupying the two portals of the macrocycle and thereby avoiding destabilization of the complex by electrostatic repulsion of the positive charges. This binding mode and the long-axis symmetry of **ANT-D** lead to a single head-to-tail dimerization product [**(ANT-D)$_2$** of Scheme 5.1], avoiding the occurrence of *syn* and *anti* isomers. Drawbacks for photoswitching are undesired secondary photoreactions that can hamper the efforts to achieve clean monomer-to-dimer conversions and a complete reversibility by cycloreversion of the photodimer.[56] Photooxidation reactions of anthracenes may interfere, especially when working with highly energetic UV light in aerated solutions. This obstacle can be potentially avoided or kept at least to a minimum level by using electron-poor aromatic systems such as the **ANT-D** dye.

With these design outsets, the **ANT-D** dye and its supramolecular interactions with CB8 were characterized by UV/vis and fluorescence measurements, titrations, mass spectrometry (ESI-MS), and NMR spectroscopy. The photodimer **ANT-D$_2$** formation was effectuated by irradiation with a 150 W Xe-lamp at λ_{exc} > 395 nm, and the cycloreversion back to the monomeric **ANT-D** was achieved at λ_{exc} = 254 nm; see Scheme 5.1.

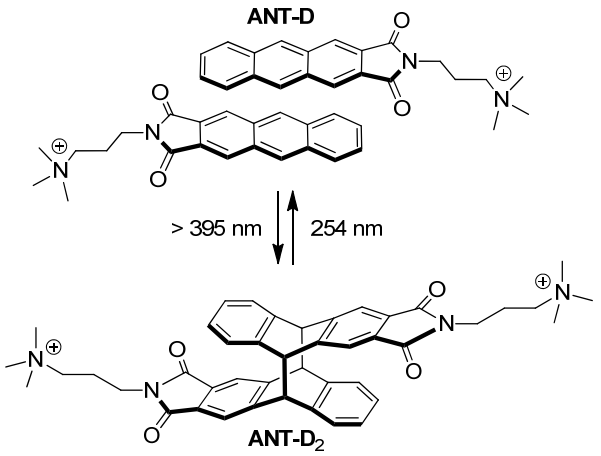

Scheme 5.1 – Reversible photoswitching between the **ANT-D** and its [4+4] photodimer **(ANT-D)$_2$**.

The construction of a supramolecular keypad lock demanded not only the use of light but also chemical inputs (see below). Being so, 1-aminoadamantane, known strong competitor for the CB8 cavity, was used. All experiments were performed in water at a pH 7 to assimilate working conditions that are favorable in bio-relevant contexts.

5.3 Design of a Supramolecular Keypad Lock

In order to successfully design a supramolecular keypad lock, it is imperative to first characterize the **ANT-D** dye (see previous section and Scheme 5.1), its supramolecular interaction with CB8, and its templated [4+4] photodimerization reaction.

In aqueous solution (pH 7) the **ANT-D** dye presents a characteristic long-wavelength $\lambda \leq 360$ nm absorption band with a molar absorption coefficient of ε = 6400 M^{-1} cm^{-1} at its maximum at 412 nm (see Figure 5.1). As shown in Figure 5.2, adding CB8 significantly changes the UV/vis spectra, implying a bathochromic shift of *ca*. 16 nm. The uniformity of the complexation reaction is confirmed by the occurrence of various isosbestic points at 319, 349, and 424 nm. The **ANT-D** fluorescence spectrum underwent similar changes in the titration with the CB8

host, leading to the observation of a practically quantitative quenching of the inherently strong emission of non-complexed **ANT-D** (λ_{max} = 494 nm, Φ_f = 0.44, τ = 6.72 ns). This is explained by an enhanced non-radiative deactivation caused by π–π interactions between the face-to-face organized aromatic guest molecules (see Scheme 5.1). The fitting of the titration data gave a binding constant of K_b = 4.5 × 10^{12} M^{-2}, pointing to a strong supramolecular interaction.

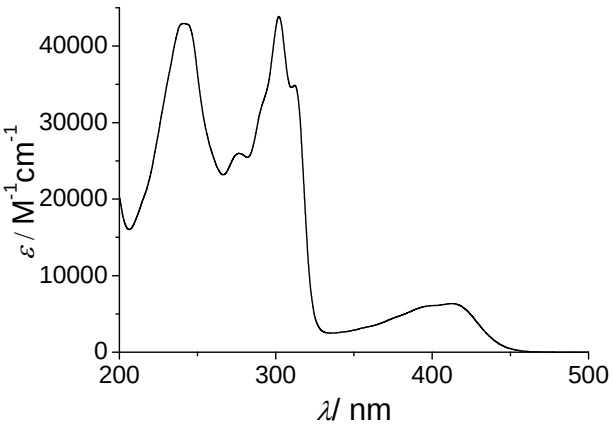

Figure 5.1 – UV/vis molar extinction coefficient of **ANT-D** at pH 7.

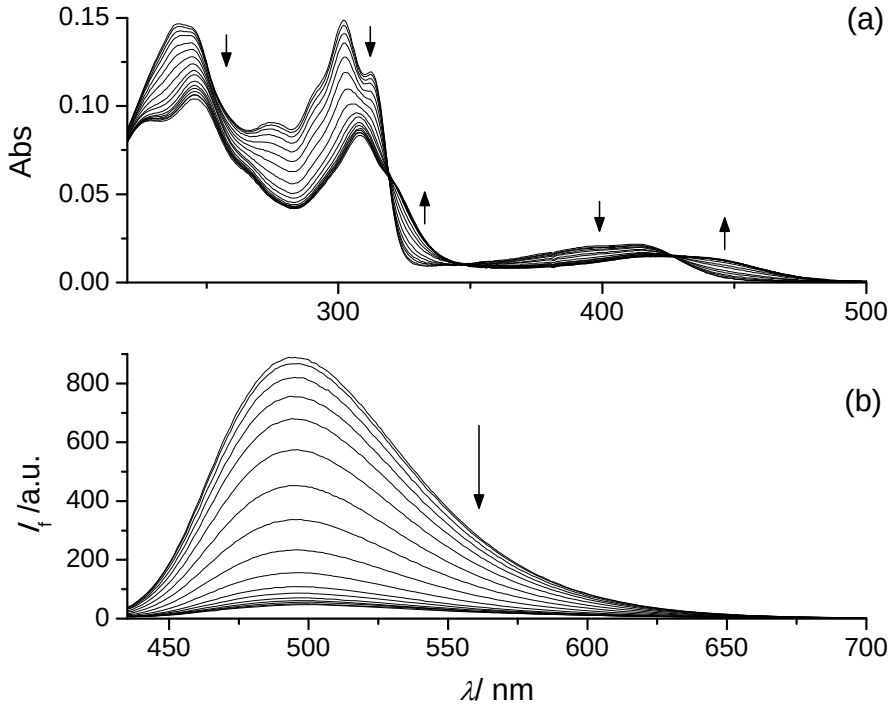

Figure 5.2 – Spectral changes of the UV/vis absorption (a) and the fluorescence (b) upon titration of **ANT-D** (3.6 μM) with CB8 (0–6.2 μM) in pH-neutral aqueous solution.

The titration curves levelled-off at *ca*. 0.5 equivalents of CB8, in agreement with the predicted formation of a ternary **ANT-D**/**ANT-D**/CB8 complex. This stoichiometry was independently confirmed by a Job's plot analysis (Figure 5.3), and the existence of a 2:1 complex was corroborated for the gas phase by electrospray-ionization mass (ESI-MS) spectrometry (Figure 5.4). Furthermore, ^{1}H NMR studies evidenced pronounced upfield shifts of the aromatic proton signals of the guest dye, coinciding with its deep immersion into the CB8 macrocycle (Figure 5.5).

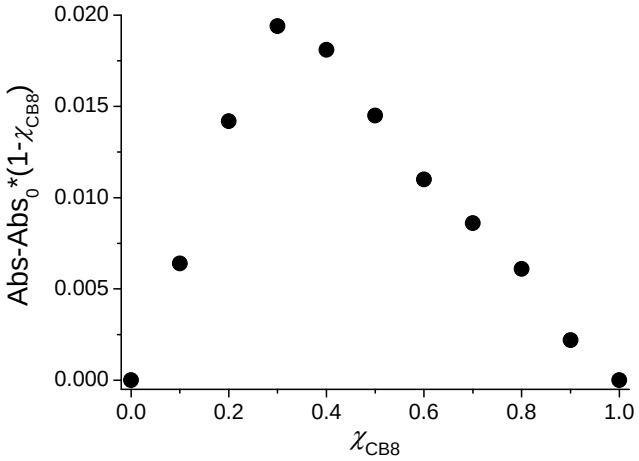

Figure 5.3 – Job's plot for the complexation of **ANT-D** by CB8. The total concentration of both components was fixed at 20 μM. The formation of a 2:1 complex is evident by the maximum at 0.3.

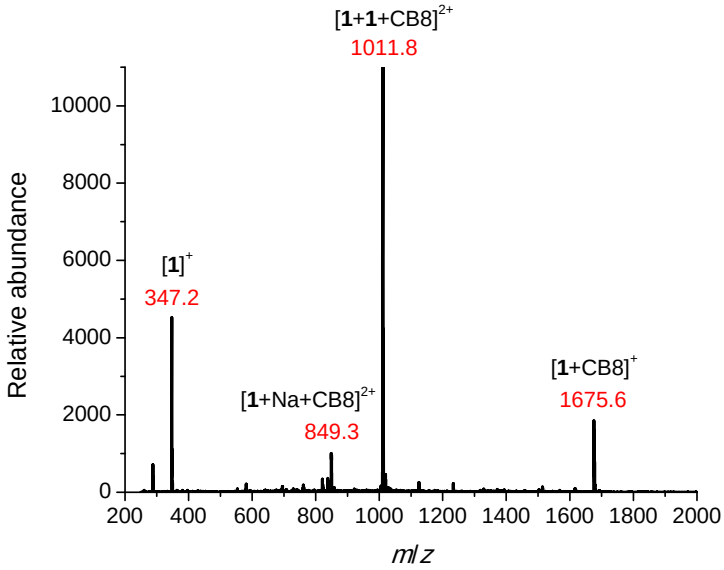

Figure 5.4 – Electrospray ionization mass spectrum of a mixture of **ANT-D** (30 μM) and CB8 (15 μM) in neutral water.

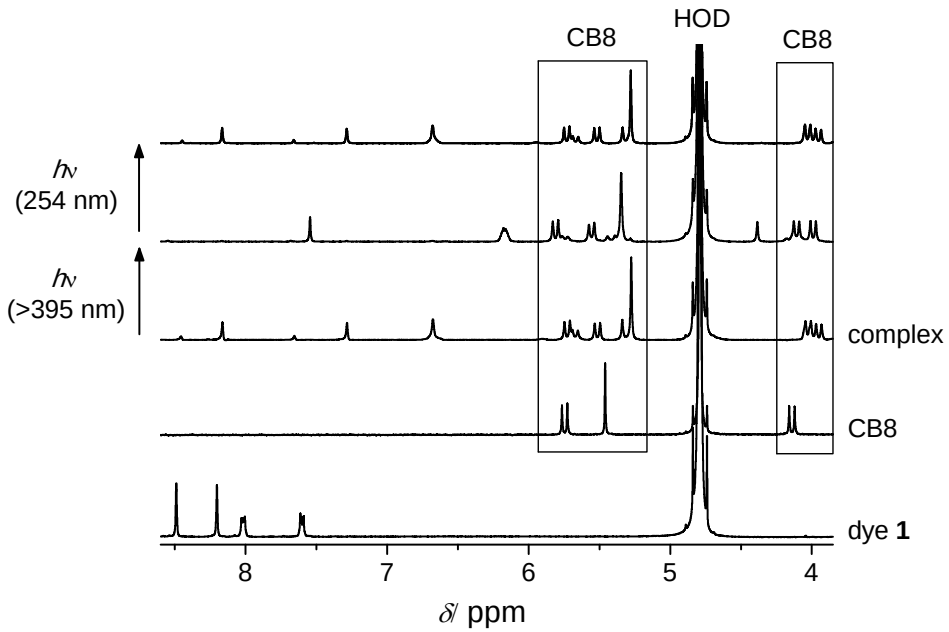

Figure 5.5 – Partial ^{1}H NMR spectra (in D2O) of **ANT-D** dye, CB8, the **ANT-D**/CB8 (250 μM/125 μM), the irradiated (>395 nm for 45 min) mixture, and the mixture after cycloreversion (irradiation at 254 nm for 4 min of the CB8-complexed photodimer that was generated previously by irradiation at >395 nm for 45 min), from bottom to top.

Having established the strong binding of **ANT-D** to CB8 and its photophysical consequences, the photodimerization of the dye was attempted. Irradiation at λ > 395 nm of a diluted solution of **ANT-D** in the presence of 0.5 equivalents of CB8, resulted in a uniform photoreaction that was monitored by ^{1}H NMR spectroscopy (Figure 5.5), UV/vis absorption (Figure 5.6, presence of a clear isosbestic point at 243 nm), and liquid chromatography (LC) (Figure 5.7). Under the employed conditions *ca*. 75% of the long-wavelength absorption band (between *ca*. 350 and 500 nm) of the complex depleted within 30 min of irradiation. In comparison, the free dye showed only a *ca*. 10% decrease of the long-wavelength absorption band under identical irradiation conditions (inset o Figure 5.6). This confirms a much faster photoreaction in the presence of CB8 (*ca*. 10 times faster under comparable irradiation conditions, time constant of 11 min for complexed **ANT-D** *versus* 115 min for the non-complexed dye) and also a good photostability of the dye itself in diluted solutions.

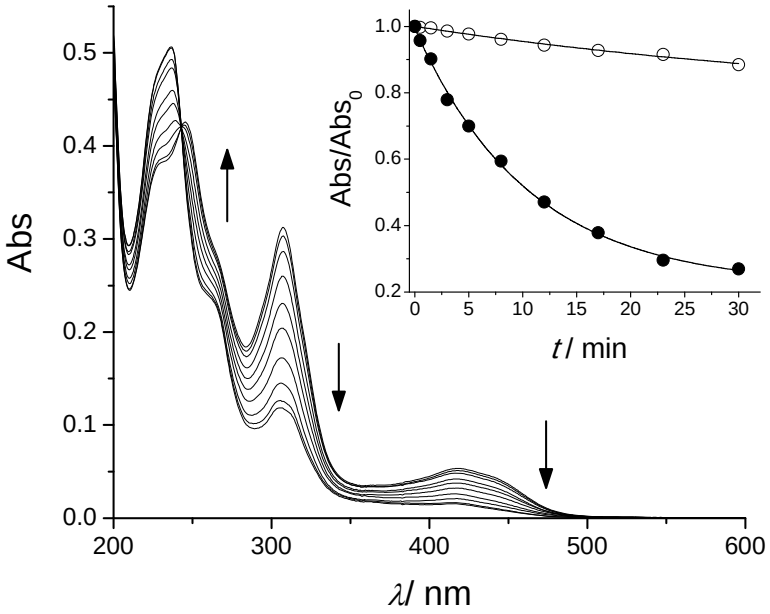

Figure 5.6 – UV/vis absorption spectral changes upon irradiation of **ANT-D** dye (10 μM) in the presence of CB8 (5 μM) at λ > 395 nm in pH-neutral aqueous solution. The inset shows the kinetic curves and themono-exponential fittings for the irradiation of **ANT-D** in the absence (empty circles) and the presence of CB8 (filled circles); observation at 412 nm (free dye) or 424 nm (presence of CB8).

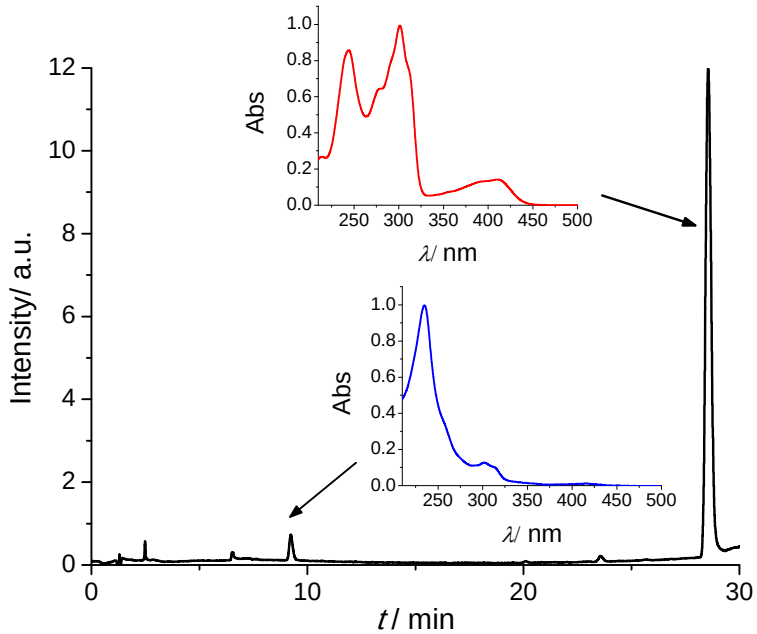

Figure 5.7 – Liquid chromatography with diode array detection (observed at 300 nm) after partial photodimerization of **ANT-D** in presence of 0.5 equivalents CB8 by irradiation at λ >395 nm. The insets show the corresponding UV/vis spectra of **ANT-D** (red) and the photodimer **ANT-D$_2$** (blue) as detected by the diode array.

In liquid chromatography with mass spectrometric detection (LC-MS), the CB8-templated formation of the dimerization product was unequivocally confirmed through the monitorization of the molecular ion peak at m/z = 347 with an isotope pattern spacing of Δm = 0.5 amu, indicative of a doubly charged dimer (see Figure 5.8 and 5.9). On the other hand, no photodimer was noted for the irradiation (λ > 395 nm) of the free dye. Furthermore, the UV/vis spectrum of the corresponding band of the dimerization product, monitored with diode-array detection, resembled the spectroscopic observations made by UV/vis spectroscopy. ^{1}H NMR studies provided structural proof for the formation of photodimer **ANT-D$_2$**. Namely, pronounced changes in the aromatic region and a new signal at ca. 4.4 ppm, indicative of the bridgehead protons of the dimer, were observed (Figure 5.5).

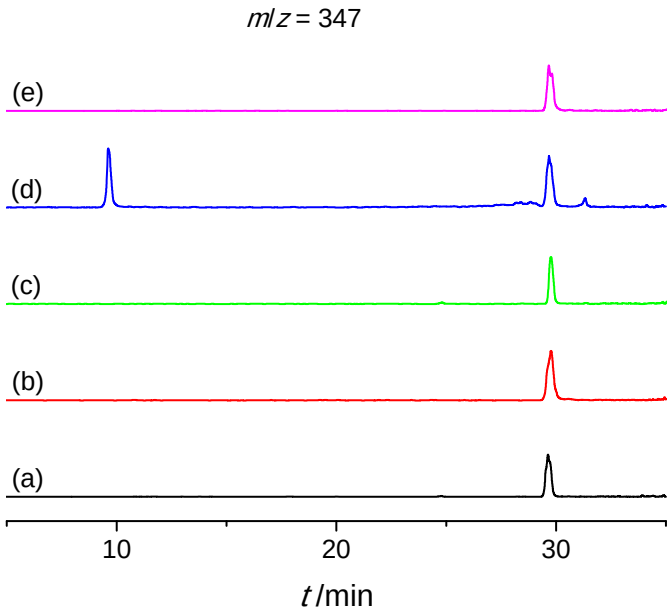

Figure 5.8 – Single ion LC-MS traces at m/z 347 of (a) the non-complexed **ANT-D**, (b) the dye in presence of CB8, (c) after irradiation of the non-complexed **ANT-D** at >395 nm, (d) after partial photodimerization by irradiation of the complex at >395 nm, (e) after cycloreversion of the complexed dimer by irradiation at 254 nm. The concentrations were adjusted to [**ANT-D**] = 30 µM and [CB8] = 15 µM (whenever present). All solutions were prepared in high purity water at pH 7. Note that the host-guest complexes do not withstand to the chromatographic separation, only the guests are observed.

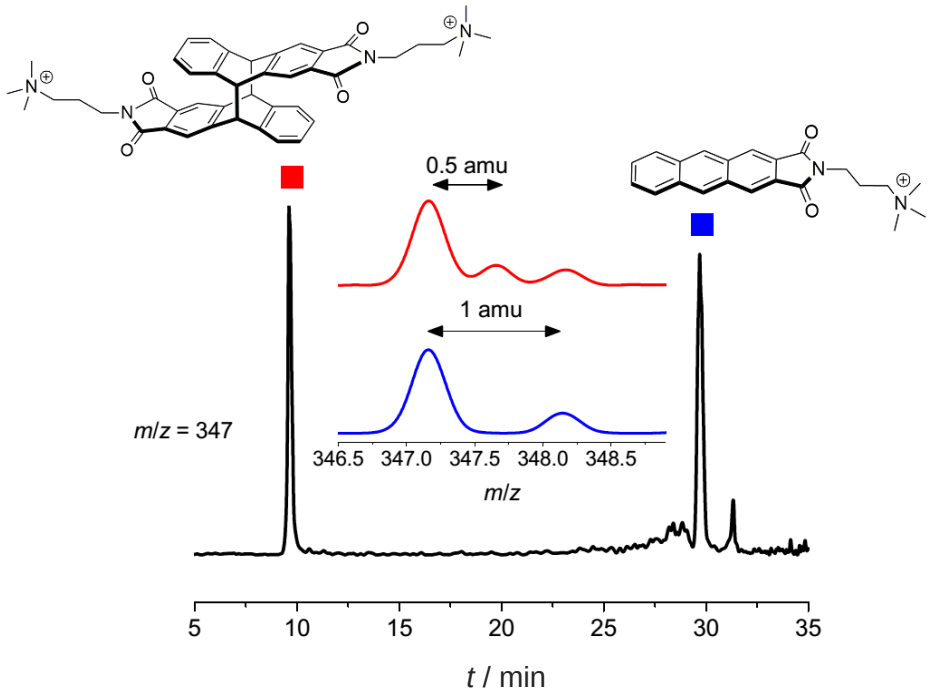

Figure 5.9 – Single ion LC-MS trace at *m/z* 347 observed after irradiation of **ANT-D** (30 μM) in presence of CB8 (15 μM). The photoreaction was not completed to demonstrate the signals of both the monomer dye and the photodimer. The color-coded inset graphs show the molecular ion peak and the isotope pattern spacing (blue: **ANT-D**, red: photodimer **ANT-D$_2$**). Note that the host-guest complexes do not withstand to the chromatographic separation, only the guests are observed.

Anthracene [4+4] photodimerization in CB8 was recently demonstrated.[56] However, undesired secondary photoreactions hampered the efforts to achieve a completely reversible photoswitching by back-isomerization on irradiation at $\lambda \leq$ 300 nm of the photodimer and it was emphasized that different designs were required if system reversibility is desired. This issue is overcome with the present system. The cycloreversion of the photodimer **ANT-D$_2$** (see Scheme 5.1) back to its monomeric form was achieved by irradiation at 254 nm for a short period of time (30 s). The efficient back reaction was signaled by the recovery of more than 90% of the absolute signal of the long-wavelength absorption band of **ANT-D**. In addition, the recovery of the aromatic signals that correspond to the complexed monomeric dye and the concomitant disappearance of the respective photodimer signals were evident in the ^{1}H NMR spectra (see Figure 5.5). The reversibility of

the dimerization/cycloreversion sequence was shown for at least 5 cycles, submitting the CB8 complexes to successive irradiations at >395 nm and 254 nm (see Figure 5.10).

This reversion works well inside the CB8 cavity as well as for the released dimer that was obtained by addition of a strongly CB8-binding competitor such as 1-aminoadamantane (amantadine) or 1-amino-3,5-dimethyladamantane (memantine). While the photodimer **ANT-D$_2$** is non-fluorescent (both in absence and presence of CB8), the cycloreversion of the unbound dimer back to **ANT-D** is accompanied by a significant recovery of the fluorescence. However, the same process inside the CB8 macrocycle leads to no significant increase in fluorescence, due to the emission quenching of the monomeric dye in the ternary **ANT-D**/**ANT-D**/CB8 complex.

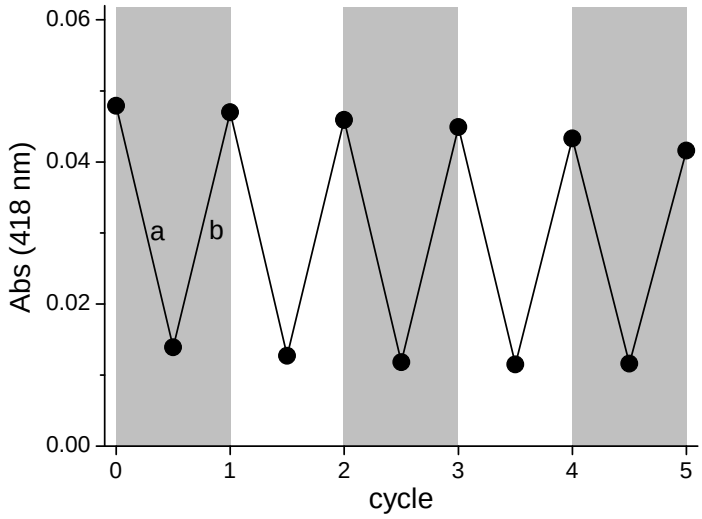

Figure 5.10 – Reversible photoswitching of **ANT-D** (10 μM) in the presence of 0.5 equivalents of CB8 monitored at λ_{obs} = 418 nm; a: 20 min irradiation at > 395 nm; b: 20 s irradiation at 254 nm.

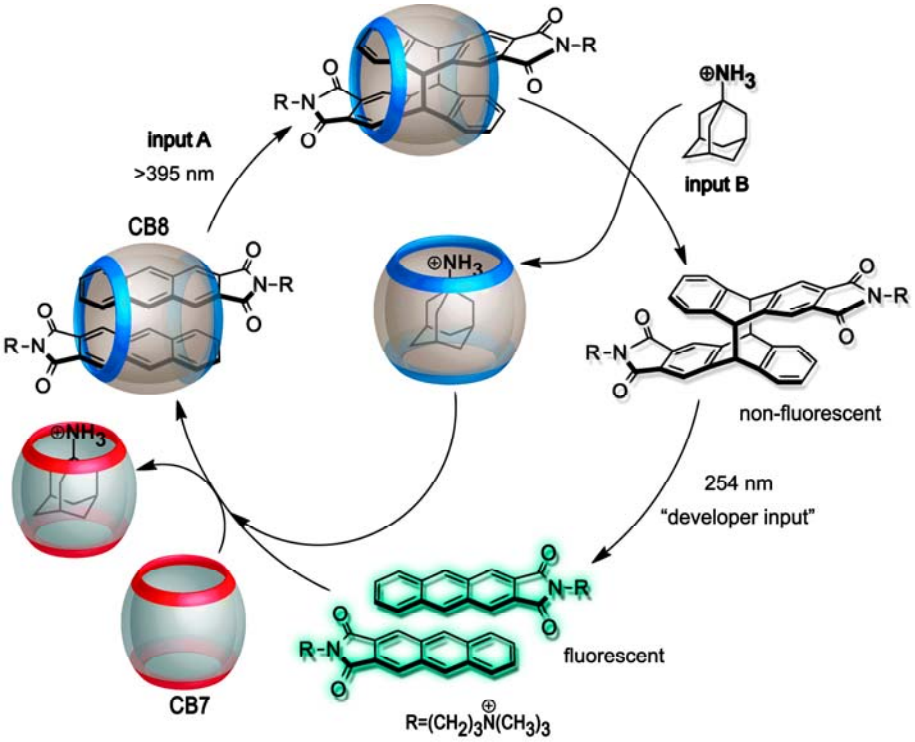

Scheme 5.2 – Supramolecular keypad lock by applying the correct input order, reading the output with the help of the ''developer input'', and resetting by CB7.

The described CB8 template effect on the photodimerization of **ANT-D** and the reversible photoswitching form the chemical basis for the announced supramolecular keypad lock device (see Scheme 5.2). For this purpose, the inputs are defined as the irradiation at λ > 395 nm (input A) and the addition of the strongly binding competitor amantadine (input B).[51,58] Noteworthy, the latter is able to displace the monomeric **ANT-D** dye as well as the dimer **ANT-D$_2$** from the CB8 macrocycle. The output of the system is defined as the observation of uncomplexed photodimer. The analytical detection of this situation would in principle demand the time-consuming application of NMR spectroscopy or mass spectrometry. In order to visualize the output situation more conveniently, the irradiation at 254 nm ("developer input" in Scheme 5.2) together with the resulting change of the fluorescence intensity ($\Delta I = I_{254} - I_0$, where the subscripts 254 and 0 refer to after and before irradiation at 254 nm, respectively) were monitored. Integrating over all situations and in accordance with the results that were discussed above, the only high output in form ΔI (being defined as 1 and

corresponding to the situation of the *open lock*) is observed for the sequential input order of first A and then B, coinciding with the formation of free photodimer (see Scheme 5.2). All other combinations and sequences lead to no photodimer (input combinations 00, B0, 0B, BA) or the formation of photodimer residing inside the CB8 cavity (A0 and 0A), see Figure 5.11. Note, that the input combinations contemplate also the fact that one or both inputs may not be activated (0). Hence, for the correct functioning of the described supramolecular keypad lock, the herein demonstrated reversibility of the photoswitching is a precondition, as the cycloreversion induced by 254 nm light is the "developer input" of the system. With respect to input A, stronger light sources would enable the shortening of the irradiation time, which under the herein employed conditions is *ca*. 45 min.

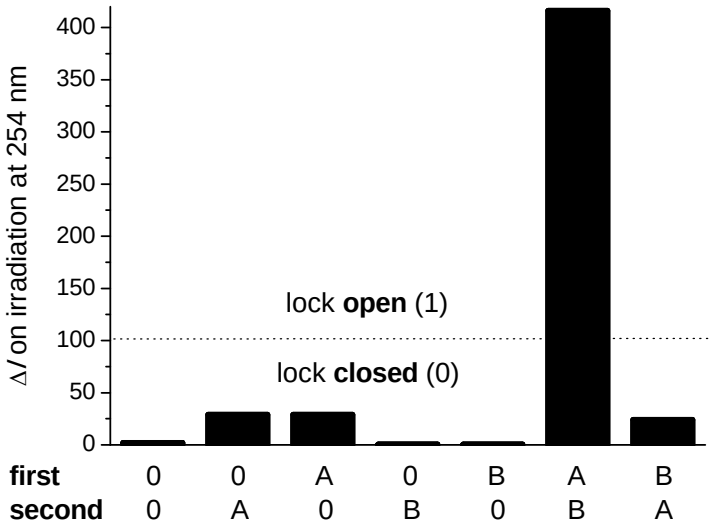

Figure 5.11 – Operation of the supramolecular keypad lock (10 μM **ANT-D**, 5 μM CB8) upon application of the corresponding inputs (A: irradiation at λ > 395 nm for 45 min; B: addition of 1-aminoadamantane; 20 μM). The output is read as the change of the fluorescence upon irradiation at 254 nm for 30 s. The dotted line shows the threshold.

A controllable resetting of the system to its initial state would be a valuable asset, guaranteeing that the logic operation could be repeated. The reversible nature of the photoreaction and the involved supramolecular interactions enable such feature. Taking for example the situation of the open keypad lock (shown in

Scheme 5.2), the competitor (amantadine) is encapsulated by CB8 and the non-complexed **ANT-D** is the species after application of the "developer input". Given the fact that the binding constant of amantadine to CB7 is three orders of magnitude higher (K_b = 1.2 × 10^{10} M^{-1}) than for CB8 (K_b = 3.3 × 10^7 M^{-1}),[51] and that **ANT-D** dye has a much smaller binding constant with CB7 (K_b = 3.0 × 10^5 M^{-1}; Figure 5.12), thermodynamic self-sorting can be used to achieve resetting.[58] Indeed, as expected from these binding constants, adding CB7 to the mixture after irradiation at 254 nm leads to complexation of amantadine by CB7 and of **ANT-D** by CB8, thereby closing the cycle shown in Scheme 5.2. Thus, the characteristic spectral signatures of the ternary **ANT-D**/**ANT-D**/CB8 complex are re-constituted by addition of CB7, i.e., a red-shift of the long-wavelength absorption band and efficient fluorescence quenching (see Figure 5.13 to 5.15). From this point on the logic operations can be repeated. This was shown for 5 cycles, after which a fatigue effect of *ca*. 30% was noted (Figure 5.16).

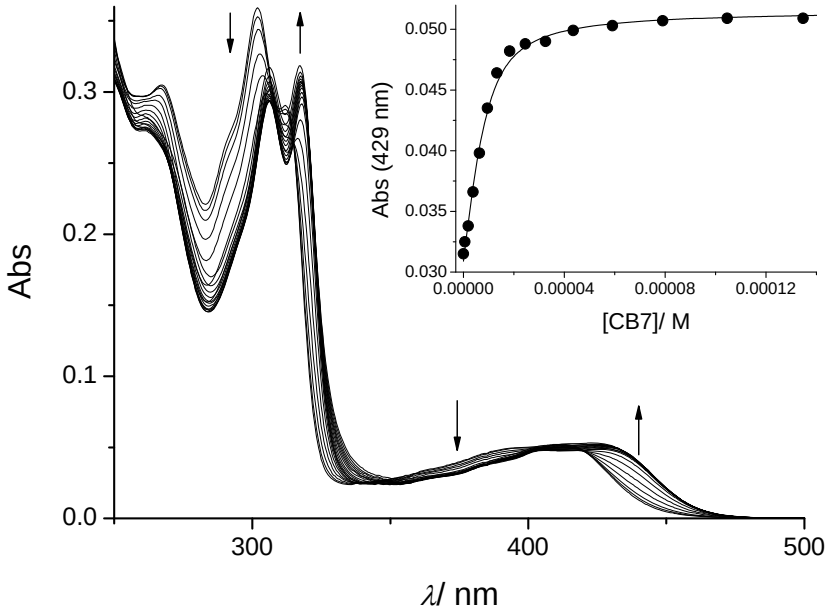

Figure 5.12 – Spectral changes of the UV/vis absorption upon titration of **ANT-D** (8 μM) with CB7 (0-200 μM) in pH-neutral aqueous solution. The inset shows the titration curve at λ_{obs} = 429 nm, and the straight line indicate the fitting according to a 1:1 binding.

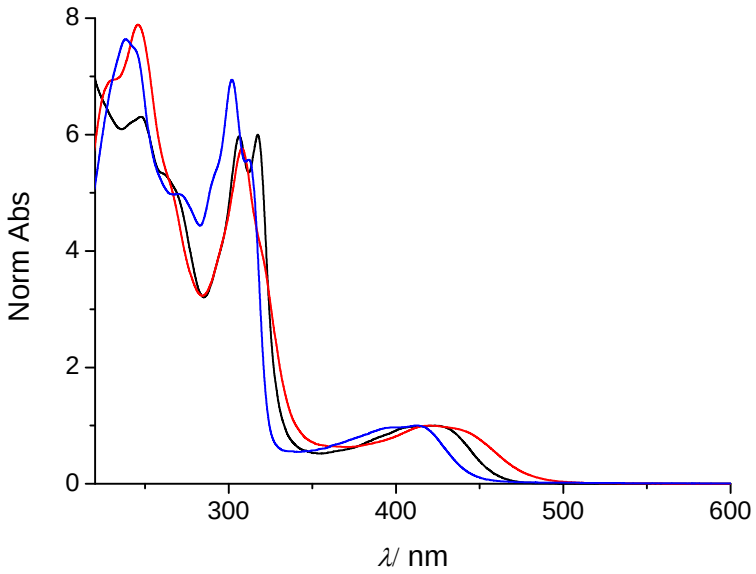

Figure 5.13 – Comparison of the UV/vis absorption spectra of **ANT-D** dye (blue line), the complex **ANT-D**/CB7 (black line), and the complex **ANT-D**/**ANT-D**/CB8 (red line).

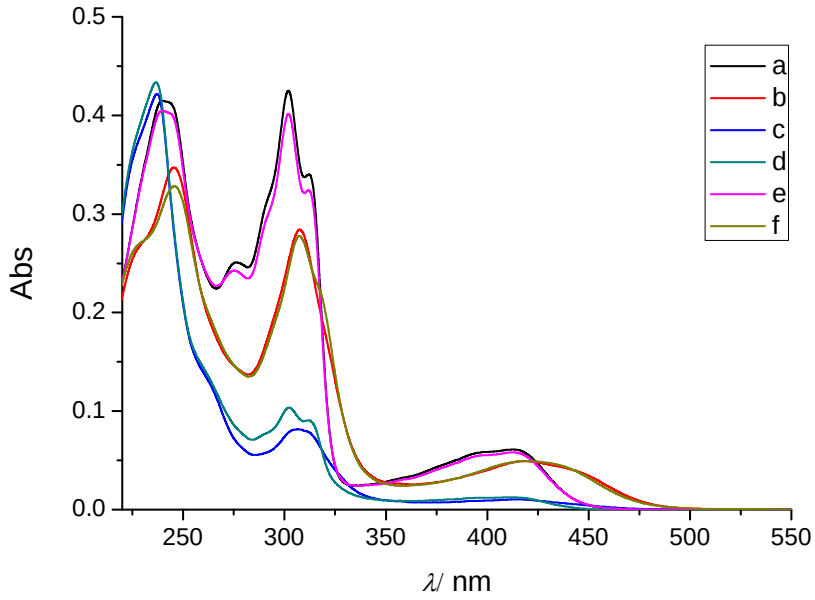

Figure 5.14 – UV/vis absorption changes for the recycling of the supramolecular keypad lock. a: 10 μM **ANT-D**; b: after addition of CB8 (5 μM) to solution a; c: after irradiation of solution b at >395 nm for 45 min; d: after addition of 1-aminoadamantane (20 μM) to solution c; e: after irradiation of solution d at 254 nm for 30 s; f: after addition of CB7 (35 μM) to solution e. Note that the spectra corresponding to the cases b and f are hardly distinguishable.

It has to be taken in account that the self-sorting process on adding CB7 involves a multicomponent mixture with several coupled equilibria, and that CB7 and 1-aminoadamantane are used in slight excess. Thus, these chemicals accumulate over the various cycles. Comparing the Figures 5.13 and 5.14, it can be seen that the characteristic spectral fingerprint of the **ANT-D**/**ANT-D**/CB8 complex is obtained after completion of each cycle. In this intricate multi-equilibrium situation[59] the reproducibility is very good, and a concentration optimization of the four components involved should improve the performance of the keypad lock even further.

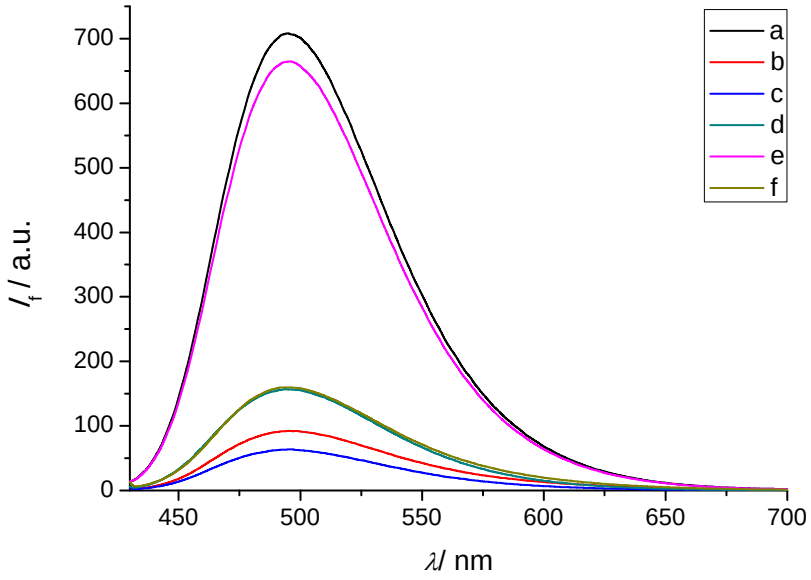

Figure 5.15 – Fluorescence changes for the recycling of the supramolecular keypad lock. a: 10 μM **ANT-D**; b: after addition of CB8 (5 μM) to solution a; c: after irradiation of solution b at >395 nm for 45 min; d: after addition of 1-aminoadamantane (20 μM) to solution c; e: after irradiation of solution d at 254 nm for 30 s; f: after addition of CB7 (35 μM) to solution e. Note that the spectra corresponding to the cases d and f are hardly distinguishable.

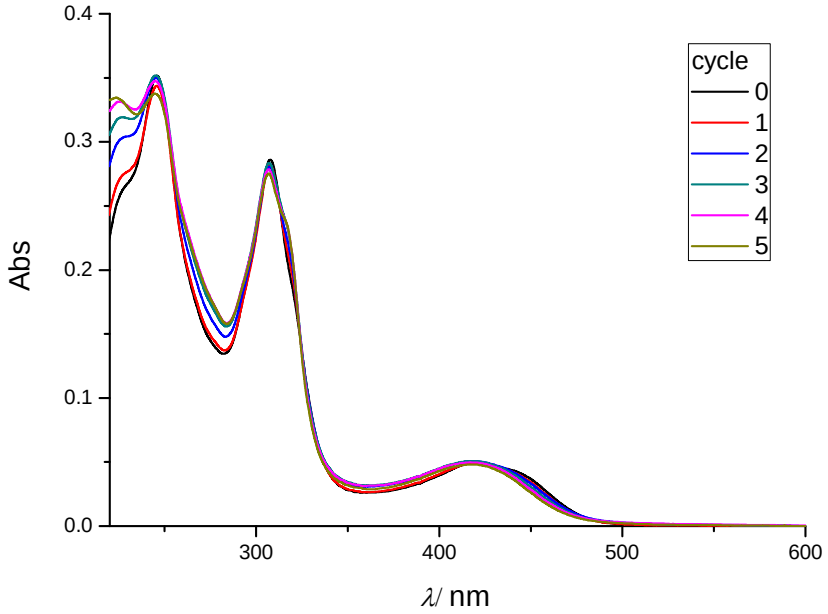

Figure 5.16 - Absorption spectra after the final addition of CB7 for several cycles corresponding to the sequences c)-f) shown in Figure 5.14.

5.4 Conclusion

In conclusion, the **ANT-D** dye forms a reversibly photoswitchable complex with CB8, harnessing the template effect exerted by the organic macrocycle.[56] This was used to demonstrate a supramolecular keypad lock, where the formation of a free photodimer, indirectly signaled by the fluorescence enhancement upon photoinduced cycloreversion, was the output. Only by application of the right input order (first irradiation at λ > 395 nm and then addition of 1-aminoadamantane) the lock was opened. By exploitation of self-sorting upon adding CB7, the system was reset to the initial **ANT-D**/**ANT-D**/CB8 complex. These results demonstrate the utility of CB*n* chemistry for resettable complex logic operations with all-organic systems in aqueous solution. Applications as functional switches in bio-relevant contexts could be foreseen.

References

(1) de Silva, P. A.; Gunaratne, N. H. Q.; McCoy, C. P. *Nature* **1993**, *364*, 42.

(2) Carvalho, C. P.; Pischel, U. In *Molecular and Supramolecular Information Processing*; Wiley-VCH Verlag GmbH & Co. KGaA: 2012, p 99.

(3) De Silva, A. P.; RSC Pub.: Cambridge, UK, 2013.

(4) Szaciłowski, K. *Chem. Rev.* **2008**, *108*, 3481.

(5) Prasanna de Silva, A.; James, M. R.; McKinney, B. O. F.; Pears, D. A.; Weir, S. M. *Nat Mater* **2006**, *5*, 787.

(6) Hammarson, M.; Andersson, J.; Li, S.; Lincoln, P.; Andreasson, J. *Chem. Commun.* **2010**, *46*, 7130.

(7) Xie, Z.; Wroblewska, L.; Prochazka, L.; Weiss, R.; Benenson, Y. *Science* **2011**, *333*, 1307.

(8) Elstner, M.; Weisshart, K.; Müllen, K.; Schiller, A. *J. Am. Chem. Soc.* **2012**, *134*, 8098.

(9) Chen, S.; Yang, Y.; Wu, Y.; Tian, H.; Zhu, W. *J. Mater. Chem.* **2012**, *22*, 5486.

(10) Erbas-Cakmak, S.; Akkaya, E. U. *Angew. Chem. Int. Ed.* **2013**, *52*, 11364.

(11) Pischel, U.; Andréasson, J.; Gust, D.; Pais, V. F. *ChemPhysChem* **2013**, *14*, 28.

(12) Uchiyama, S.; McClean, G. D.; Iwai, K.; de Silva, A. P. *J. Am. Chem. Soc.* **2005**, *127*, 8920.

(13) de Silva, A. P.; Dobbin, C. M.; Vance, T. P.; Wannalerse, B. *Chem. Commun.* **2009**, 1386.

(14) Bag, B.; Bharadwaj, P. K. *Chem. Commun.* **2005**, 513.

(15) Bozdemir, O. A.; Guliyev, R.; Buyukcakir, O.; Selcuk, S.; Kolemen, S.; Gulseren, G.; Nalbantoglu, T.; Boyaci, H.; Akkaya, E. U. *J. Am. Chem. Soc.* **2010**, *132*, 8029.

(16) Bi, S.; Yan, Y.; Hao, S.; Zhang, S. *Angew. Chem. Int. Ed.* **2010**, *49*, 4438.

(17) Ikeda, M.; Tanida, T.; Yoshii, T.; Kurotani, K.; Onogi, S.; Urayama, K.; Hamachi, I. *Nat Chem* **2014**, *6*, 511.

(18) Baytekin, H. T.; Akkaya, E. U. *Org. Lett.* **2000**, *2*, 1725.

(19) Goodman, A.; Breinlinger, E.; Ober, M.; Rotello, V. M. *J. Am. Chem. Soc.* **2001**, *123*, 6213.

(20) Ashton, P. R.; Ballardini, R.; Balzani, V.; Boyd, S. E.; Credi, A.; Gandolfi, M. T.; Gómez-López, M.; Iqbal, S.; Philp, D.; Preece, J. A.; Prodi, L.; Ricketts, H. G.; Stoddart, J. F.; Tolley, M. S.; Venturi, M.; Venturi, M.; White, A. J. P.; Williams, D. J. *Chem. – Eur. J.* **1997**, *3*, 152.

(21) Leigh, D. A.; Morales, M. Á. F.; Pérez, E. M.; Wong, J. K. Y.; Saiz, C. G.; Slawin, A. M. Z.; Carmichael, A. J.; Haddleton, D. M.; Brouwer, A. M.; Buma, W. J.; Wurpel, G. W. H.; León, S.; Zerbetto, F. *Angew. Chem. Int. Ed.* **2005**, *44*, 3062.

(22) Qu, D.-H.; Wang, Q.-C.; Tian, H. *Angew. Chem. Int. Ed.* **2005**, *44*, 5296.

(23) Semeraro, M.; Credi, A. *J. Phys. Chem. C* **2010**, *114*, 3209.

(24) Qu, D. H.; Ji, F. Y.; Wang, Q. C.; Tian, H. *Adv. Mater.* **2006**, *18*, 2035.

(25) Periyasamy, G.; Collin, J.-P.; Sauvage, J.-P.; Levine, R. D.; Remacle, F. *Chem. – Eur. J.* **2009**, *15*, 1310.

(26) Luo, Y.; Collier, C. P.; Jeppesen, J. O.; Nielsen, K. A.; DeIonno, E.; Ho, G.; Perkins, J.; Tseng, H.-R.; Yamamoto, T.; Stoddart, J. F.; Heath, J. R. *ChemPhysChem* **2002**, *3*, 519.

(27) Collier, C. P.; Wong, E. W.; Belohradský, M.; Raymo, F. M.; Stoddart, J. F.; Kuekes, P. J.; Williams, R. S.; Heath, J. R. *Science* **1999**, *285*, 391.

(28) de Silva, A. P.; Dixon, I. M.; Gunaratne, H. Q. N.; Gunnlaugsson, T.; Maxwell, P. R. S.; Rice, T. E. *J. Am. Chem. Soc.* **1999**, *121*, 1393.

(29) Carvalho, C. P.; Uzunova, V. D.; Da Silva, J. P.; Nau, W. M.; Pischel, U. *Chem. Commun.* **2011**, *47*, 8793.

(30) Praetorius, A.; Bailey, D. M.; Schwarzlose, T.; Nau, W. M. *Org. Lett.* **2008**, *10*, 4089.

(31) Shaikh, M.; Mohanty, J.; Bhasikuttan, A. C.; Uzunova, V. D.; Nau, W. M.; Pal, H. *Chem. Commun.* **2008**, 3681.

(32) Pischel, U. *Angew. Chem. Int. Ed.* **2010**, *49*, 1356.

(33) Guo, Z.; Zhu, W.; Shen, L.; Tian, H. *Angew. Chem. Int. Ed.* **2007**, *46*, 5549.

(34) Margulies, D.; Felder, C. E.; Melman, G.; Shanzer, A. *J. Am. Chem. Soc.* **2007**, *129*, 347.

(35) Rout, B.; Milko, P.; Iron, M. A.; Motiei, L.; Margulies, D. *J. Am. Chem. Soc.* **2013**, *135*, 15330.

(36) de Ruiter, G.; Motiei, L.; Choudhury, J.; Oded, N.; van der Boom, M. E. *Angew. Chem. Int. Ed.* **2010**, *49*, 4780.

(37) de Ruiter, G.; Tartakovsky, E.; Oded, N.; van der Boom, M. E. *Angew. Chem. Int. Ed.* **2010**, *49*, 169.

(38) Andréasson, J.; Straight, S. D.; Moore, T. A.; Moore, A. L.; Gust, D. *Chem. – Eur. J.* **2009**, *15*, 3936.

(39) Andréasson, J.; Pischel, U.; Straight, S. D.; Moore, T. A.; Moore, A. L.; Gust, D. *J. Am. Chem. Soc.* **2011**, *133*, 11641.

(40) Remón, P.; Bälter, M.; Li, S.; Andréasson, J.; Pischel, U. *J. Am. Chem. Soc.* **2011**, *133*, 20742.

(41) Zou, Q.; Li, X.; Zhang, J.; Zhou, J.; Sun, B.; Tian, H. *Chem. Commun.* **2012**, *48*, 2095.

(42) Pischel, U.; Uzunova, V. D.; Remon, P.; Nau, W. M. *Chem. Commun.* **2010**, *46*, 2635.

(43) Gao, C.; Silvi, S.; Ma, X.; Tian, H.; Venturi, M.; Credi, A. *Chem. Commun.* **2012**, *48*, 7577.

(44) Hennig, A.; Bakirci, H.; Nau, W. M. *Nat Meth* **2007**, *4*, 629.

(45) Chinai, J. M.; Taylor, A. B.; Ryno, L. M.; Hargreaves, N. D.; Morris, C. A.; Hart, P. J.; Urbach, A. R. *J. Am. Chem. Soc.* **2011**, *133*, 8810.

(46) Lee, D.-W.; Park, K. M.; Banerjee, M.; Ha, S. H.; Lee, T.; Suh, K.; Paul, S.; Jung, H.; Kim, J.; Selvapalam, N.; Ryu, S. H.; Kim, K. *Nat Chem* **2011**, *3*, 154.

(47) Biedermann, F.; Elmalem, E.; Ghosh, I.; Nau, W. M.; Scherman, O. A. *Angew. Chem. Int. Ed.* **2012**, *51*, 7739.

(48) Ma, D.; Hettiarachchi, G.; Nguyen, D.; Zhang, B.; Wittenberg, J. B.; Zavalij, P. Y.; Briken, V.; Isaacs, L. *Nat Chem* **2012**, *4*, 503.

(49) Lee, H. H.; Choi, T. S.; Lee, S. J. C.; Lee, J. W.; Park, J.; Ko, Y. H.; Kim, W. J.; Kim, K.; Kim, H. I. *Angew. Chem. Int. Ed.* **2014**, *53*, 7461.

(50) Carvalho, C. P.; Dominguez, Z.; Da Silva, J. P.; Pischel, U. *Chem. Commun.* **2015**, *51*, 2698.

(51) Vázquez , J.; Remón , P.; Dsouza, R. N.; Lazar, A. I.; Arteaga, J. F.; Nau, W. M.; Pischel, U. *Chem. – Eur. J.* **2014**, *20*, 9897.

(52) Wang, R.; Yuan, L.; Ihmels, H.; Macartney, D. H. *Chem. – Eur. J.* **2007**, *13*, 6468.

(53) Pemberton, B. C.; Singh, R. K.; Johnson, A. C.; Jockusch, S.; Da Silva, J. P.; Ugrinov, A.; Turro, N. J.; Srivastava, D. K.; Sivaguru, J. *Chem. Commun.* **2011**, *47*, 6323.

(54) Mohanty, J.; Dutta Choudhury, S.; Upadhyaya, H. P.; Bhasikuttan, A. C.; Pal, H. *Chem. – Eur. J.* **2009**, *15*, 5215.

(55) Yang, C.; Mori, T.; Origane, Y.; Ko, Y. H.; Selvapalam, N.; Kim, K.; Inoue, Y. *J. Am. Chem. Soc.* **2008**, *130*, 8574.

(56) Biedermann, F.; Ross, I.; Scherman, O. A. *Polym. Chem.* **2014**, *5*, 5375.

(57) Bouas-Laurent, H.; Desvergne, J. P. In *Photochromism*; Bouas-Laurent, H. D., Ed.; Elsevier Science: Amsterdam, 2003, p 561.

(58) Liu, S.; Ruspic, C.; Mukhopadhyay, P.; Chakrabarti, S.; Zavalij, P. Y.; Isaacs, L. *J. Am. Chem. Soc.* **2005**, *127*, 15959.

(59) Zhang, Q.; Tian, H. *Angew. Chem. Int. Ed.* **2014**, *53*, 10582.

Chapter 6

General Conclusions

In this chapter the main conclusions of the described work are summarized.

6.1 General Conclusions

Having in mind that the focus of this work was the development of new biologically related applications with CB*n* macrocycles, Chapter 1 provides a concise review of this host system and its ability to tune the photophysical and chemical properties of encapsulated guests. The following chapters describe the development of new or improved systems potentially applicable in bio-relevant contexts.

In Chapter 2, the dissociation of the host–guest complex between CB7 and the Hoechst 33258 dye by a phototriggered pH jump is presented. The sudden pH jump from 7 to 9 (achieved by a phototriggered reaction) lowers the binding constant of the dye by two orders of magnitude, resulting in an immediate (on the time scale of the photolysis) release of the guest, which was employed as a model for a potential drug. The release event is conveniently signaled by fluorescence modulations. This approach opens an unconventional and conceptually novel pathway for photo-controlled guest (drug) release.

In Chapter 3, an improved supramolecular strategy for the rate-accelerated formation of the merocyanine form of an anchor-substituted photo- and acidochromic spiropyran in the presence of the macrocyclic CB7 host was described. This approach allowed the observation of an outstanding hydrolytic stability of the merocyanine form in aqueous solution, without negative effects on the photoinduced back conversion to the ring-closed spiro form. The observed

kinetic and thermodynamic effects can be rationalized based on the strong binding of the macrocycle to the cadaverine-derived anchor of the spiropyran. The importance of an adequate anchor design is underlined by comparison with other spiropyrans.

In Chapter 4, it was shown for the first time that CB*n* macrocycles can inhibit the activity of type II endonucleases. Furthermore, a simple method to control the reactivation of enzymatic hydrolysis of the DNA substrates by addition of strongly binding competitors for CB*n* was demonstrated. The mechanistic nature of the interaction of the supramolecular host with the enzymes could not be clarified in the last details due to experimental limitations. However, it was clearly shown that the underlying reasons for the supramolecular control are not related to the interaction of the CB*n* macrocycles with the DNA substrates or co-factors of the enzyme. The effects were shown for a series of enzymes and DNA substrates, pointing to the general nature of the observations.

In Chapter 5 a keypad lock function, where an anthracene dye derivative forms a reversibly photoswitchable complex with CB8, harnessing the template effect exerted by the host macrocycle, was discussed. The input information, constituted by irradiation at >395 nm (input A) and a competitive guest (input B; 1-aminoadamantane), has to be applied in the right order (first input A and then input B) to produce un-complexed photodimer. The output of the system was related to relative fluorescence changes upon cycloreversion (irradiation at 254 nm). By exploitation of self-sorting upon addition of CB7 the system resets to the initial ternary CB8 complex. These results demonstrate the utility of CB*n* chemistry for the development of resettable complex logic operations with all-organic systems in aqueous solution.

6.2 Conclusiones Generales

Teniendo en cuenta que el objetivo de este trabajo fue el desarrollo de nuevas aplicaciones relacionadas biológicamente con macrociclos CB*n*, el Capítulo 1 proporciona una revisión concisa de este sistema anfitrión y su capacidad para modular las propiedades fotofísicas y químicas de los huéspedes encapsulados. Los siguientes capítulos describen el desarrollo de sistemas nuevos o mejorados potencialmente aplicables en contextos bio-relevantes.

En el Capítulo 2, se presenta la disociación del complejo anfitrión-huésped entre CB7 y el colorante Hoechst 33258 por medio de un salto de pH modulado por irradiación con luz. El salto de pH repentino de 7 a 9 (que se logra mediante una reacción fotoquímica) disminuye la constante de unión del colorante por dos órdenes de magnitud, lo que resulta en una inmediata (en la escala de tiempo de la fotólisis) liberación del huésped, el cual se empleó como modelo potencial para un fármaco. El evento de liberación está convenientemente señalizado por modulaciones en la fluorescencia. Este enfoque abre una vía no convencional y conceptualmente novedosa para la liberación foto-controlada de huéspedes (fármacos).

En el Capítulo 3 se describe una estrategia supramolecular mejorada para la formación a velocidad acelerada de la forma merocianina de un espiropirano foto- y acido-crómico modificado con un anclaje, en presencia del huésped macrocíclico CB7. Ésta estrategia permite la observación de una excelente estabilidad hidrolítica de la forma merocianina en solución acuosa, sin efectos negativos sobre la retro-conversión foto-inducida a la forma espiro. Los efectos cinéticos y termodinámicos observados pueden ser racionalizados en base a la fuerte unión del macrociclo al anclaje del tipo cadaverina del espiropirano. Queda subrayada la importancia de un diseño de anclaje adecuado por medio de la comparación con otros espiropiranos.

En el Capítulo 4 se demostró por primera vez que los macrociclos CB*n* pueden inhibir la actividad de las endonucleasas tipo II. Además, se demostró que es un método simple para controlar la reactivación de la hidrólisis enzimática de los sustratos de ADN mediante la simple adición de competidores fuertes. La

naturaleza mecanística de la interacción del huésped supramolecular con las enzimas no pudo aclararse en el último detalle, debido a limitaciones experimentales. Sin embargo, se demostró claramente que las razones subyacentes para el control supramolecular no están relacionadas con la interacción de los macrociclos CB*n* con los sustratos de ADN o co-factores de la enzima. Los efectos se muestran para una serie de enzimas y sustratos de ADN, que apuntan a una naturaleza generalizada de estas observaciones.

En el capítulo 5 se discutió una función *keypad lock*, donde un colorante derivado de antraceno forma un complejo con CB8 que puede ser modulado de forma reversible y fotocontrolada, aprovechando el efecto plantilla ejercido por el macrociclo anfitrión. La información del *input* (señal de entrada) constituida por la irradiación a >395 nm (*input* A) y por un huésped competitivo (*input* B; 1-aminoadamantano), se debe aplicar en el orden correcto (primer *input* A y después *input* B) para producir un foto-dímero libre. El *output* (señal de salida) del sistema se relacionó con los cambios de fluorescencia relativa a la cicloreversión (irradiación a 254 nm). Por el uso de un *self-sorting* tras la adición de CB7 el sistema restablece el complejo ternario inicial de CB8. Estos resultados demuestran la utilidad de la química de los CB*n* para el desarrollo de operaciones lógicas complejas y reajustables siendo todos los sistemas empleados orgánicos y en solución acuosa.

Chapter 7

Detailed Experimental Procedures

This chapter loom the information that is complementary to the previous sections, like symbols and abbreviations used, the experimental section of the distinct studies, CB7 synthesis, and characterization of the macrocycles.

I Symbols & Abbreviations

Δm	Isotope spacing	**ESI**	Electrospray ionization
ε	Molar extinction coefficient	**H33258**	Hoechst 33258
τ	Fluorescence lifetime	**^{1}H NMR**	Proton nuclear magnetic Resonance
δ	Chemical shift		
λ	Wavelength	K_b	Binding constant
Φ_f	Fluorescence quantum yield	l	Optical pathlength
A	Preexponential factor	**LC**	Liquid chromatography
ANT-D	Anthracene derivative	**MC**	Merocyanine form
BSA	Bovine serum albumin	**MCH**	Protonated MC
bz	Benzimidazole ring	**MG$^+$**	Malachite green cation
CB*n*	Cucurbiturils; Cucurbit[*n*]uril	**MGOH**	Malachite green leucohydroxide
CD	Circular dichroism	**MS**	Mass spectrometry
DAD	Photodiode array detector	**SP**	Spiro form
E_a	Apparent activation energy	**pK_a**	Negative decadic logarithm of the acidity dissociation constant
E_{photon}	Photon energy	U	Light flux
EDTA	Ethylenediaminetetraacetic acid		

II Experimental Section

II.1 Equipment, Materials and Procedure

II.1.1 Chapter 2

Hoechst 33258 trihydrochloride pentahydrate (FluoroPure™ grade) was supplied by Invitrogen and used without further purification. CB7 was provided by Prof. Nau (Jacobs University Bremen, Germany) and synthesized by me according to a published procedure discussed in section II.2.[1] I also acknowledge the implication of Dra. Uzunova (from Jacobs University Bremen, Germany), which performed the NMR studies. Malachite green leucohydroxide (90%) was from Aldrich and used as received. Water was of Millipore quality (mQ).

All UV/vis absorption and fluorescence measurements have been done at ambient temperature (297 K) in air-equilibrated aqueous solutions, using quartz cuvettes with 1 cm optical pathlength. Absorption spectra were recorded on a UV-1603 spectrophotometer from Shimadzu. Steady-state fluorescence measurements were performed on a Varian Cary Eclipse instrument. Fluorescence titration experiments with CB7 were executed by administering aliquots of a stock solution and the chosen excitation wavelength was always a correspondent absorption isosbestic or quasi-isosbestic point. The fitting of the binding curves was done by a 1:1 complexation model as described in the literature.[2,3] Generally, the dye concentration was kept low (≤ 10 μM; in most cases 1 μM) to avoid aggregation.[4] All pH titration experiments were carry out in the same day to allow comparisons between the spectra.

Time-resolved fluorescence measurements were performed with a time-correlated single-photon-counting setup from Edinburgh Instruments (FLS 920) using a pulsed light-emitting diode (LED) PLS-280 from PicoQuant (λ_{exc} = 280 nm, fwhm *ca*. 450 ps) as excitation source. The fluorescence lifetime measurements were performed at a somewhat higher dye concentration (*ca*. 100 μM). The pH in the respective titrations was adjusted by addition of acid (HCl) or base (NaOH) and monitored during the course of the experiments with a pH meter (model HI221,

HANNA Instruments). Where indicated, phosphate buffer (1 mM or 10 mM) was used. Fluorescence quantum yields were measured with quinine sulfate in 0.05 M H_2SO_4 as standard (Φ_f = 0.55).[5] The Job's plots were performed according to published methods.[6]

The mass spectrometric experiments were achieved with a Bruker Daltonics HCT-Ultra mass spectrometer (ion trap), equipped with an electrospray ionization source (Agilent) that utilized a nickel-coated glass capillary with an inner diameter of 0.6 mm. Ions were continuously generated by infusing the aqueous solution samples into the source with a syringe pump (KdScientific, model 781100, USA) at flow rates of 4 μL min^{-1}. The measurement parameters were adjusted and were typically as follows; polarity: positive; capillary voltage: -4.0 kV; capillary exit voltage: CE = 200 V; skimmer voltage: 25 V; temperature of drying gas: 573 K. The spectra were obtained in the "ultrascan mode" (fwhm 0.6 m/z). The experiments were carried out with a nebulizer gas pressure of 30 psi and a drying gas flow of 8 L min^{-1}. The measurements were carried out with mixtures of 3 μM **H33258** and 10 μM CB7 either at pH 4.5 and 7.

^{1}H NMR spectra were recorded on an ECX400 spectrometer from Jeol. Solutions were prepared in D_2O (99.9 atom% D) and if required their acidity was adjusted by addition of DCl (99 atom% D).

For the pH jump experiments, solutions containing 1 μM **H33258**, 30 μM CB7, and 100 μM MGOH were prepared at pH 7.2 (buffered or non-buffered). The MGOH was added in form of a few microliters of a 100 mM MGOH stock solution in dimethylsulfoxide. This solution was allowed to equilibrate for *ca*. 1.5 h in the dark before photopysis. During this time small fraction (< 10%; as rated by change in the UV/vis absorption spectrum) of the MGOH converted thermally to MG^+. At the end of the equilibration, the pH was measured and then the solution was irradiated for 10 min with a 302 nm light, generated by a UVP hand-held UV lamp (Model UVM-57, 1.5 mW cm^{-2} power density). Subsequently, the fluorescence spectrum was recorded (λ_{exc} = 340 nm) and the pH was measured again. Finally, the solution was allowed to re-equilibrate in the dark and fluorescence spectra were recorded periodically. At the final point, the pH was controlled once more.

II.1.2 Chapter 3

Compounds **1** to **3** were a courtesy of Prof. Andréasson (Chalmers University of Technology, Sweden), prepared according to literature procedures.[7] I also acknowledge the implication of Dr. Nilsson (from the same group at Chalmers University) with who parts this work was developed. Specifically, in the calculation of rates constants, ^{1}H NMR spectra, Arrhenius type data analysis, reversible switching, and helped in steady illumination experiments whit SP form. CB7 was synthesized according to a published procedure discussed in section II.2.[1] The ring-opened forms of spiropyran **1** (merocyanine **1MC** and protonated merocyanine **1MCH**) were prepared by heating **1SP** in an aqueous solution containing 0.1% trifluoroacetic acid at 353 K for 3 min, according to a described method, and if required (for **1MC**) this was followed by an adjustment of pH (phosphate buffer).[8]

Spectroscopic measurements were made in aerated water (milli-Q quality) or phosphate buffer (pH 7, 10 mM), using 1 cm quartz cuvettes. All necessary pH adjustments were performed with HCl and NaOH and controlled with a pH meter (model HI221, HANNA Instruments). The UV/vis absorption measurements were carried out with a Cary Bio 50 UV/vis spectrometer equipped with a Varian PCB 1500 Water Peltier System thermostat for temperature control. Typically, the measurements were executed at 293 K. The visible light was generated by a 500 W Xe lamp equipped with a hot mirror (A = 1.8 at 900 nm) to reduce IR intensity and suitable optical filters. For quantum yield determinations, interference filters (maximum transmission at 503 nm for MC isomerization and maximum transmission at 430 nm for MCH isomerization) were used. This yielded power densities of about 33 and 28 mW cm^{-2} for the application of the 503 and 430 nm filters, respectively. Around half of the sample volume was exposed to light at any given time. For the cycling experiment, CB7 (20 equiv) was added to a 10 μM **1SP** solution (t = 0 s) in 10 mM phosphate buffer (pH 7). Thermal ring opening was monitored for 30 min at λ_{obs} = 526 nm. This was followed by a 40 s irradiation period (500 W Xe lamp with 465 nm long-pass filter, power density of 1.67 W cm^{-2}) with simultaneous UV/vis absorption monitoring. The thermal-ring-opening/photoinduced-ring-closing cycle was repeated ten times.

The titration experiments with CB7 were done by administering aliquots of a CB7 to the photochrome guest solution (in its **1MC** or **1MCH** form). After each addition, the UV/vis absorption spectrum was recorded. The binding constants were determined by a global fit according to a model of consecutive 1:1 and 1:2 (guest/CB7) complexation.[9] Attempts to fit the data only with a 1:1 binding model or according to 2:1 (guest/CB7) complexation yielded unsatisfactory fits or physically meaningless data. The Job's plots were performed according to published methods.[6] The following errors were estimated for the different kinetic and thermodynamic data obtained in this work: binding constants 20%; activation energies 5%; protonation constants ± 0.1 pH unit; kinetic rate constants 15%; isomerization quantum yields 40%.

^{1}H NMR spectra was performed on an Eclipse 400 spectrometer from JEOL, in D_2O. The saturated solution of spiropyran **1** was recorded and allowed to reach the maximum conversion (90%) to the **1MC** form by thermal ring opening and measured before notable hydrolysis took place. For the characterization of the CB7 complex, an excess of the macrocycle was added to a saturated photochrome solution.

ESI-MS spectra were obtained on a Bruker Daltonics HCT-ultra mass spectrometer (ion trap), equipped with an ESI source (Agilent) and using a nickel-coated glass capillary (inner diameter of 0.6 mm). The ions were continuously generated by infusing the aqueous sample solution (4 mL min^{-1}) into the source with the help of a syringe pump (KdScientific, model 781100, USA). The solutions contained 10 μM **1MCH** at pH 2.5 in the absence or presence of 10 μM CB7 and were studied in the positive polarity mode. Typical experimental conditions were as follows: capillary voltage, 3.5 kV; capillary exit voltage, 75 V; skimmer voltage, 15 V; drying gas, 573 K at 6 L min^{-1}; nebulizer gas pressure, 20 psi. The host–guest complexes were stable in the gas phase and could be seen over a wide range of CE potentials (50 – 300 V).

The quantum yields for ring closure of **1MC** and **1MCH** were determined by monitoring the absorption decay rates (e.g., see insets of Figure 7.1) of the open forms upon irradiation with visible light (503 nm interference filter for **1MC** and 430 nm interference filter for **1MCH**), with resort to Equation 7.1.

$$\Phi_{open\rightarrow close} = \frac{\frac{-\Delta A \times V \times N_A}{\varepsilon_{open} \times l}}{\frac{U \times \Delta t \times area}{E_{photon}} \times (1-10^{-\bar{A}})} \times \frac{1}{0.4} \qquad \textbf{Equation 7.1}$$

ΔA is the absorbance variation in the time interval Δt (in s), *area* is the irradiated sample area (in cm^2), l is the optical pathlength (in cm), V is the sample volume (in L), N_A is Avogadro's constant (in mol^{-1}), ε_{open} is the molar extinction coefficient of the open form (in $M^{-1}\,cm^{-1}$) at the monitoring wavelength, U is the light flux of the isomerizing light (in $W\,cm^{-2}$), E_{photon} is the photon energy (in Ws), and $\bar{A}$ is the average absorbance in the time interval Δt. The factor 1/0.4 accounts for the fact that only 40% of the total sample volume was irradiated.

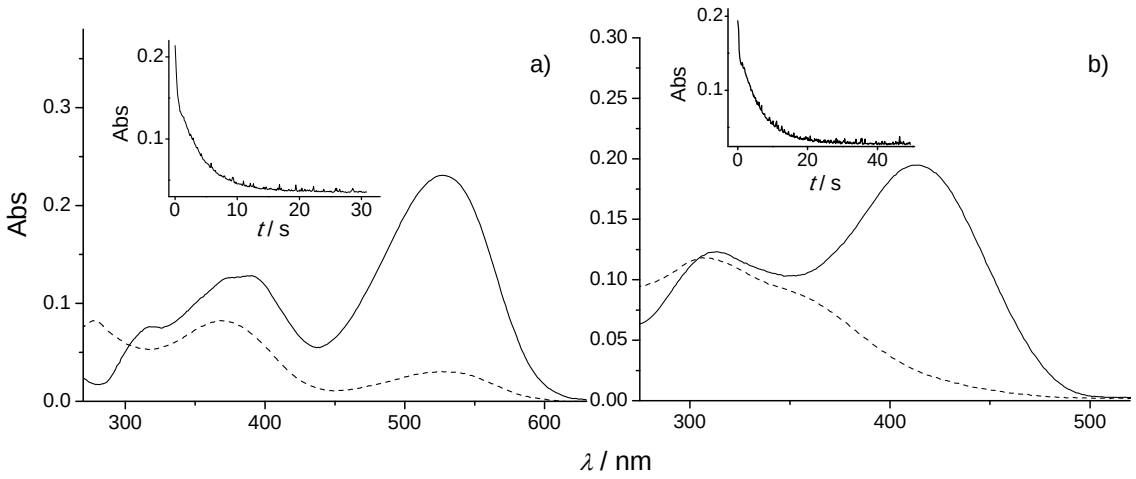

Figure 7.1 – Absorption spectra of a) **1MC**, and b) **1MCH**, in presence of 20 equivalents CB7 before (—) and after (···) irradiation with visible light (503 nm interference filter for **1MC** and 430 nm interference filter for **1MCH**). The insets show the corresponding kinetics, monitored at a) 510 nm, and b) 410 nm.

II.1.3 Chapter 4

CB6 was purchased from Sigma-Aldrich and CB7 was synthesized following a published procedure discussed in section II.2.[1] The water was of milli-Q quality, all polyamines (putrescine, cadaverine, spermine, spermidine) were purchased as hydrochloride salts from Sigma-Aldrich in the highest purity available (>98%). pGL3-Basic vector and *Sac*I restriction enzyme were provided by Promega Co., while enzymes *Kpn*I, *Xap*I, *Pdm*I, and λDNA/Eco91I (*BstE*II) marker were purchased from Thermo Scientific. *Kpn*I in BSA-free storage solution was supplied by Sigma-Aldrich. NucleoBond® Xtra Midi EF kit was acquired from Macherey-Nagel, and Green Safe Premium from NZY Tech. Additional information about the enzymes is available at http://rebase.neb.com.[10,11]

Chemically competent DH5α *E. coli* cells were slowly thawed and incubated with 100 ng of pGL3-Basic plasmid DNA (Scheme 7.1) on ice for 30 minutes. The cell suspension was incubated for 40 seconds at 315 K (heat shock) and then immediately placed on ice for 5 minutes. Prior to plating the cells were incubated in Super Optimal Broth with Catabolyte repression (2% w/v tryptone, 0.5% w/v yeast extract, 10 mM NaCl, 2.5 mM KCl, 10 mM $MgCl_2$, 10 mM $MgSO_4$, 20 mM glucose) for 2 h at 310 K with orbital agitation at 220 rpm. After recovery, the cells were plated in pre-warmed Lysogeny Broth agar plates containing ampicillin (100 μg μL^{-1}), and incubated overnight at 310 K. The following day, one single colony was selected and inoculated into 200 mL Lysogeny Broth containing 100 μg μL^{-1} of ampicillin. The cell suspension was incubated overnight at 310 K with orbital agitation at 220 rpm. Finally, the cells were centrifuged and processed for plasmid DNA extraction using a NucleoBond® Xtra Midi EF kit.

The plasmid DNA was linearized by total restriction with P*dm*I endonuclease ([DNA] = 383.8 nM; [PdmI] = 2 U μL^{-1}, 33 mM Tris-acetate buffer (pH 7.9), 10 mM $Mg(OAc)_2$, 66 mM KOAc, 0.1 mg mL^{-1} BSA; at 310 K for 12 h), verified by 1% agarose gel electrophoresis, and purified by standard ethanol precipitation.

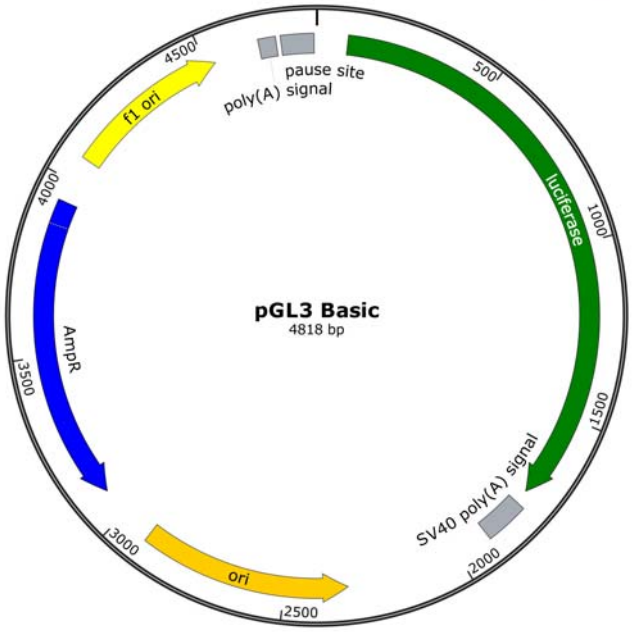

Scheme 7.1 – pGL3-Basic Vector circle map. Additional description: AmpR, gene conferring ampicillin resistance in *E. coli*; f1 ori, origin of replication derived from filamentous phage; ori, origin of replication in *E. coli*. Arrows within luciferase (cDNA encoding the modified firefly luciferase) and the AmpR gene indicate the direction of transcription; the arrow in the f1 ori indicates the direction of ssDNA strand synthesis.

Quantification and purity of the obtained circular and linear DNA was confirmed by measurements with a NanoDrop 2000c UV/vis spectrophotometer from Thermo Scientific. The required quality parameter for the DNA was set to $Abs_{260/280} \approx 1.8$ and $Abs_{260/230} \approx 2.0$.[12]

The reaction conditions for the restriction assays were: [DNA] = 9.6 nM corresponding to [bp] = 46.3 µM; [*Kpn*I] = 0.5 U μL^{-1} in a 10 mM Tris-HCl buffer (pH 7.5) containing 10 mM MgCl2, 0.02% Triton X-100, 0.1 mg mL^{-1} BSA; [*Sac*I] = 0.5 U μL^{-1} in 10 mM Tris-HCl buffer (pH 7.5) containing 7 mM $MgCl_2$, 50 mM KCl, 1 mM DTT; [*Xap*I] = 0.025 U μL^{-1} in 33 mM Tris-acetate buffer (pH 7.9) containing 10 mM $Mg(OAc)_2$, 66 mM KOAc, 0.1 mg mL^{-1} BSA; all at 310 K for 3 h. Additionally, assays in the same described conditions for each enzyme were executed in presence of one or combined combination of the follow: CB7, CB6, putrescine, cadaverine, spermine, spermidine, and EDTA. The concentrations used for the macrocycles were optimized to achieve *ca*. 50% enzyme activity inhibition, while

the polyamine/macrocycle ratio was adjusted to reach complete re-activation of the enzyme (< 5% inhibition). All restriction assays were done in triplicate and monitored by 1% agarose gel electrophoresis stained with Green Safe Premium (visualization in a Gel Doc™ Imaging system). A molecular weight size marker was used to assign distinct DNA fragments. The degree of inhibition was evaluated by integration of the optical density of the electrophoresis DNA bands by using the ImageJ program.[13]

CD measurements were performed on a Jasco J-810 circular dichroism spectropolarimeter in a 0.1 cm cuvette, at room temperature. Spectra were recorded at a speed of 200 nm min^{-1} and 1 nm resolution and were averaged over five accumulations.

Spectroscopic measurements in quartz cuvettes with 1 cm optical pathlength were performed in aerated mQ water at pH 7 (NaOH used for pH adjustment) at room temperature. Absorption spectra were recorded on a UV-1603 spectrophotometer from Shimadzu, while steady-state fluorescence measurements were done on a Varian Cary Eclipse instrument. Competitive displacement fluorescence titrations experiments were executed with the **H33258**/CB7 complex (1 μM /3 μM) with cadaverine, putrescine, and spermidine, were done by administering aliquots of compensated stock solutions (see Figure 7.2). The fitting of the binding curves was done by a competitive displacement 1:1 complexation model as described in the literature.[14,15]

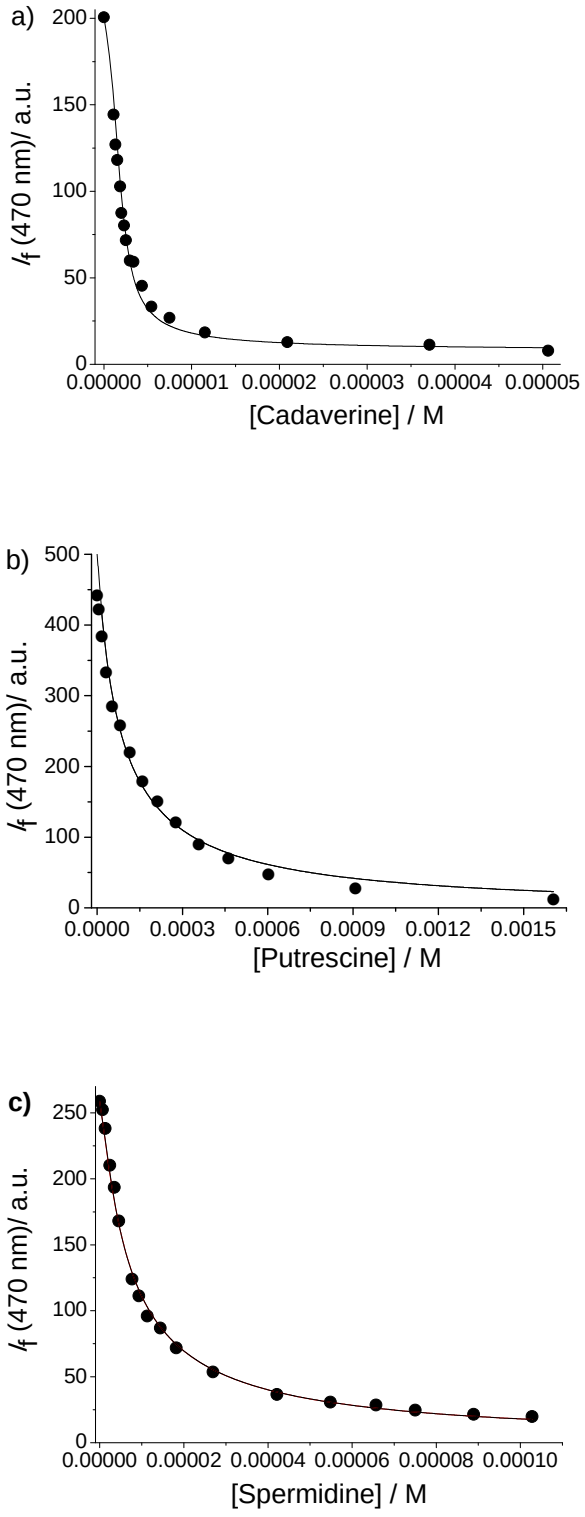

Figure 7.2 - Competitive fluorescence titrations of 1 μM H33258 / 3 μM CB7 with a) cadaverine, b) putrescine, and c) spermidine. λ_{obs} selected for the plots was 470 nm and the fluorescence measurements were made at λ_{exc} = 295 nm. The solid line is the fit according to competitive 1:1 binding model [*ca*. a) $K_b = 2.0 \times 10^7$ M^{-1}, b) $K_b = 1.0 \times 10^5$ M^{-1}, c) $K_b = 1.2 \times 10^6$ M^{-1}]

- DNA Sequence of the pGL3-Basic vector (4818 bp, one letter code)

GGTACCGAGCTCTTACGCGTGCTAGCCCGGGCTCGAGATCTGCGATCTAAGTAAGCTTGGCATTCCGGTACTGTTGGTAAAGCCACCAT
GGAAGACGCCAAAAACATAAAGAAAGGCCCGGCGCCATTCTATCCGCTGGAAGATGGAACCGCTGGAGAGCAACTGCATAAGGCTATG
AAGAGATACGCCCTGGTTCCTGGAACAATTGCTTTTACAGATGCACATATCGAGGTGGACATCACTTACGCTGAGTACTTCGAAATGT
CCGTTCGGTTGGCAGAAGCTATGAAACGATATGGGCTGAATACAAATCACAGAATCGTCGTATGCAGTGAAAACTCTCTTCAATTCTT
TATGCCGGTGTTGGGCGCGTTATTTATCGGAGTTGCAGTTGCGCCCGCGAACGACATTTATAATGAACGTGAATTGCTCAACAGTATG
GGCATTTCGCAGCCTACCGTGGTGTTCGTTTCCAAAAAGGGGTTGCAAAAAATTTTGAACGTGCAAAAAAAGCTCCCAATCATCCAAA
AAATTATTATCATGGATTCTAAAACGGATTACCAGGGATTTCAGTCGATGTACACGTTCGTCACATCTCATCTACCTCCCGGTTTTAA
TGAATACGATTTTGTGCCAGAGTCCTTCGATAGGGACAAGACAATTGCACTGATCATGAACTCCTCTGGATCTACTGGTCTGCCTAAA
GGTGTCGCTCTGCCTCATAGAACTGCCTGCGTGAGATTCTCGCATGCCAGAGATCCTATTTTTGGCAATCAAATCATTCCGGATACTGC
GATTTTAAGTGTTGTTCCATTCCATCACGGTTTTGGAATGTTTACTACACTCGGATATTTGATATGTGGATTTCGAGTCGTCTTAATG
TATAGATTTGAAGAAGAGCTGTTTCTGAGGAGCCTTCAGGATTACAAGATTCAAAGTGCGCTGCTGGTGCCAACCCTATTCTCCTTCT
TCGCCAAAAGCACTCTGATTGACAAATACGATTTATCTAATTTACACGAAATTGCTTCTGGTGGCGCTCCCCTCTCTAAGGAAGTCGGG
GAAGCGGTTGCCAAGAGGTTCCATCTGCCAGGTATCAGGCAAGGATATGGGCTCACTGAGACTACATCAGCTATTCTGATTACACCCG
AGGGGGATGATAAACCGGGCGCGGTCGGTAAAGTTGTTCCATTTTTTGAAGCGAAGGTTGTGGATCTGGATACCGGGAAAACGCTGGG
CGTTAATCAAAGAGGCGAACTGTGTGTGAGAGGTCCTATGATTATGTCCGGTTATGTAAACAATCCGGAAGCGACCAACGCCTTGATT
GACAAGGATGGATGGCTACATTCTGGAGACATAGCTTACTGGGACGAAGACGAACACTTCTTCATCGTTGACCGCCTGAAGTCTCTGA
TTAAGTACAAAGGCTATCAGGTGGCTCCCGCTGAATTGGAATCCATCTTGCTCCAACACCCCAACATCTTCGACGCAGGTGTCGCAGGT
CTTCCCGACGATGACGCCGGTGAACTTCCCGCCGCCGTTGTTGTTTTGGAGCACGGAAAGACGATGACGGAAAAAGAGATCGTGGATT
ACGTCGCCAGTCAAGTAACAACCGCGAAAAAGTTGCGCGGAGGAGTTGTGTTTGTGGACGAAGTACCGAAAGGTCTTACCGGAAAACT
CGACGCAAGAAAAATCAGAGAGATCCTCATAAAGGCCAAGAAGGGCGGAAAGATCGCCGTGTAATTCTAGAGTCGGGGCGGCCGGCCG
CTTCGAGCAGACATGATAAGATACATTGATGAGTTTGGACAAACCACAACTAGAATGCAGTGAAAAAAATGCTTTATTTGTGAAATTT
GTGATGCTATTGCTTTATTTGTAACCATTATAAGCTGCAATAAACAAGTTAACAACAACAATTGCATTCATTTTATGTTTCAGGTTCA
GGGGGAGGTGTGGGAGGTTTTTTAAAGCAAGTAAAACCTCTACAAATGTGGTAAAATCGATAAGGATCCGTCGACCGATGCCCTTGAG
AGCCTTCAACCCAGTCAGCTCCTTCCGGTGGGCGCGGGGCATGACTATCGTCGCCGCACTTATGACTGTCTTCTTTATCATGCAACTCG
TAGGACAGGTGCCGGCAGCGCTCTTCCGCTTCCTCGCTCACTGACTCGCTGCGCTCGGTCGTTCGGCTGCGGCGAGCGGTATCAGCTCA
CTCAAAGGCGGTAATACGGTTATCCACAGAATCAGGGGATAACGCAGGAAAGAACATGTGAGCAAAAGGCCAGCAAAAGGCCAGGAAC
CGTAAAAAGGCCGCGTTGCTGGCGTTTTTCCATAGGCTCCGCCCCCCTGACGAGCATCACAAAAATCGACGCTCAAGTCAGAGGTGGCG
AAACCCGACAGGACTATAAAGATACCAGGCGTTTCCCCCTGGAAGCTCCCTCGTGCGCTCTCCTGTTCCGACCCTGCCGCTTACCGGAT
ACCTGTCCGCCTTTCTCCCTTCGGGAAGCGTGGCGCTTTCTCATAGCTCACGCTGTAGGTATCTCAGTTCGGTGTAGGTCGTTCGCTCC
AAGCTGGGCTGTGTGCACGAACCCCCCGTTCAGCCCGACCGCTGCGCCTTATCCGGTAACTATCGTCTTGAGTCCAACCCGGTAAGACA
CGACTTATCGCCACTGGCAGCAGCCACTGGTAACAGGATTAGCAGAGCGAGGTATGTAGGCGGTGCTACAGAGTTCTTGAAGTGGTGG
CCTAACTACGGCTACACTAGAAGAACAGTATTTGGTATCTGCGCTCTGCTGAAGCCAGTTACCTTCGGAAAAAGAGTTGGTAGCTCTT
GATCCGGCAAACAAACCACCGCTGGTAGCGGTGGTTTTTTTGTTTGCAAGCAGCAGATTACGCGCAGAAAAAAAGGATCTCAAGAAGA
TCCTTTGATCTTTTCTACGGGGTCTGACGCTCAGTGGAACGAAAACTCACGTTAAGGGATTTTGGTCATGAGATTATCAAAAAGGATC
TTCACCTAGATCCTTTTAAATTAAAAATGAAGTTTTAAATCAATCTAAAGTATATATGAGTAAACTTGGTCTGACAGTTACCAATGCT
TAATCAGTGAGGCACCTATCTCAGCGATCTGTCTATTTCGTTCATCCATAGTTGCCTGACTCCCCGTCGTGTAGATAACTACGATACGG
GAGGGCTTACCATCTGGCCCCAGTGCTGCAATGATACCGCGAGACCCACGCTCACCGGCTCCAGATTTATCAGCAATAAACCAGCCAGC
CGGAAGGGCCGAGCGCAGAAGTGGTCCTGCAACTTTATCCGCCTCCATCCAGTCTATTAATTGTTGCCGGGAAGCTAGAGTAAGTAGT
TCGCCAGTTAATAGTTTGCGCAACGTTGTTGCCATTGCTACAGGCATCGTGGTGTCACGCTCGTCGTTTGGTATGGCTTCATTCAGCTC
CGGTTCCCAACGATCAAGGCGAGTTACATGATCCCCCATGTTGTGCAAAAAAGCGGTTAGCTCCTTCGGTCCTCCGATCGTTGTCAGAA
GTAAGTTGGCCGCAGTGTTATCACTCATGGTTATGGCAGCACTGCATAATTCTCTTACTGTCATGCCATCCGTAAGATGCTTTTCTGTG
ACTGGTGAGTACTCAACCAAGTCATTCTGAGAATAGTGTATGCGGCGACCGAGTTGCTCTTGCCCGGCGTCAATACGGGATAATACCG
CGCCACATAGCAGAACTTTAAAAGTGCTCATCATTGGAAAACGTTCTTCGGGGCGAAAACTCTCAAGGATCTTACCGCTGTTGAGATC
CAGTTCGATGTAACCCACTCGTGCACCCAACTGATCTTCAGCATCTTTTACTTTCACCAGCGTTTCTGGGTGAGCAAAAACAGGAAGGC
AAAATGCCGCAAAAAAGGGAATAAGGGCGACACGGAAATGTTGAATACTCATACTCTTCCTTTTTCAATATTATTGAAGCATTTATCA
GGGTTATTGTCTCATGAGCGGATACATATTTGAATGTATTTAGAAAAATAAACAAATAGGGGTTCCGCGCACATTTCCCCGAAAAGTG
CCACCTGACGCGCCCTGTAGCGGCGCATTAAGCGCGGCGGGTGTGGTGGTTACGCGCAGCGTGACCGCTACACTTGCCAGCGCCCTAGC
GCCCGCTCCTTTCGCTTTCTTCCCTTCCTTTCTCGCCACGTTCGCCGGCTTTCCCCGTCAAGCTCTAAATCGGGGGCTCCCTTTAGGGTT
CCGATTTAGTGCTTTACGGCACCTCGACCCCAAAAAACTTGATTAGGGTGATGGTTCACGTAGTGGGCCATCGCCCTGATAGACGGTTT
TTCGCCCTTTGACGTTGGAGTCCACGTTCTTTAATAGTGGACTCTTGTTCCAAACTGGAACAACACTCAACCCTATCTCGGTCTATTCT
TTTGATTTATAAGGGATTTTGCCGATTTCGGCCTATTGGTTAAAAAATGAGCTGATTTAACAAAAATTTAACGCGAATTTTAACAAAA
TATTAACGCTTACAATTTGCCATTCGCCATTCAGGCTGCGCAACTGTTGGGAAGGGCGATCGGTGCGGGCCTCTTCGCTATTACGCCAG
CCCAAGCTACCATGATAAGTAAGTAATATTAAGGTACGGGAGGTACTTGGAGCGGCCGCAATAAAATATCTTTATTTTCATTACATCT
GTGTGTTGGTTTTTTGTGTGAATCGATAGTACTAACATACGCTCTCCATCAAAACAAAACGAAACAAAACAAACTAGCAAAATAGGCT
GTCCCCAGTGCAAGTGCAGGTGCCAGAACATTTCTC TATCGATA

- Sequence of *Kpn*I (228 aminoacids, one letter code)

MDVFDKVYSDDNNSYDQKTVSQRIEALFLNNLGKVVTRQQIIRAATDPKTGKQPENWHQRLSELRTDKGYTILSWRDMKVLAPQEYIM
PHATRRPKAAKRVLPTKETWEQVLDRANYSCEWQEDGQHCGLVEGDIDPIGGGTVKLTPDHMTPHSIDPATDVNDPKMWQALCGRH
QVMKKNYWDSNNGKINVIGILQSVNEKQKNDALEFLLNYYGLKR

- Sequence of *SacI* (358 aminoacids, one letter code)

MGITIKKSTAEQVLRKAYEAAASDDVFLEDWIFLATSLREVDAPRTYTAALVTALLARACDDRVDPRSIKEKYDDRAFSLRTLCHGVVVP
MSVELGFDLGATGREPINNQPFFRYDQYSEIVRVQTKARPYLDRVSSALARVDEEDYSTEESFRALVAVLAVCISVANKKQRVAVGSAIVE
ASLIAETQSFVVSGHDVPRKLQACVAAGLDMVYSEVVSRRINDPSRDFPGDVQVILDGDPLLTVEVRGKSVSWEGLEQFVSSATYAGFRR
VALMVDAASHVSLMSADDLTSALERKYECIVKVNESVSSFLRDVFVWSPRDVHSILSAFPEAMYRRMIEIEVREPELDRWAEIFPET

- Sequence of *XapI* (237 aminoacids, one letter code)

MAQKARLRQNRYGTVINTTSSKQELQLGDALVDATERLTAKFGIAFTHEKKVMLADIVTSLRRSFPTVSFDDPLPNTYMSPDGGILSIMA
ADGERTFPVLITEVKNQGTNDLRAQEGLKKQAMGNAIERLGKNVIGFRAMMLEDGIIPFVCFGYGWDFHEGSSILDRVKTIAMFGELNQ
VNVIPEGEEGLFNRGSFFFRMEPWSLEEMSDVMFDVGSRAIHYYFAKFGDSAFKMIGS

II.1.4 Chapter 5

The **ANT-D** dye was synthesized and duly characterized by Zoe Dominguez at the University of Huelva (Scheme 7.2).[16] CB8 was purchased from Sigma Aldrich, while CB7 was prepared according to the procedure discussed in section II.2.

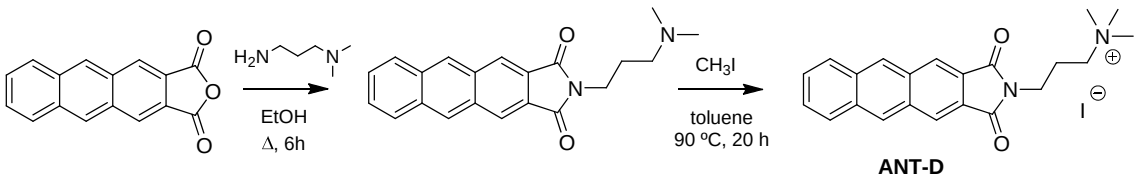

Scheme 7.2 – Schematic synthesis of **ANT-D** dye.

All measurements and photoreactions were performed with freshly prepared air-equilibrated aqueous solutions at room temperature. The pH of the solutions was adjusted to pH 7 by the addition of NaOH and controlled during the titration experiments with a pH meter (model HI221, HANNA Instruments). NMR measurements were done on an Agilent 400 MHz spectrometer.

All photophysical measurements were carried out in quartz cuvettes with 1 cm optical path length. The UV/vis absorption spectra were recorded with a UV-1603 spectrophotometer from Shimadzu. Steady-state fluorescence measurements were executed on a Cary Eclipse fluorimeter from Varian. The fluorescence quantum yield was determined by employing quinine sulfate in 0.05 M H_2SO_4 as standard

(Φ_f = 0.55).[5] Time-resolved fluorescence measurements were performed with a time-correlated single-photon-counting setup from Edinburgh Instruments (FLS 920) using a picosecond pulsed diode laser EPL-445 (λ_{exc} = 442.2 nm, pulse width 78.3 ps) as excitation source. The deconvolution analysis of the decay curve yielded the corresponding fluorescence lifetime.

A 150 W Xenon Lamp (Oriel GmbH & Co. KG) was used as light source for the photodimerization of **ANT-D**. The irradiation light was passed through a 395-nm optical cut-off filter. For the cycloreversion of the photodimer a hand-held UV lamp with output at 254 nm (VL-4.LC, 4 W) was used.

The titration experiments were done by administering aliquots of stock solutions of the CB*n* macrocycles (CB7 or CB8) to solutions containing the guest **ANT-D** dye. The excitation wavelength in the fluorescence titration was chosen to coincide with an isosbestic point of the UV/vis absorption titration. The fitting of the titration curves was done with a 1:1[2,3] and 2:1[17] complexation models for CB7 and CB8, respectively. The Job plot was obtained for a constant total (host and guest) concentration of 20 μM, and performed according to the literature.[6]

The chromatographic separation was achieved using an Hamilton PRP-1 reversed phase column (15.0 cm length, 2.1 mm internal diameter, 5 μm particle diameter), stabilized at 298 K. The mobile phase consisted of water and acetonitrile, both with 0.1% of formic acid at 0.4 mL min^{-1} flow. Two gradient programs were used. In the first program the mobile phase started with 95% of H_2O and 5% of acetonitrile and then changed to 0% of H_2O and 100% of acetonitrile within 10 min. This composition was kept for 4 min and then the initial composition was recovered within 30 s and stabilized for additional 5 min before the next run. In the second program the mobile phase started with 95% of H_2O and 5% of acetonitrile, was changed to 70% of H_2O and 30% of acetonitrile within 25 min and then to 0% of H_2O and 100% of acetonitrile within 5 min. This composition was kept for 4 min, and then the initial composition was recovered within 30 s, and finally stabilized for additional 5 min before the next run.

The LC-MS system is an Agilent Technologies 1200 Series LC, equipped with a photodiode array detector (DAD) and coupled to a Bruker Daltonics HCT ultra (ion

trap). The UV/vis absorption spectra of the separated products were obtained using the DAD. LC-DAD traces were acquired at 300 nm. The parameters of the electrospray ionization mass spectrometry detection were set as follows: polarity, positive; capillary voltage, –4.0 kV; capillary exit voltage, 180 V; skimmer voltage, 60 V; temperature of drying gas, 603 K; nebulizer gas pressure, 40 psi; drying gas flow, 8 L min^{-1}.

The mass spectrometric experiments to identify the **ANT-D**/**ANT-D**/CB8 complex were performed with a Bruker Daltonics HCT ultra mass spectrometer (ion trap), equipped with an electrospray ionization source (Agilent) that utilized a nickel-coated glass capillary with an inner diameter of 0.6 mm. The ions were continuously generated by infusing the aqueous solution sample into the source with a syringe pump (KdScientific, model 781100, USA) at a flow rate of 4 μL min^{-1}. The parameters used to detect host-guest complexes in the gas phase were typically as follows: polarity, positive; capillary voltage, –4.0 kV; capillary exit voltage, 20 V; skimmer voltage, 100 V; temperature of drying gas, 573 K; nebulizer gas pressure, 20 psi; drying gas flow, 5 L min^{-1}.

II.2 Cucurbit[7]uril Synthesis and CB*n* Characterization

The CB7 synthesis was based on an optimized standard literature procedure described by Nau and collaborators (Scheme 7.3).[1]

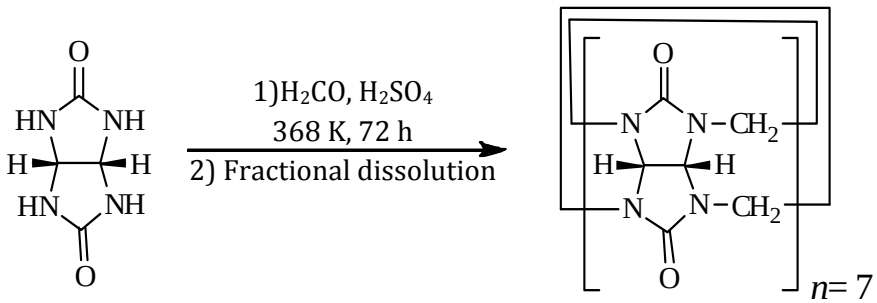

Scheme 7.3 – Synthesis of CB7 and its fractional isolation.

All reagents and materials were purchased from Fluka, except glycoluril (≥ 98%) and maleic acid that were from Aldrich and acetone from VWR. Formaldehyde (20 mL of 37% aqueous solution) was mixed with sulfuric acid (60 mL of 9 M aqueous solution) and with the use of an ice bath the magnetically stirred mixture was cooled down to 278 K. Glycoluril (11.4 g) was slowly added and the temperature was set to 368 K for 72 h. During this time an initially formed viscous gel completely redissolved. The reaction mixture was then poured into 200 mL deionised water and 800 mL acetone was added. This induced the precipitation of all CB*n* oligo- and polymers. The suspension was then decanted and the solid was washed with 1.5 L of a mixture of acetone/water (8:2 v/v) to remove the acid. This yielded a mixture of CB*n* homologues as a white powder. In order to remove the maximum amount of CB6, 400 mL deionised water was added (CB6 solubility in water is limited to around 20 μM, while the CB7 solubility is *ca*. 5 mM)[18] and the suspension was filtered. Then 300 mL acetone was added to the filtrate, leading to the precipitation of mainly CB7 homologue. The solid was filtered and dried in the oven at 353 K for 24 hours. The final product was then characterized prior to use by ^{1}H NMR (400 MHz, D_2O) δ: 4.16 (d, 14H), 5.47 (s, 14H), 5.72 (d, 14H), using maleic acid as internal standard, and ESI-MS (see Figure 7.3 and 7.4).

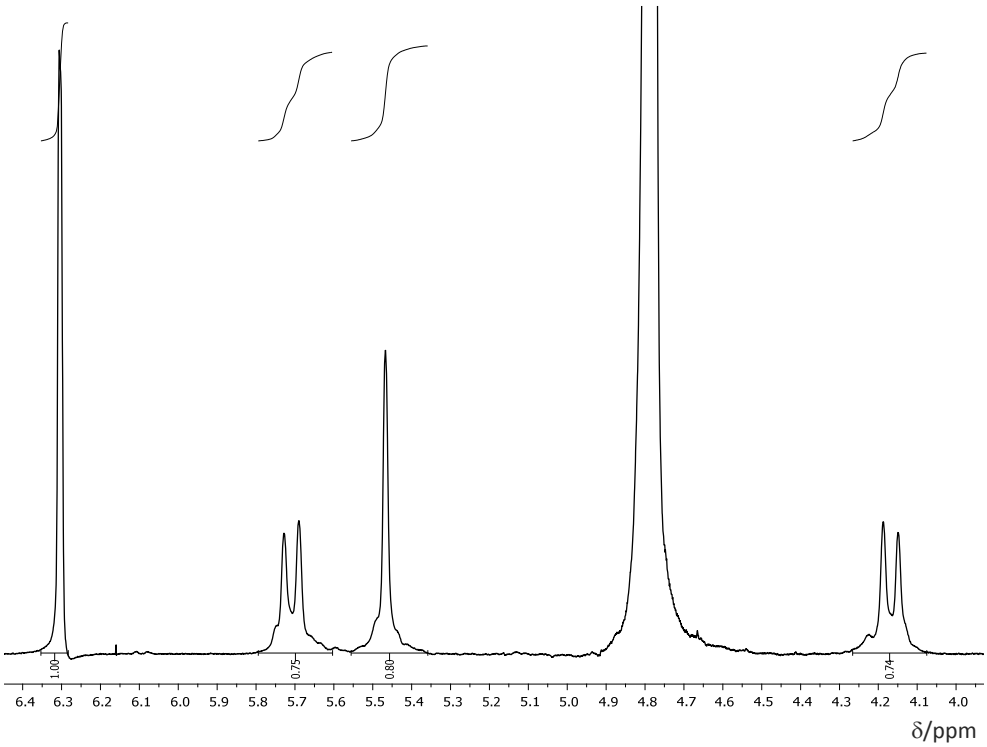

Figure 7.3 – ^{1}H NMR spectrum of CB7 in presence of equimolar amount of maleic acid, in D_2O.

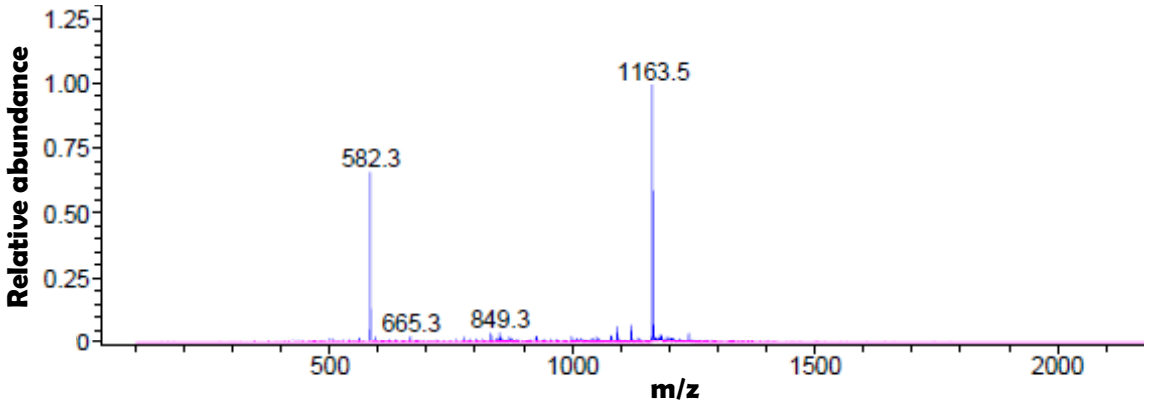

Figure 7.4 – ESI-MS spectrum of CB7 in aqueous solution. Assignments: m/z 1163: $(CB7+H)^{+}$; 582: $(CB7+2H)^{2+}$.

The cucurbiturils CB6 and CB8 that were also used in this thesis were purchased from Sigma-Aldrich and used without further purification. Due to solubility problems, it was not possible to use ^{1}H NMR spectroscopy for water-content quantification. Being so, for the CB6 host the water content was assumed as the one given by the supplier (20 wt%). For CB8 the concentration of the stock solution was quantified by direct UV/vis absorption titration of *N*,*N*-dimethylaminophenyl tropylium with the macrocycle.[19] The high 2:1 binding constant of the tropylium ion yielded a sharp leveling off which was used to determine the correct concentration. For both macrocycles the absence of other impurities was verified by ESI-MS.

References

(1) Marquez, C.; Fang, H.; Nau, W. M. *IEEE Trans. NanoBiosci.* **2004**, *3*, 39.

(2) Bakirci, H.; Zhang, X.; Nau, W. M. *J. Org. Chem.* **2005**, *70*, 39.

(3) Nau, W. M.; Zhang, X. *J. Am. Chem. Soc.* **1999**, *121*, 8022.

(4) Görner, H. *Photochem. Photobiol.* **2001**, *73*, 339.

(5) Morris, J. V.; Mahaney, M. A.; Huber, J. R. *J. Phys. Chem.* **1976**, *80*, 969.

(6) Valeur, B. *Molecular Fluorescence: Principles and Applications*; 1st ed.; Wiley-VCH Weinheim, 2001.

(7) Nilsson, J. R.; Parente Carvalho, C.; Li, S.; Da Silva, J. P.; Andréasson, J.; Pischel, U. *ChemPhysChem* **2012**, *13*, 3691.

(8) Stafforst, T.; Hilvert, D. *Chem. Commun.* **2009**, 287.

(9) Thordarson, P. *Chem. Soc. Rev.* **2011**, *40*, 1305.

(10) Vincze, T.; Posfai, J.; Roberts, R. J. *Nucleic Acids Res.* **2003**, *31*, 3688.

(11) Roberts, R. J.; Vincze, T.; Posfai, J.; Macelis, D. *Nucleic Acids Res.* **2007**, *35*, D269.

(12) Sambrook J. ; W., R. D. *Molecular Cloning: A Laboratory Manual* 3ed.; Cold Spring Harbor Laboratory, 2001.

(13) Schneider, C. A.; Rasband, W. S.; Eliceiri, K. W. *Nat Meth* **2012**, *9*, 671.

(14) Hennig, A.; Bakirci, H.; Nau, W. M. *Nat Meth* **2007**, *4*, 629.

(15) Bailey, D. M.; Hennig, A.; Uzunova, V. D.; Nau, W. M. *Chem. Eur. J.* **2008**, *14*, 6069.

(16) Carvalho, C. P.; Dominguez, Z.; Da Silva, J. P.; Pischel, U. *Chem. Commun.* **2015**, *51*, 2698.

(17) Bakirci, H.; Nau, W. M. *J. Photochem. Photobiol. A: Chem.* **2005**, *173*, 340.

(18) Lagona, J.; Mukhopadhyay, P.; Chakrabarti, S.; Isaacs, L. *Angew. Chem. Int. Ed.* **2005**, *44*, 4844.

(19) Vázquez , J.; Remón , P.; Dsouza, R. N.; Lazar, A. I.; Arteaga, J. F.; Nau, W. M.; Pischel, U. *Chem. Eur. J.* **2014**, *20*, 9897.

Scientific Contributions Derived from this Thesis

List of Publications

1. Cátia Parente Carvalho, Vanya D. Uzunova, José P. Da Silva, Werner M. Nau, and Uwe Pischel. "A Photoinduced pH jump applied to drug release from cucurbit[7]uril", *Chem. Commun.*, **2011**, *47*, 8793-8795.

2. Jesper R. Nilsson, Cátia Parente Carvalho, Shiming Li, José Paulo Da Silva, Joakim Andréasson, and Uwe Pischel. "Switching Properties of a Spiropyran-Cucurbit[7]uril Supramolecular Assembly: Usefulness of the Anchor Approach", *ChemPhysChem*, **2012**, *13*, 3691-3699.

3. Cátia Parente Carvalho, Amir Norouzy, Vera Ribeiro, Werner M. Nau, and Uwe Pischel. "Cucurbiturils as supramolecular inhibitors of DNA restriction by type II endonucleases", *Org. Biomol. Chem.*, **2015**, *13*, 2866-2869.

4. Cátia Parente Carvalho, Zoe Domínguez, José Paulo Da Silva, and Uwe Pischel. "A supramolecular keypad lock", *Chem. Commun.*, **2015**, *51*, 2698-2701.

List of Conference Contributions

1. Uwe Pischel, Cátia Parente Carvalho, Zoe Domínguez, José Paulo Da Silva. "Cucurbituril Host-Guest Chemistry for Molecular Information Processing", **Oral Communication**, 4th International Conference on Cucurbituril, Tianjin (China), **2015**.

2. Cátia Parente Carvalho, Zoe Domínguez, José Paulo Da Silva, Uwe Pischel. "A Reversibly Photoswitchable Supramolecular Complex", **Poster**, VII Mediterranean Organic Chemistry Meeting (REQOMED), Málaga (Spain), **2015**.

3. Cátia Parente Carvalho, Zoe Domínguez, José Paulo Da Silva, Uwe Pischel. "A Supramolecular Keypad Lock", **Poster and Flash Presentation**, COST Action CM1005 - Supramolecular Chemistry in Water Final Scientific Meeting, Prague (Czech Republic), **2015**.

4. C. Parente Carvalho, U. Pischel. “Cucurbiturils Inhibit the Enzymatic Activity of Type II Endonuclease” **Poster and Flash Presentation**, Workshop on *PHYSICAL ORGANIC CHEMISTRY OF COMPLEX SYSTEMS* in the European Winter School on Physical Organic Chemistry: e-Wispoc 2014, Bressanone (Italy), **2014**.

5. Uwe Pischel, Cátia Parente Carvalho, Jesper R. Nilsson, Shiming Li, José Paulo Da Silva, Joakim Andréasson. “Anchoring of a Spiropyran to Cucurbit[7]uril: Photochromic Performance and Chemical Stability in Water”, **Oral Communication**, 3rd International Conference on Cucurbiturils, Canberra (Australia), **2013**.

6. Cátia Parente Carvalho, Uwe Pischel. “Cucurbiturils Inhibit Enzymatic Activity of Type II Endonucleases”, **Poster**, 3rd International Conference on Cucurbiturils, Canberra (Australia), **2013**.

7. U. Pischel, C. Parente Carvalho, J. R. Nilsson, S. M. Li, J. P. Da Silva, J. Andréasson. "Photochromic switching of a spiropyran-cucurbit[7]uril supramolecular complex”, **Oral Communication**, 23rd Lecture Conference on Photochemistry, Potsdam (Germany), **2012**.

8. C. Parente Carvalho, V. D. Uzunova, J. P. da Silva, W. M. Nau, U. Pischel. “Photoinduced pH jump – Application to drug release from cucurbit[7]uril”, **Poster**, XXIV IUPAC Symposium on Photochemistry, Coimbra (Portugal), **2012**.

9. Jesper R. Nilsson, Cátia P. Carvalho, Shiming Li, Joakim Andréasson, Uwe Pischel. “Cucurbit[7]uril alters spiropyran pKa values, hinders hydrolysis and accelerates isomerization in aqueous solution”, **Poster**, Central European Conference on Photochemistry (CECP), Bad Hofgastein (Austria), **2012**.

10. U. Pischel, C. P. Carvalho, V. D. Uzunova, J. P. da Silva, W. M. Nau. “Phototriggered drug release from a supramolecular assembly”, **Oral Communication**, COST Meeting - Supramolecular Chemistry in Water, Frascati (Italy), **2011**.

11. C. P. Carvalho, V. D. Uzunova, J. P. da Silva, W. M. Nau, U. Pischel. "Phototriggered drug release from a supramolecular assembly", **Poster**, III Jornadas Ibéricas de Fotoquímica, Granada (Spain), **2011**.

12. Pischel U., Parente Carvalho C., Uzunova V. D., Nau W. M.. "Biomimetic Encapsulation of a Fluorescent DNA Binder by Cucurbit[7]uril", **Oral Communication**, 22nd Lecture Conference of the GDCh-Divsion of Photochemistry, Erlangen (Germany), **2010**.

Curriculum Vitae

Cátia Diana Parente Caldeira Carvalho

Date of Birth: 28/08/1984

Nationality: Portuguese

Contacts: e-mail: catia.diana@hotmail.com;

Telf: +351 961610684

Education

2015 Ph.D. studies in Chemical Science and Technology, at the University of Huelva, Spain.
Ph.D. thesis supervised by Prof. Dr. Uwe Pischel: *Supramolecular Cucurbituril Complexes for Applications in Bio-relevant Contexts.*

Scientific Exchange Visits:
- Prof. Dr. José Paulo Da Silva, *University of Algarve (Portugal).*
- Prof. Dr. Werner M. Nau, *Jacobs University (Germany).*
- Prof. Dr. Joakim Andréasson, *Chalmers University of Technology (Sweden).*
- Prof. Dr. Carlos Baleizão, *Technical University of Lisbon (Portugal).*
- Prof. Dr[a]. Vera Ribeiro, *University of Algarve (Portugal).*
- Prof. Dr. Fernando Pina, *New University of Lisbon (Portugal).*

17/12/2012 Master Degree in Chemical Science and Technology, at the University of Huelva, Spain.
Master thesis with Prof. Dr. Uwe Pischel: *An aminonaphthalimide-putrescine conjugate as fluorescent probe for cucurbituril host-guest complexes.*

20/12/2010 Master Degree in Biomedical Sciences, at the University of Algarve, Portugal.
Master thesis supervised by Prof. Dr. Uwe Pischel and Prof. Dr. José Paulo da Silva: *Supramolecular biomimetic binding of the DNA-dye Hoechst 33258 by a synthetic macrocycle.*

03/06/2008 Diploma Degree in Biochemistry, at the University of Algarve, Portugal.
Thesis supervised by Prof. Dra. Vera Ribeiro in the field of Molecular Biology: *The Role of Apical Sodium-dependent Bile Acid Transporter Variants in the Susceptibility for Colorectal Cancer.*

Scientific Competences and Skills

2012 - 2015 Tutor in several research projects of undergraduate and master students.

7/04/2015 Laboratory protective equipment: assortment and selection, course by Fremap

2009 - 2011 Research trainee at the University of Huelva (Spain).

2006 - 2008 Research trainee at the Faculty of Sciences and Technology University of Algarve, Faro (Portugal), under the supervision of Prof. Dra. Vera Ribeiro.

Techniques: UV/vis and Fluorescence spectroscopy, time-correlated single-photon-counting, ESI-MS, LC-DAD, CD, ITC, ^{1}H and ^{13}C-NMR, PCR-RFLP, RT-PCR, several molecular biology techniques, and multi-step organic synthesis.

Software: Endnote, Origin, ChemBioDraw, ImageJ, MesteReNova, DataAnalysis.

Languages: Portuguese *(native)*, English *(fluent speech and vast technical vocabulary)*, and Spanish *(advanced)*.

Honors & Awards

2012 – 2015 Ph.D. Fellowship from the Portuguese Ministry of Science/FCT (01/01/2012 to date). Four years of salary for doctoral studies in Spain plus project support fees.

06/02/2014 WISPOC Poster Prize, at the European Winter School on Physical Organic Chemistry, Bressanone (Italy).

02/02/2014 Trainee Grant from the Management Committee of the COST Action CM1005 to assist e-COST Training School.

2009 – 2011 Research Fellowships, RISE and I2TEP projects, and also from the Center for Research in Sustainable Chemistry (CIQSO), at the University of Huelva (Spain).

20/05/2009 ISSX Poster Prize, at the 11th European Regional ISSX Meeting, Lisbon (Portugal)

Publications in peer-reviewed Journals

1. Cátia Parente Carvalho, Zoe Domínguez, José Paulo Da Silva, and Uwe Pischel. "A supramolecular keypad lock", *Chem. Commun.*, **2015**, *51*, 2698-2701.
2. Cátia Parente Carvalho, Amir Norouzy, Vera Ribeiro, Werner M. Nau, and Uwe Pischel. "Cucurbiturils as supramolecular inhibitors of DNA restriction by type II endonucleases", *Org. Biomol. Chem.*, **2015**, *13*, 2866-2869.
3. Patricia Rémon, Cátia Parente Carvalho, Carlos Baleizão, Mario Nuno Berberan-Santos, and Uwe Pischel. "Highly Efficient Singlet-Singlet Energy Transfer in Light-Harvesting [60,70]Fullerene-4-Amino-1,8-naphthalimide Dyads", *ChemPhysChem*, **2013**, *14*, 2717-2724.
4. Cátia Parente Carvalho, Rita Ferreira, José Paulo Da Silva, and Uwe Pischel. "An aminonaphtalimide-putrescine conjugate as fluorescet probe for cucurbituril host-guest complexes", *Supramol. Chem.*, **2013**, *25*, 92-100.
5. Jesper R. Nilsson, Cátia Parente Carvalho, Shiming Li, José Paulo Da Silva, Joakim Andréasson, and Uwe Pischel. "Switching Properties of a Spiropyran-Cucurbit[7]uril Supramolecular Assembly: Usefulness of the Anchor Approach", *ChemPhysChem*, **2012**, *13*, 3691-3699.
6. Cátia Parente Carvalho, Vanya D. Uzunova, José P. Da Silva, Werner M. Nau, and Uwe Pischel. "A Photoinduced pH jump applied to drug release from cucurbit[7]uril", *Chem. Commun.*, **2011**, *47*, 8793-8795.
7. Cátia Carvalho, Vera Ribeiro, José Estevens. "Relationship between Variants of Apical Sodium-dependent Bile Acid Transporter Gene (SLC10A2) and the Development of Colorectal Cancer", *Drug Metab Rev*, **2009**, *41*, 21.

Book Chapters

1. Cátia Parente Carvalho and Uwe Pischel. (**2012)** Supramolecular assemblies for information processing, In Katz E. (Ed) "Molecular and Biomolecular Information Processing: From Molecular Switches to Logic Systems" (pp 99 – 119). Wiley-VCH, Weinheim, Germany.

Conferences and Workshops Contributions

1. Uwe Pischel, Cátia Parente Carvalho, Zoe Domínguez, José Paulo Da Silva. "Cucurbituril Host-Guest Chemistry for Molecular Information Processing", **Oral Communication**, 4th International Conference on Cucurbituril, Tianjin (China), **2015**.

2. Cátia Parente Carvalho, Zoe Domínguez, José Paulo Da Silva, Uwe Pischel. "A Reversibly Photoswitchable Supramolecular Complex", **Poster**, VII Mediterranean Organic Chemistry Meeting (REQOMED), Málaga (Spain), **2015**.

3. Cátia Parente Carvalho, Zoe Domínguez, José Paulo Da Silva, Uwe Pischel. "A Supramolecular Keypad Lock", **Poster and Flash Presentation**, COST Action CM1005 - Supramolecular Chemistry in Water Final Scientific Meeting, Prague (Czech Republic), **2015**.

4. C. Parente Carvalho, U. Pischel. "Cucurbiturils Inhibit the Enzymatic Activity of Type II Endonuclease" **Poster and Flash Presentation**, Workshop on *PHYSICAL ORGANIC CHEMISTRY OF COMPLEX SYSTEMS* in the European Winter School on Physical Organic Chemistry: e-Wispoc 2014, Bressanone (Italy), **2014**.

5. Uwe Pischel, Cátia Parente Carvalho, Jesper R. Nilsson, Shiming Li, José Paulo Da Silva, Joakim Andréasson. "Anchoring of a Spiropyran to Cucurbit[7]uril: Photochromic Performance and Chemical Stability in Water", **Oral Communication**, 3rd International Conference on Cucurbiturils, Canberra (Australia), **2013**.

6. Cátia Parente Carvalho, Uwe Pischel. "Cucurbiturils Inhibit Enzymatic Activity of Type II Endonucleases", **Poster**, 3rd International Conference on Cucurbiturils, Canberra (Australia), **2013**.

7. U. Pischel, C. Parente Carvalho, J. R. Nilsson, S. M. Li, J. P. Da Silva, J. Andréasson. "Photochromic switching of a spiropyran-cucurbit[7]uril supramolecular complex", **Oral Communication**, 23rd Lecture Conference on Photochemistry, Potsdam (Germany), **2012**.

8. Cátia Diana Parente Carvalho. "Supramolecular Encapsulation of Bio-Inspired Models by Cucurbiturils: Progress Report", **Oral Communication**, II Workshop Transfronterizo Proyeto I2TEP: Investigación y transferencia transfronteriza España-Portugal", Beja (Portugal), **2012**.

9. C. Parente Carvalho, V. D. Uzunova, J. P. da Silva, W. M. Nau, U. Pischel. "Photoinduced pH jump – Application to drug release from cucurbit[7]uril", **Poster**, XXIV IUPAC Symposium on Photochemistry, Coimbra (Portugal), **2012**.

10. Jesper R. Nilsson, Cátia P. Carvalho, Shiming Li, Joakim Andréasson, Uwe Pischel. "Cucurbit[7]uril alters spiropyran pKa values, hinders hydrolysis and accelerates isomerization in aqueous solution", **Poster**, Central European Conference on Photochemistry (CECP), Bad Hofgastein (Austria), **2012**.

11. U. Pischel, C. P. Carvalho, V. D. Uzunova, J. P. da Silva, W. M. Nau. "Phototriggered drug release from a supramolecular assembly", **Oral Communication**, COST Meeting - Supramolecular Chemistry in Water, Frascati (Italy), **2011**.

12. C. P. Carvalho, V. D. Uzunova, J. P. da Silva, W. M. Nau, U. Pischel. "Phototriggered drug release from a supramolecular assembly", **Poster**, III Jornadas Ibéricas de Fotoquímica, Granada (Spain), **2011**.

13. Pischel U., Parente Carvalho C., Uzunova V. D., Nau W. M.. "Biomimetic Encapsulation of a Fluorescent DNA Binder by Cucurbit[7]uril", **Oral Communication**, 22nd Lecture Conference of the GDCh-Divsion of Photochemistry, Erlangen (Germany), **2010**.
14. Cátia Carvalho, José Estevens and Vera Ribeiro; "Relationship between Variants of Apical Sodium-dependent Bile Acid Transporter Gene (SLC10A2) and the Development of Colorectal Cancer", **Poster**, 11th European Regional ISSX Meeting, Lisbon (Portugal), **2009**.
15. Cátia Carvalho, José Estevens and Vera Ribeiro; "Effect of Polymorphism in the Apical Sodium-dependent Bile Salt Transporter Gene (SLC10A2) in Colorectal Cancer Risk" **Poster**, VIII International symposium on experimental techniques, Faro (Portugal), **2007**.
16. Piedade R., Carvalho C., Gaspar J., Rueff J., Ribeiro V.; "PXR genotyping in the Portuguese population", **Poster**, XIV Congresso Nacional de Bioquímica, Vilamoura (Portugal), **2004**.